THE IMPORTANCE OF SUBMARINE GROUNDWATER DISCHARGE ON NUTRIENT FLUXES AND DISSOLVED ORGANIC MATTER MOLECULAR COMPOSITION IN A SEMI-ARID, HIGHLY DISTURBED ESTUARY

A Dissertation

by

AUDREY RUTH DOUGLAS

BS, University of Oregon, 2007

Submitted in Partial Fulfillment of the Requirements for the Degree of

DOCTOR OF PHILOSOPHY

in

COASTAL AND MARINE SYSTEM SCIENCE

Texas A&M University-Corpus Christi
Corpus Christi, Texas

December 2020

December 2020

SUBMARINE GROUNDWATER DISCHARGE, NUTRIENT FLUXES, AND DISSOLVED ORGANIC MATTER MOLECULAR COMPOSITION IN A SEMI-ARID, HIGHLY DISTURBED ESTUARY

A Dissertation

by

AUDREY RUTH DOUGLAS

This dissertation meets the standards for scope and quality of
Texas A&M University-Corpus Christi and is hereby approved.

Dorina Murgulet, Ph.D.
Chair

Paul Montagna, Ph.D.
Committee Member

Hussain Abdulla, Ph.D.
Committee Member

Joseph David Felix, Ph.D.
Committee Member

Richard Peterson, Ph.D.
Committee Member

Jim Lee, Ph.D.
Graduate Faculty Representative

December 2020

ABSTRACT

This dissertation advances our understanding of the temporal and spatial variability of submarine groundwater discharge (SGD) rates, SGD-derived nutrient fluxes and its role in the nitrogen budget, and the dissolved organic matter (DOM) molecular composition of surface water and porewater in semi-arid, hydrological disturbed estuaries. Nueces Bay was selected as the study area because it is highly disturbed both anthropogenically (e.g., dredging, oil/gas development, and reduced freshwater inflows) and naturally (e.g., drought, flooding) and the nitrogen budget remains unbalanced after multiple attempts. This study collected surface water and porewater samples quarterly for 2 years and employed radon and radium mass balances and Darcy estimates to assess SGD rates, principal components analysis and a partial hierarchical two-way ANOVA to evaluate the water quality and relative importance of SGD-derived nutrient fluxes to the overall nutrient budget, and PPL-SPE and UPLC-Orbitrap Fusion Tribrid mass spectrometry to assess DOM molecular composition. This study found significant spatial and temporal variability in SGD rates that vary over 1-2 orders of magnitude depending on method (i.e., radon or radium mass balance, Darcy estimate), location, and groundwater endmember. The high SGD rates, compared to literature, are driven by steeper gradients nearshore, short-circuiting of confining layers due to substantial oil/gas development and dredging, sediment heterogeneity, and reduced confining layer integrity favoring vertical advective flux. The observed spatiotemporal variability in SGD was related to nutrient fluxes and nitrogen budgets, suggesting that SGD brings 2-4 orders of magnitude more nitrogen and other nutrients into the system than surface runoff under all hydroclimatic conditions. Thus, the average SGD flux supplies more nitrogen to the system than previously accounted for creating an excess of

$370.6x10^9$ g $N \cdot yr^{-1}$. Finally, a molecular characterization of the DOM indicates that surface water DOM composition is significantly different from flooding and baseflow conditions (6- and 9-months post flooding) during flood recession (3-months post flooding) with more heteroatom compounds detected. Surface water and porewater are most similar during flooding recession, indicating greater SGD-derived DOM. While other studies have suggested that semi-arid systems receive significant SGD, this dissertation further suggests that SGD in highly anthropogenically disturbed systems may be derived from both shorter (shallower) and longer (deeper) flowpaths and lag the climatic conditions by weeks (surficial aquifers) and months or longer (deeper aquifers). As anthropogenic disturbances continue to increase along with a changing climate, the groundwater-surface water interactions will be impacted and the long-term effects of these changes on nutrient and DOM composition might be significant, though potential consequences remain largely unknown.

DEDICATION

I dedicate this to my father and mother, for your endless love and support and for teaching me to persist.

ACKNOWLEDGEMENTS

I would like to thank Texas A&M University-Corpus Christi, the Center for Water Supply Studies, Texas Sea Grant (Contract NO. NA14OAR4170102), Texas Sea Grant's Grants in Aid of Research (2017 and 2018), and the Texas Water Development Board for their financial and research support.

Special thanks is given to my committee chair, Dr. Dorina Murgulet, who invested enormous amounts of time guiding me from a student with a Bachelor's degree returning to academic research and scholastic life after years away and almost no related background to a now independent researcher contributing to the body of scientific literature. I also appreciate all the support and guidance from my committee members, Drs. Hussain Abdulla, Paul Montagna, Joseph David Felix, and Richard Peterson.

Thanks also go to my colleagues and the department faculty and staff for making my time at Texas A&M University-Corpus Christi an enjoyable experience. In particular, Paula Rose and Chriss Shope for a memorable introduction to field work my first month in the program, Alessandra Garcia and Kari Nease for always being there to assist or advise with anything administrative, Nick Spalt and Melissa Treviño for many long days in the field and lab filled with humor and Spanish lessons, and undergraduates Zoe Ruben and Megan Greige for their hard work and long hours in the lab and helping me become a better instructor and mentor.

I would like to thank my friends, Kevin, Lindsey, Megan, and Polly, for helping keep me sane and grounded and for providing much needed laughter and nourishment for body and soul. Without your support and understanding I would not have been able to navigate the stress and anxiety. I also want to extend my gratitude to my roommates, who have helped look after my

house and my four-legged child while I put in long days in the field and lab and wrote my dissertation. Namely, Yu, Nina, and Shufei Chen who fed me home-cooked Chinese meals the last year of my dissertation writing.

Finally, I want to thank my parents and my four-legged child, Casey, who provided ears to listen, or scratch, and endless encouragement and love throughout my pursuit of a doctoral degree.

TABLE OF CONTENTS

LIST OF FIGURES

FIGURES PAGE

LIST OF TABLES

TABLES PAGE

CHAPTER I: INTRODUCTION

1.1 Groundwater-Surface Water Interactions

The interaction between groundwater and surface water occurs at a range of spatial and temporal scales and its magnitude is highly variable depending on meteorological, fluvial, hydrological, geological, and anthropogenic processes (Murgulet et al. 2016; Oberdorfer et al. 2008; Santos et al. 2012b). Only in the past couple of decades has research begun to focus on the role of groundwater as a source of freshwater, nutrients, and contaminants to coastal embayments (Burnett et al. 2006; Moore 2010). Thus, to assess freshwater inflows and nutrient inputs and cycling in coastal embayments for development of comprehensive management practices, studies of submarine groundwater discharge (SGD) and the corresponding nutrient inputs and composition must be performed.

Groundwater is a key source of freshwater in many parts of the world (Schwartz and Zhang 2003). The chemistry of groundwater is influenced by local geology, aquifer residence times, flow paths, pollution, and other anthropogenic or natural processes (Santos et al. 2008a). Pollution from industrial processes and agricultural fertilizers and pesticides can reach and contaminate local groundwater supplies (Charette and Allen 2006). The local geology, geography, and land use land cover not only impact local groundwater quality, but they are also significant factors in the movement of groundwater through influences on aquifer recharge or groundwater uses.

Human population growth and its associated activities (i.e., fossil fuel consumption, wastewater, and agriculture, among others), have significantly increased the flux of nitrogen (N) and phosphorous (P) to terrestrial and aquatic systems (Bruesewitz et al. 2015; Kennish 2002; Paerl 2009; Rabalais 2002; Scavia and Bricker 2006). Subsequently, the high flux of nutrients

from the enriched soils to the water table is causing excess N and P contamination in groundwater. The importance of groundwater is not so much due to the magnitude of flow rates, but rather owing to its elevated nutrient concentrations compared to receiving surface waters (Oberdorfer et al. 2008; Oberdorfer et al. 1990). Several studies have demonstrated that SGD can constitute an ecologically significant source of nutrients (Luo et al. 2014; Maher et al. 2019; Slomp and Van Cappellen 2004; Spalt et al. 2020; Urquidi-Gaume et al. 2016) and metals (Charette and Buesseler 2004; Montluçon and Sañudo-Wilhelmy 2001; Mori et al. 2019; Rodellas et al. 2014; Spalt et al. 2020) to coastal ecosystems. For instance, although groundwater nutrient concentrations vary greatly, NO_3^- concentrations in discharging coastal groundwater may be up to five orders of magnitude greater than levels in the receiving seawater bodies (Valiela et al. 1990). Consequently, though groundwater discharge volumes may be small, its nutrient content may be great enough to make significant contributions to coastal nutrient budgets, particularly in shallow estuaries with limited surface runoff inputs.

1.2 Submarine Groundwater Discharge

Similarly to surface waters, groundwater flows downgradient and as hydostratigraphic units continue out under coastal embayments and oceans, groundwater flows directly into the sea at points of aquifer outcrop (Burnett et al. 2003). These coastal aquifers can be classified as shallow/local flow systems or and deep/intermediate or regional flow systems, depending on their hydrogeologic settings. Shallow aquifers tend to have higher rates of recharge and higher rates of groundwater flow velocities (1-30 cm/yr and 1-100 m/yr, respectively) compared to deep aquifers (0.01-1 cm/yr and 0.1-1 m/yr, respectively) (Slomp and Van Cappellen 2004). Groundwater discharge from a coastal aquifer into a bay or estuary requires a hydraulic connection and a positive pressure gradient from the aquifer to the sea. Thus, SGD occurs mainly

as diffuse seepage from shallow unconfined aquifers along the shoreline, and offshore seepage at breaks in the confining layer of the deep aquifer or spring discharge (Burnett et al. 2008; Slomp and Van Cappellen 2004). Through these hydraulic connections, groundwater is a source of freshwater discharge into marine environments, including estuaries while oceans are a source of saltwater intrusion into coastal aquifers (Kroeger and Charette 2008; Zektser et al. 2007). Furthermore, groundwater may be a significant source of dissolved constituents from water-sediment interactions within the subterranean estuary and infiltration of contaminants into aquifers to oceans (Kroeger and Charette 2008; Longnecker and Kujawinski 2011; Zektser et al. 2007).

SGD comprises any flow of water from the seabed to the coastal ocean regardless of composition or driving force (Burnett 2003; Moore 2010; Santos et al. 2012b). SGD is thus defined irrespective of its composition (e.g., fresh or saline), origin (e.g., terrestrial or oceanic, shallow or deep), or driving force (e.g., hydraulic gradient, tidal forces, wave setup and pumping, sea level changes, salt fingering, bioirrigation, and more) (Martin et al. 2004; Michael et al. 2005; Oberdorfer et al. 1990; Robinson et al. 2007; Santos et al. 2012b). Taniguchi et al. (2002) conducted a comprehensive review of previous studies attempting to estimate the magnitude of SGD around the world. The review found SGD to be a nearshore process due to a systematic decrease in SGD rates as water depth increases (i.e., move further offshore) causing the pressure to increase from the weight of the water column, thus decreasing the hydraulic gradient and reducing, or limiting, SGD. Estimates of the role of SGD in the global water budget range over three orders of magnitude from a low of approximately 0.1% of riverine input to a high of approximately 10% of riverine input, with most estimates between 6-10% (Burnett et al. 2001; Slomp and Van Cappellen 2004; Taniguchi et al. 2002). Regardless of the wide range of

magnitudes, SGD may be both volumetrically and biogeochemically important to coastal and geochemical cycling of major and minor elements, including N and P, that may be strongly influenced by recirculation of seawater or direct discharge of groundwater into the sea (Burnett and Dulaiova 2003).

1.3 Nutrients

Nutrient input via SGD rivals riverine inputs in certain regions and may play a significant part in nutrient cycling and primary productivity in coastal oceans (Lee et al. 2012; Peterson et al. 2008; Slomp and Van Cappellen 2004; Stewart et al. 2018; Valiela et al. 1990; Wang et al. 2017). Additional nutrients from SGD to coastal oceans may be beneficial to the coastal ecology in some areas but may also be detrimental in other areas due to the extent and timing of transport or excessive nutrient inputs, i.e., eutrophication.

A better understanding of the extent and controls of inorganic and organic nutrient fluxes associated with SGD is necessary to inform coastal ocean functionality and its response to anthropogenic or natural stressors. However, the majority of SGD and groundwater nutrient studies only include the dissolved inorganic nitrogen (DIN) pool, nitrite + nitrate (NO_2^-+NO_3^-) and ammonium (NH_4^+), and the total dissolved nitrogen (TDN) but do not consider the remaining dissolved organic nitrogen (DON) (Longnecker and Kujawinski 2011; Sipler and Bronk 2015; Slomp and Van Cappellen 2004). Bioavailable dissolved N comprises DIN and a portion of DON. Under N-limiting conditions, common to many coastal zones, while the concentration of DIN is low, the concentration of DON may be high due to biologically recalcitrant forms and some of these biologically refractory DON can be photochemically transformed into bioavailable forms, NH_4^+or amino acids, upon exposure to solar radiation (Vahatalo and Jarvinen 2007). However, whether these reactions produce or incorporate

bioavailable N depends on the concentration of reactants. In particular, at high concentrations NH_4^+ is incorporated into DON and at low concentrations NH_4^+ is produced from DON.

The DON pool comprises thousands of different compounds. Longnecker and Kujawinski (2011) found that 15% to 30% of the dissolved organic matter (DOM) in groundwater was DON, a range higher than that observed in marine and riverine environments and freshwater from inland rivers. In general, deep oceans have the lowest mean concentrations of DON and the rivers have the highest, with concentrations and variability becoming progressively higher in coastal, then estuarine, and then riverine waters (Sipler and Bronk 2015). Except for the deep ocean and high nutrient low chlorophyll South Ocean, all environments contain ~58-77% of the bulk TDN pool as DON. Additionally, the carbon:nitrogen (C:N) ratio of DOM, of which DON is included, increases along a decreasing salinity gradient from 14 in surface oceans to 32 in rivers (Sipler and Bronk 2015). Previous time-series studies of DON in the Gulf of Mexico suggest a seasonal increase in DON concentration in late spring and summer (Lopez-Veneroni and Cifuentes 1994). Such increases in DON as the seasons warm have also been documented in other locations adjacent to the Atlantic Ocean, such as Chesapeake Bay, North Inlet, SC, and the English Channel, but no seasonal pattern has been found in areas that are generally oligotrophic, i.e., Pacific and Atlantic Ocean gyres (Sipler and Bronk 2015). Furthering our understanding of the composition of DOM, and DON specifically, in SGD will enable more holistic studies into the fate and reactivity of DOM compounds.

1.4 Study Area

The study area, located in the south-central coast of Texas, U.S.A., focuses on the highly disturbed, semi-arid Nueces Bay, a secondary bay adjacent to Corpus Christi Bay (CCB) in the Nueces Estuary system with no direct connection to the Gulf of Mexico. Nueces Bay falls within

a subsection of the Gulf Coast Aquifer (GCA) which consists of both confined and unconfined aquifers in a layered stratigraphy of alternating and intermixed lenses of silt, clay, sand, and gravel (Shafer 1968) forming the Chicot, Evangeline, and Jasper aquifers (Ashworth and Hopkins 1995; Waterstone and Parsons 2003). The Nueces Estuary system is microtidal with persistent southeasterly winds and is thus more sensitive to meteorological forcing (Diener 1975; Ockerman 2001). These persistent winds result in a generally well-mixed water column year-round. Sources of freshwater inflow to Nueces Bay include Nueces River and other surface runoff, return flows from municipal, industrial, agricultural sources, and direct precipitation (TDWR 1981). The head of Nueces Bay is surrounded by large areas of salt, brackish, and freshwater marshes (TDWR 1981). Nueces River, the primary source of surface water to the bay, flows along the southern edge of the Nueces Delta complex and discharges directly into the bay away from the delta (NBBEST 2011). Almost 98% of the river flows are controlled by the Choke Canyon Reservoir and Lake Corpus Christi dam system which provides water to the City of Corpus Christi, San Patricio County Municipal Water District, and others (NBBEST 2011). Due to these water demands, the lower part of the river has experienced extensive hydrological alterations (i.e., major modification and channelization redirecting flow away from the delta toward the lower bay) as a result of management practices. The implemented practices have changed the flow regime, ecology, and physical characteristics of the region. Previous studies have attributed reductions in riverine freshwater inflows of ~55% to the bay and ~99% to the delta to these alterations and drought (Bureau of Reclamation 2000). The bay experiences recurrent drought and flood conditions resulting in large seasonal salinity variations, with lows in the spring wet season and highs in the late summer dry season. Consequently, Nueces Bay is

often a reverse estuary with higher salinities in the delta than in the bay and higher bay salinities than the Gulf of Mexico (NBBEST 2011).

Potential sources of contamination and nutrients to the bay may include oil/gas industry, pipelines running across the bay, and agricultural land-use. Dry land crop agriculture (i.e., grain sorghum, corn, and cotton) and ranching activities dominate the area's land use (TDWR 1981). Nueces Bay and the areas of Nueces and San Patricio counties immediately surrounding the bay have been heavily developed for oil and gas extraction. The discharge of produced waters, which is often extremely high in dissolved solids and may contain elevated concentrations of radioactive substances, into coastal estuaries was a longstanding practice in Texas until a new rule, 40 CFR Part 435, passed in 1996 effectively banned such practices (D'Unger et al. 1996). As a consequence of brine disposal directly into the bay, bottom sediments may be enriched in Ur, Th and Ra.

1.5 Previous Studies

The Nueces River and Corpus Christi and Baffin Bays Basin and Bay Expert Science Team (NBBEST) submitted its environmental flow analyses and regime recommendations with findings that the Nueces Bay and Delta system is ecologically unsound due to the loss/alteration of habitat features and flow regimes required by indicator species and compromised nutrient elemental cycling and sediment loading (NBBEST 2011). The other bays within the Nueces River Basin (Corpus Christi Bay, Baffin Bay, Oso Bay, and Laguna Madre) were found to be ecologically sound though vulnerable to further decreases in inflows due to an already limited natural water supply. The now requisite modification and management of freshwater inflow regimes to Nueces Bay concentrates on surface water flows only and does not account for submarine groundwater flows that could also impact bay salinities and nutrient loading even

though numerous studies have identified groundwater discharge as the most important contributor of freshwater and nutrients to coastal embayments (Kroeger and Charette 2008). An attempt by Brock (2001) to develop a balanced nitrogen budget for Nueces Estuary (which includes Corpus Christi Bay, Oso Bay, and Nueces Bay) could not account for 30% of the exported nitrogen using known nitrogen inputs. Possible reasons for this imbalance are underestimates of nitrogen fixation and an additional unaccounted for contribution from SGD (Breier and Edmonds 2007). In neighboring Corpus Christi Bay, several instances of low salinity spikes have been recorded during monitoring of hypoxic events from May to September 2008. These rapid decreases in salinity were typically less than 30 minutes in duration and ranged from 0.8 to 12 ppt less than the baseline (Nelson and Montagna 2009). SGD provides one possible explanation for these occurrences. Additionally, a previous SGD study in Nueces Bay using radio-isotopes found very high dissolved Ra activities, as high as 1000 $dpm \cdot m^3$ for ^{226}Ra, in excess of riverine and bay bottom sediment sources indicating a large positive flux of groundwater into the bay (Breier and Edmonds 2007)).

1.6 Rational and Purpose

The unique approach of this research that applies geophysical and geochemical techniques (i.e., underwater geophysical imaging and geochemical tracers) to identify SGD sources in combination with biochemical methods will improve our comprehension of the impact groundwater-derived nutrients have on coastal ecosystem health. At a local/regional scale this research is important because regions within the Nueces Estuary have been shown to experience episodic hypoxia and harmful algal blooms (HABs) from spring-fall, causing adverse effects on benthic communities, fisheries, and human health, yet, up to date, the source(s) and fate of the nutrients fueling these events is not well understood. On a broader scale, the results of this

research will better inform SGD-derived nutrient fluxes in semi-arid, hydrologically stressed embayments. This new information will allow for updated management regimes and improved monitoring that comprises both surface-water and groundwater inflows as an integral part of the hydrologic and nutrient cycles. This research is important because it seeks to further the scientific understanding related to the bioavailability of nitrogen nutrients, which are a limiting factor of coastal primary productivity. Of these, groundwater contributions may account for approximately 50% of total DON inputs to coastal regions, beyond the traditional focus on the inorganic forms of nitrogen (Santos et al. 2009). Further understanding the role of SGD in nutrient transport to coastal waters will allow for more impactful monitoring and policy making regarding water management best practices and HAB monitoring and prediction.

The purpose of this research is to advance the scientific understanding of what role SGD and its associated nutrient fluxes play into the nutrient budget and health of ecologically unsound semi-arid estuaries using the south Texas Nueces Bay as a case study. In addition to quantifying seasonal and spatial SGD trends and the associated nutrient contributions, this study investigated the sources and fate of DON delivered to surface waters via SGD as a source of nitrogen nutrients that was previously unaccounted for. More specifically, this research aims to answer the following research questions:

1. What is the spatial and temporal extent of SGD in a semi-arid embayment across different hydroclimatic regimes?
2. What factors contribute to the spatial and temporal variations in SGD in a semi-arid coastal embayment?

3. What is the spatial and temporal variability of nutrient concentrations and SGD-derived nutrient fluxes in a semi-arid estuary across different hydroclimatic conditions?
4. How does SGD-derived N fluxes impact the nitrogen budget in a semi-arid estuary?
5. How does the concentration and chemical characterization of DOM in the groundwater/SGD differ from the surface water?

To address these questions, this dissertation has three main chapters that have led to three research journal papers. The first manuscript focuses on quantifying the spatial and temporal variability in SGD rates in a highly disturbed, semi-arid estuary. Geochemical tracer mass balances (radon and radium) and Darcy estimates using porewater and shallow and deep groundwater endmembers are used to constrain potential SGD variability (Chapter II, Douglas et al. 2020b). The second manuscript uses the SGD rates from the first study to calculate groundwater nutrient fluxes to the system and assess the contribution of SGD-derived N to the system's N budget. The inorganic and organic nutrient concentrations and water quality parameters are analyzed by principal component analysis and analysis of variance with a mixed effects model to assess the spatial and temporal variability across variable hydroclimatic conditions (Chapter III, Douglas et al. 2020a). The third manuscript focuses on the spatial and temporal variability of surface water and porewater dissolved organic matter molecular composition. The DOM molecular composition was determined from Orbitrap Fusion Tribrid mass spectrometry and surface water and porewater compositions are compared with principal components analysis and volcano plots (Chapter IV). Finally, a summary of the findings from this dissertation is provided in Chapter V.

CHAPTER II: SUBMARINE GROUNDWATER DISCHARGE IN AN ANTHROPOGENICALLY DISTURBED, SEMI-ARID ESTUARY

Published as: Douglas, A. R., D. Murgulet, R. Peterson (2020). "Submarine groundwater discharge in an anthropogenically disturbed, semi-arid estuary." Journal of Hydrology **580**: 124369.

Graphical Abstract 2.1

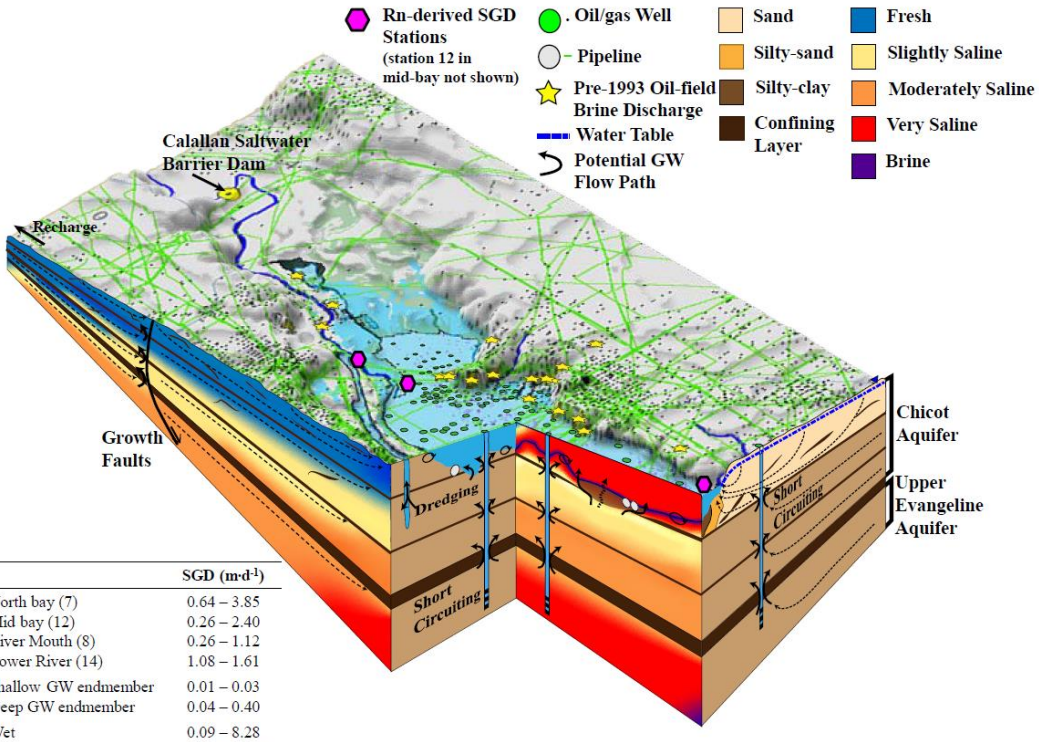

METHOD		SGD ($m \cdot d^{-1}$)
Rn-derived (average terrestrial groundwater endmember)	North bay (7)	0.64 – 3.85
	Mid bay (12)	0.26 – 2.40
	River Mouth (8)	0.26 – 1.12
	Lower River (14)	1.08 – 1.61
Radium	Shallow GW endmember	0.01 – 0.03
	Deep GW endmember	0.04 – 0.40
Local Darcy Estimates	Wet	0.09 – 8.28
	Dry	-0.02 – 7.84

Abstract

Quantification of submarine groundwater discharge (SGD) remains a challenge due to its large spatial and temporal variability exacerbated by natural heterogeneity (e.g., climatic conditions and hydrogeologic settings) and anthropogenic disturbances (e.g., dredging, oil/gas extraction, and oil-field brine discharges). This study investigates the spatial and temporal variability of SGD during different hydroclimatic conditions in a semi-arid, anthropogenically

disturbed estuary using Darcy's law (i.e., fresh/terrestrial SGD) and radon (^{222}Rn, total SGD) and radium (^{226}Ra, saline/recirculated SGD) isotope mass balances. Continuous electrical resistivity imaging and ^{222}Rn surveys revealed potential subsurface influences on SGD with the highest SGD rates in areas with sandier substrates and near transitions from low hydraulic conductivity to higher hydraulic conductivity bottom sediments. Darcy estimates ranged over two orders of magnitude and were slightly higher following the flooding recession (0.09–8.28 $m \cdot d^{-1}$) than following a period of low precipitation (−0.02–7.84 $m \cdot d^{-1}$). Mobile continuous ^{222}Rn estimates (0.79–1.81 $m \cdot d^{-1}$) support higher and more variable SGD rates, similar trends to those previously reported from time-series ^{222}Rn measurements (0.13–3.85 $m \cdot d^{-1}$ across seasons). Radium-226 derived SGD ($1.3 \times 10{-}2–2.7 \times 10{-}2$ $m \cdot d^{-1}$ using the average groundwater endmember) fall short of ^{222}Rn-derived SGD due to inability to account for radium tracer reactivity within the sediment. However, local Darcy estimates agree well with the range of ^{222}Rn, likely due to the steeper gradients near shore. Radium activity ratios and SGD rates reflect mixing of shallow and deep groundwater beneath the bay, likely due to anthropogenic disturbances with a greater influence from deep groundwater 3–6 months following major precipitation events. This study strongly suggests that semi-arid systems receive significant SGD, which in highly anthropogenically disturbed systems are derived from both shallower and deeper groundwater flowpaths and lag the climatic conditions by weeks (shallow inputs) and months or longer (deeper inputs).

2.1 Introduction

The interaction between groundwater and surface water occurs at a range of spatial and temporal scales and is highly variable depending on meteorological, fluvial, geological, and

anthropogenic processes. Various studies have demonstrated that submarine groundwater discharge (SGD) can constitute an ecologically significant source of nutrients (Slomp and Van Cappellen 2004; Urquidi-Gaume et al. 2016) and metals (Charette and Buesseler 2004; Montluçon and Sañudo-Wilhelmy 2001; Rodellas et al. 2014) to estuaries and embayments. SGD may contribute to surface water quality degradation and mobilization of potentially toxic contaminants like nutrients, heavy metals, radionuclides, and organic compounds from the sediment. Thus, an improved understanding of SGD rates into coastal systems and corresponding groundwater solute fluxes is necessary to develop comprehensive biogeochemical budgets and management practices.

SGD is defined as any flow of water across the sediment-water interface, irrespective of its composition (e.g., fresh or saline), origin (e.g., terrestrial or oceanic), or driving force (e.g., terrestrial hydraulic gradients or tidal pumping) (Burnett et al. 2008; Moore 2010; Santos et al. 2012b). Yet, individual SGD measurement techniques may not account for all discharge components. For example, regional estimates based on Darcy's law account for terrestrial-derived SGD based on the hydraulic gradient between the aquifer and surface water but few account for recirculated seawater (Li et al. 2009), whereas estimates based on a radium mass balance approach (Charette et al. 2003) may provide a reasonable estimate of saline, recirculated SGD but fail to represent lower salinity SGD due to the salinity dependence of dissolved radium (Mulligan and Charette 2006). Contrastingly, a radon mass balance approach may account for total SGD (i.e., fresh and saline; terrestrial and recirculated) as radon is non-reactive and does not behave differently in different salinity regimes (Mulligan and Charette 2006). Thus, a combination of techniques is necessary to account for different components of SGD.

Quantification of groundwater fluxes is difficult due to significant spatial and temporal heterogeneity and the inherent logistical complications of measuring a dispersed flux of water. Efforts to identify and quantify SGD have relied upon several techniques: direct measurements using seepage meters (Lee 1977; Sholkovitz et al. 2003; Taniguchi and Fukuo 1993); electrical resistivity profiling to identify subsurface seepage faces and/or porewater salinity (Bighash and Murgulet 2015; Dimova et al. 2012; Stieglitz et al. 2008); thermal imaging of discharge plumes (Danielescu et al. 2009; Johnson et al. 2008; Kelly et al. 2013); groundwater flow modeling (Murgulet and Tick 2016; Wilson 2005); and mass balance models using geochemical tracers such as radium (Ra) (Rodellas et al. 2014), radon (Rn) (Burnett and Dulaiova 2003; Urquidi-Gaume et al. 2016), and methane (CH_4) (Breier et al. 2010). However, each of these techniques has varying spatial and temporal integration scales to consider in the final SGD estimates (Mulligan and Charette 2006). Few studies have applied a combination of geochemical (Rn and Ra isotopes) and geophysical (electrical resistivity) methods (Breier et al. 2005; Stieglitz et al. 2008; Swarzenski et al. 2006a) with theoretical estimates to study SGD (Mulligan and Charette 2006; Santos et al. 2009).

It is likely that the variability of SGD can be caused by spatial changes in estuarine bottom sediment type and anthropogenic disturbances (e.g., dredging, oil/gas pipelines, oil-field brine discharges) in conjunction with temporal changes in hydrological conditions (e.g., drought vs. flood). Some studies have: 1) investigated SGD in arid and semi-arid estuaries with high evaporation rates and seasonally variable precipitation (Boehm et al. 2006; Breier and Edmonds 2007; El-Gamal et al. 2012; Murgulet et al. 2018; Shellenbarger et al. 2006; Urquidi-Gaume et al. 2016), or 2) used both radon (i.e., total SGD) and radium (i.e., saline SGD) methods (Baudron et al. 2015; Johnson et al. 2008; Mulligan and Charette 2006; Sadat-Noori et al. 2015;

Swarzenski et al. 2007b) to better constrain SGD. Furthermore, these studies were mainly performed in higher permeability and sandier environments with minimum disturbances from anthropogenic activities. Some of these studies show generally good agreement (i.e., on the same order of magnitude and/or overlapping ranges) between the radon and radium SGD estimates (Baudron et al. 2015; Johnson et al. 2008; Sadat-Noori et al. 2015; Swarzenski et al. 2007b) and indicate that saline recirculated seawater accounts for most SGD, while just one study suggests that a larger fresh, terrestrial SGD component is necessary to account for the greater radon estimate (Mulligan and Charette 2006).

A previous study of SGD in such an estuary (Nueces Bay) by Breier and Edmonds (2007) using radium mass balance methods found that SGD required to balance a ^{226}Ra budget was 160% of river inflows. Murgulet et al. (2018) report SGD rates 1 – 3 orders of magnitude greater (0.13 – 3.85 $m \cdot d^{-1}$) than Breier and Edmonds (2007) ($5x10^{-3}$ $m \cdot d^{-1}$) using stationary continuous radon methods, which further suggest high SGD fluxes in Nueces Bay and indicate a possible underestimation by the radium method. We hypothesize that in a system with a high occurrence of dredging, oil/gas drilling, and buried pipelines, SGD may be locally enhanced by contributions from deeper aquifers along conduits created by these disturbances below the estuary (i.e., short circuiting). Furthermore, prolonged oil-field brine discharges to a system such as this would influence the fate of reactive groundwater tracers (i.e., radium).

This study aims to improve understanding of spatial and temporal variability of SGD in a highly anthropogenically disturbed, semi-arid estuary that is dominated by low permeability sediments (i.e., fine silt to clay sediment), seasonally variable precipitation, high evaporation rates, and low freshwater inflows. We present and compare geophysical surveys, hydrogeological estimates, and geochemical tracer data collected quarterly over two years to

estimate SGD behaviors during different climatological conditions and in different sedimentary environments. We use radon and radium as conservative and non-conservative tracers, respectively, to investigate the potential influence of historic oil-field brine discharges on SGD estimates.

2.2 Methods

2.2.1 Study Area

The study area, located in the south-central coast of Texas, was chosen because of its many anthropogenic disturbances and altered flow regimes that have contributed to its classification as ecologically unsound (NBBEST 2011). Nueces Bay is a secondary bay adjacent to Corpus Christi Bay (CCB) within the Nueces Estuary system and has no direct connection to the Gulf of Mexico (Figure 2.1). Nueces Bay is ~75 km2 in area with an average depth of 0.7 m and has the highest concentration per area of oil/gas wells and pipelines (Figure 2.2) of the south Texas bays (Breier et al. 2010; RRC 2018). Oil-field brines produced during oil/gas extraction activities were discharged directly to the bay (Figure 2.1C) from the turn of the century until the practice was banned in the mid-1990's (D'Unger et al. 1996). These oil-field brines were often extremely high in dissolved solids (which may exceed 100 parts per thousand) and contained elevated concentrations of metals and radioactive substances. The sediments in the vicinity of the discharges were found to contain high concentrations of oil-field brine contaminants. Additionally, oyster shell dredging occurred in the open bay prior to 1972, which further disturbed the bay sediments (Pulich Jr. 2007). Consequently, Nueces Bay has some of the most disturbed sediment beds in Texas.

The Nueces Estuary is a microtidal system, with a reported mean daily tidal range of 0.1 m to 0.15 m (Diener 1975; NBBEST 2011). Given the shallow, microtidal characteristics, water

level fluctuations in this bay are controlled primarily by wind (NBBEST 2011). Average monthly wind speeds range from 17 to 18 km·h-1 with a southeasterly dominant wind direction (Ockerman 2001). These persistent winds result in a generally well-mixed water column and increased turbidity due to sediment resuspension. The area is characterized as dry to sub-humid with possible tropical disturbances during summer and fall (Shafer 1968). Annual average precipitation and evaporation rates are around 76 and 145 cm, respectively (Ockerman 2001). Sources of freshwater inflow to Nueces Bay include runoff (i.e., Nueces River, lateral flow, and return flows from municipal, industrial, and agricultural sources) and direct precipitation (TDWR 1981). While the Nueces River is the primary source of freshwater to Nueces Bay, low precipitation rates within the watershed as well as hydrologic alterations (i.e., dams and diversions on the river; Figure 2.1B) lead to typically low riverine discharge into the bay. As a result, the bay receives low amounts of riverine nutrients while experiencing increased salinity levels (Longley et al. 1994). Murgulet et al. (2017) present more information on the climatology of the area, including fluctuations of annual precipitation and streamflow. Entering the study period (December 2014 through August 2016), the state of Texas was experiencing one of the strongest multi-year (4 – 5 years) droughts on record (Murgulet et al. 2017; TWDB 2017), which ended in spring 2015 with a large flooding event (Figure 2.3). Consequently, our study captures the progression from extreme dry conditions to extreme wet conditions (rising limb and peak flood) to post-flood recession, and back to normal conditions (Murgulet et al. 2018).

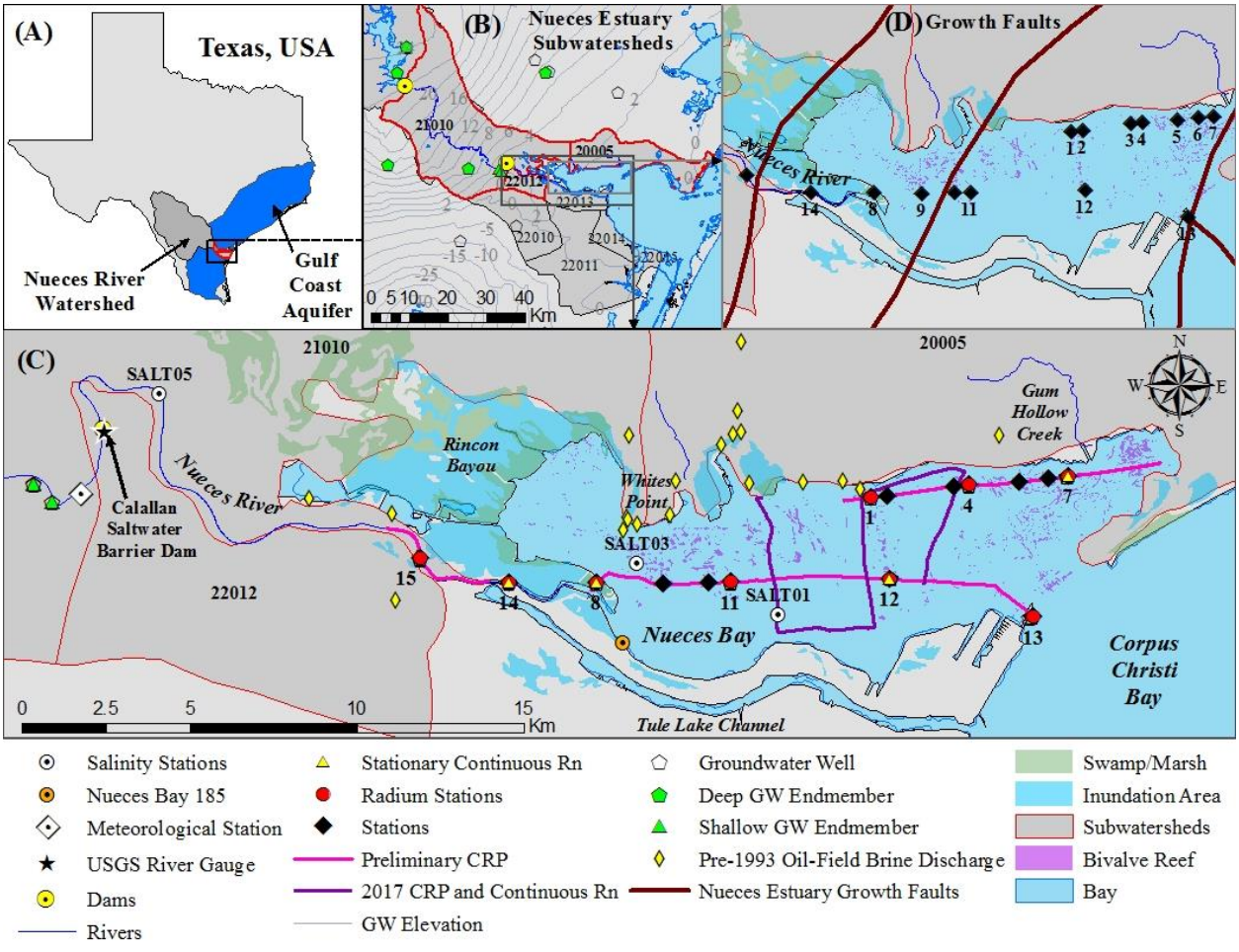

Figure 2.1: Study site. (A) Gulf Coast Aquifer and Nueces River Watershed within Texas, USA. (B) Nueces Estuary Subwatersheds used in the TWDB freshwater inflow estimates (TWDB 2018), dams on the Nueces River, groundwater elevation contours (m above mean sea level) from TWDB Groundwater Database Reports for wells with average screened intervals <245 m below ground surface (bgs) (TWDB 2017), and sampled groundwater (GW) wells. (C) Meteorological and hydrological monitoring stations, surface water and porewater sampling stations, stationary continuous ^{222}Rn stations, historic oil-field brine discharge outfalls (D'Unger et al. 1996), preliminary CRPs, and 2017 CRP with continuous mobile ^{222}Rn. (D) Surface water sampling stations in relation to growth faults as generalized by Brown Jr et al. (2004) from 3-D seismic and well-data analyses. Figure best viewed in color.

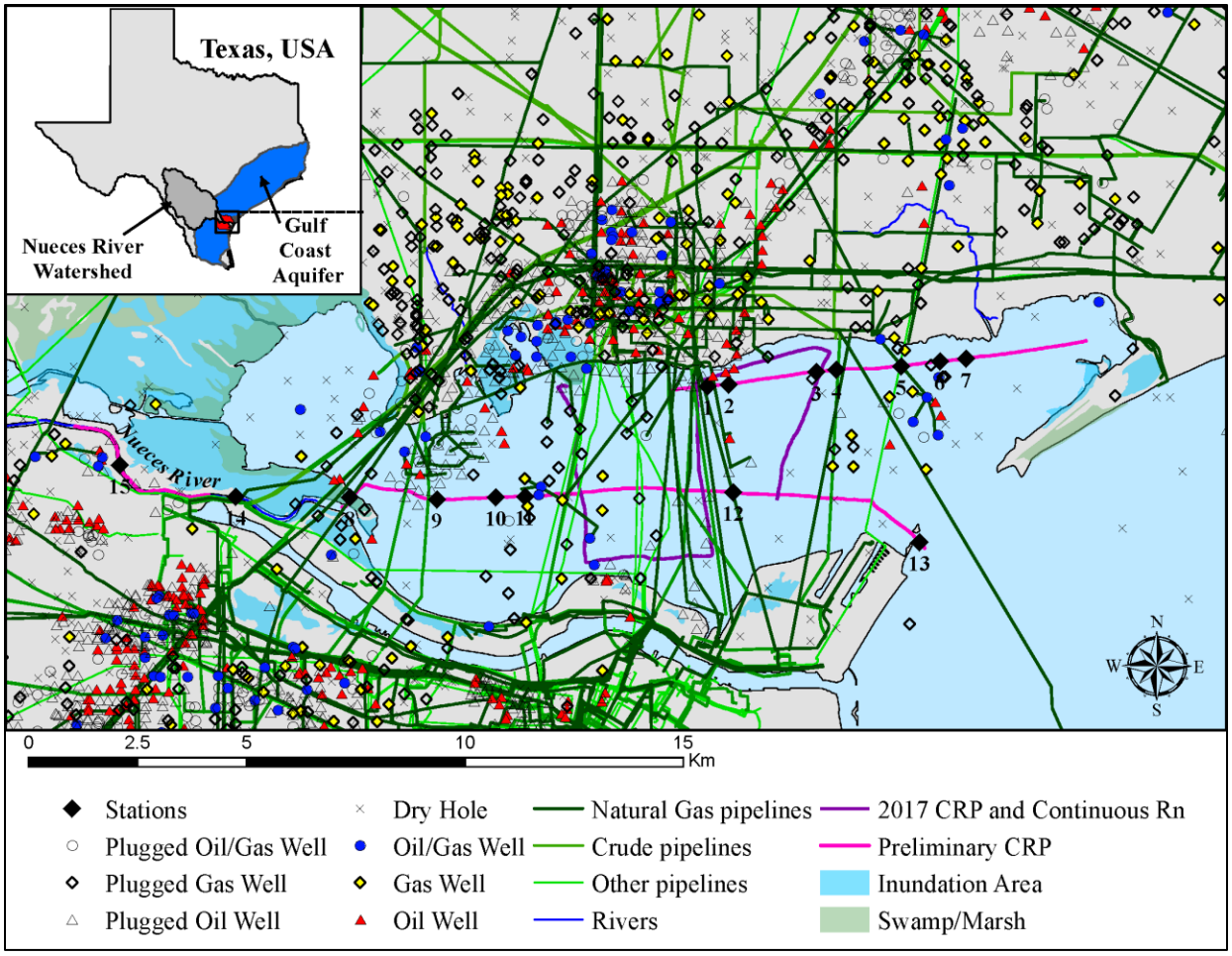

Figure 2.2: Locations of oil and gas wells and pipelines in relation to sampling stations and CRP transects. All oil and gas well and pipeline data was provided by the Railroad Commission of Texas and accessible through the Public GIS Viewer (RRC 2018).

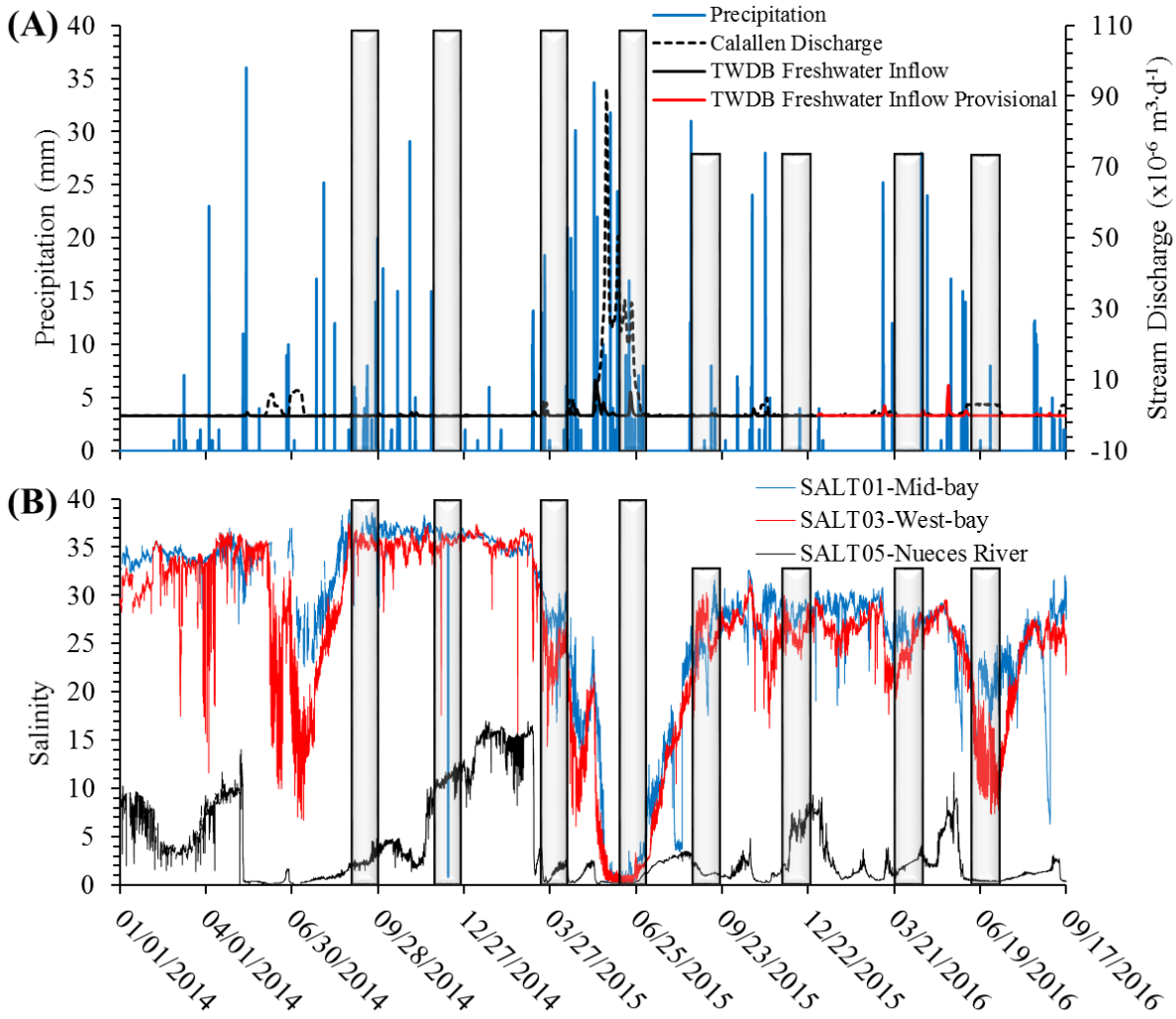

Figure 2.3: (A) Total daily Nueces River discharge (dashed black line) at Calallen, TX (USGS gauge 08211500), TWDB Freshwater Inflow (solid black lines), total daily precipitation (mm, blue line) at the Corpus Christi Meteorological Station #7 on Nueces River (in close proximity to the saltwater barrier dam). Provisional TWDB Freshwater Inflow data (solid red line) includes TxRR modelled streamflow, but not diversions and return flows as TWDB had not made this data available at time of publication. (B) Conrad Bluchar Institute salinity stations (**Figure 2.1C**): SALT01 (in the middle of the bay, blue line), SALT03 (in close proximity to the Nueces

River mouth, red line), and SALT05 (in Nueces River downstream of the saltwater barrier dam, black line). Sampling events are indicated by vertical grey bars.

Nueces Bay falls within a subsection of the Gulf Coast Aquifer (**Figure 2.1A**), which is described as a leaky artesian aquifer in a layered stratigraphy of alternating and intermixed silt, clay, sand, and gravel lenses forming the Chicot, Evangeline, and Jasper aquifers (Ashworth and Hopkins 1995; Shafer 1968; Waterstone and Parsons 2003). Nueces Bay and the surrounding systems are generally in direct contact with the Chicot aquifer, extending 366 m below ground surface (bgs), which consists of an alluvial formation overlying the Beaumont and Lissie formations (Chowdhury et al. 2004; Mace et al. 2006). Additionally, a considerable amount of water discharges upward from the Evangeline, extending 793 m bgs, into the Chicot aquifer in southern Texas. Most of south Texas is underlain by brackish to saline groundwater at depths <150 m bgs with areas of high salinity occurring locally (Kreitler 1993). Hydraulic conditions generally dictate that groundwater flows toward the river and the north shore and eventually discharges into the bays and estuaries (Bighash and Murgulet 2015; Breier et al. 2010; Nyquist et al. 2008). Bay surface sediments are predominantly sandy to silty-sand across the north-bay, silty-sand at the Nueces River mouth, clayey-sand to clayey-silt throughout the west-bay and across the south-bay, and silty-clay in the middle of the bay and the lower Nueces River (Shideler et al. 1981).

2.2.2 Sample Collection

The study was designed to investigate spatial and temporal differences in SGD. Surface water, porewater, and terrestrial groundwater were sampled according to methods outlined in Murgulet et al. (2018). Briefly, samples were collected quarterly from September 2014 through

July 2016 from 13 to 15 stations selected from continuous resistivity profiles (CRPs) to characterize the different environments in the bay. For the purpose of this paper, the following station classifications are used for presenting and discussing results: north-bay: 1-7; river: 14, 15; west-bay: 8-11; mid-bay: 12; and CCB: 13 (**Figure 2.1**). Water column samples were collected from approximately 0.2 m above the sediment-water interface. Porewater samples (n = 25) were extracted using an AMS retract-a-tip piezometer from depths ranging from 0.5-2 m below the sediment-water interface. Ten groundwater wells with varying screened depths from 2.2 – 91.5 m below ground surface were sampled in May 2015 and October 2015 to characterize the shallow (<10 m, n = 4) and deep (>15 m, n = 6) groundwater endmembers (**Figure 2.1B**). The hydraulic gradient of the regional aquifer was inferred from groundwater level data mined from the Texas Water Development Board's Groundwater Database (GWDB).

All porewater and groundwater samples for ^{222}Rn analysis were collected in 250 mL gas-tight borosilicate bottles filled from the bottom and allowed to overflow for one volume before being sealed with no headspace. Rn-222 measurements were conducted with a Durridge RAD-7 following the WAT250 protocol (Durridge Company Inc. 2017) within 2 days of sample collection to prevent loss due to decay (half-life 3.8 days) and decay corrected to time of sampling.

A total of 68 surface water samples were measured for ^{224}Ra and ^{226}Ra from 9 stations (north-bay: 1, 4, 7; river: 14, 15; west-bay: 8, 11; mid-bay: 12; and CCB: 13) and 8 sampling events. Large volume samples (50 – 100L) were filtered in the field through a 1μm and 0.5μm filter sequence to remove suspended sediments. Radium was extracted by passing through ~15 g of acrylic fibers impregnated with MnO_2 (Dimova et al. 2007; Kim et al. 2001; Sun and Torgersen 1998). These fibers were analyzed for ^{224}Ra (half-life 3.6 days) within 3 days of collection on a

Durridge RAD-7 following Kim et al. (2001) and Dimova et al. (2007). Fibers were then sealed for >21 days to reach secular equilibrium before running for ^{226}Ra (half-life 1600 years) on a Durridge RAD-7 following Kim et al. (2001) and Johnson et al. (2008). Extraction efficiencies of Mn fibers were determined to be 98% for ^{224}Ra and 96% for ^{226}Ra by processing random samples through a second Mn cartridge. Analytical errors, determined from RAD-7 counting statistics, were less than 20% for ^{224}Ra and 8% for ^{226}Ra at the 95% confidence interval.

2.2.3 Continuous Resistivity Profiles

Electrical resistivity (ER) measurements were conducted using a Marine Supersting R8-IP resistivity meter (Advanced Geosciences 2016) with a 112 m cable consisting of 56 graphite electrodes spaced 2 m apart which has the capacity to image to a depth of ~ 22.5 m (for more detail see Douglas et al. 2017; Murgulet et al. 2016). Surveys were conducted on calm water with boat speeds <4 $km \cdot hr^{-1}$ to minimize noise. GPS data and depth soundings were recorded simultaneously within the instrument using a Lowrance LMS-480M with an LGC-2000 GPS Antenna while a YSI Professional Plus data sonde recorded continuous water column salinity and temperature. These field measurements of surface water salinity and thickness of the water column below the electrode array are applied in the inversion to constrain the results so that changes in surface water conditions do not affect the resistivity model results for the sediment underlying the electrode array (Bighash and Murgulet 2015; Nyquist et al. 2008). The system allows imaging of both the water column and the underlying sediments when the cable is deployed at the water surface. Two CRPs were measured in early September 2014 for a preliminary exploration of Nueces Bay from the river to Corpus Christi Bay and across the north-bay (**Figure 2.1C**). At the time, accessibility was restricted in the river and throughout the bay due to lower than normal water levels during the drought. As such, the lower Nueces River

was not surveyed until February 2015 when water levels had risen in the river. Sampling stations for geochemical sampling were selected from anomalously low or high resistivities appearing in the inverted resistivity images and with consideration for the geologic environments within the bay. Most selected stations correspond to locations with potential for high SGD, but control stations with the least potential for SGD occurrence were also selected.

An additional survey was conducted in May 2017 focusing on north-south transects (**Figure 2.1C**). This CRP was performed in conjunction with a spatial survey of water quality parameters (i.e., temperature, salinity, dissolved oxygen (DO), and pH) and radon activity (see section 2.2.5).

2.2.4 Darcy Discharge Rate Estimates

Darcy's law estimates of "local" shallow, brackish SGD were derived using water level and hydraulic conductivity data from four groundwater monitoring wells (<10 m depth) located near the Calallen saltwater barrier dam. Standard slug-in tests with the Hvorslev method (1951) were conducted at the monitoring wells with a pressure data logger collecting data at 1 Hz to estimate horizontal hydraulic conductivity of the shallow aquifer sediments. As all four shallow wells were brackish, the point-water heads were converted to freshwater heads (Fetter 2001) before hydraulic gradients were determined. Darcy's law estimates of "regional" deep freshwater SGD were determined from TWDB monitoring wells water level data from 2014, 2015, and 2016. Only wells less than ~245 m (800 ft) deep (i.e., Chicot aquifer) were included in the construction of groundwater elevation contours (**Figure 2.1B**) and calculation of hydraulic gradients. The Chicot Aquifer has been found to have average horizontal hydraulic conductivities of 14.2 $m \cdot d^{-1}$ (range: 9.8 $m \cdot d^{-1}$ to 19.2 $m \cdot d^{-1}$) within 121 km of the coast, with the highest conductivities ($\overline{x}$: 18.6 $m \cdot d^{-1}$) occurring within 80 km of the coast (Young et al. 2016). A specific yield (i.e.,

effective porosity) of 0.05 for the Chicot Aquifer (Young et al. 2016) was applied to convert from specific discharge to groundwater velocity.

2.2.5 ^{222}Rn-derived SGD

Time-series ^{222}Rn measurements at four locations within the study area (**Figure 2.1**) presented by Murgulet et al. (2018) are used for spatial analysis and temporal comparison with the Darcy and ^{226}Ra-derived SGD estimates in the current study. Given the spatial heterogeneity observed in the time-series SGD estimates, continuous mobile ^{222}Rn measurements were conducted in May 2017. Surface water (~0.5 m below the air-water interface) was continuously pumped to an air-water exchanger ("RAD Aqua") by a peristaltic pump while a closed air loop continuously pumped the gas through three RAD-7 radon detectors connected in parallel. The use of multiple detectors connected in parallel yields increased spatial resolution and greater precision constraining spatial heterogeneity of SGD. The ^{222}Rn activities were integrated every 10 minutes (or one measurement every ~660 m at a survey speed of 4 km·hr^{-1}) and were used to estimate SGD fluxes following Dulaiova et al. (2005) and Smith and Robbins (2012). Resulting ^{222}Rn activities and CRPs were mapped in ArcGIS for visual analysis.

Continuous mobile ^{222}Rn measurements were used in a mass balance to estimate SGD as described by Dulaiova et al. (2005); Murgulet et al. (2018); Smith and Robbins (2012). Briefly, the model accounts for radon sinks (atmospheric evasion, radioactive decay, and mixing with lower activity waters offshore) and sources (sediment supported ^{222}Rn and ^{226}Ra supported ^{222}Rn) over time, assigns any further source of radon mass to SGD inputs, and converts to SGD fluxes by dividing by the radon activity in the advecting fluid. Wind speed data were obtained from the Conrad Blucher Institute monitoring station 185 Nueces Bay. The sediment supported ^{222}Rn activities and groundwater endmember activities from (Murgulet et al. 2018) were used for

the sediment supported ^{222}Rn correction and conversion to advective fluxes, respectively. For the continuous mobile ^{222}Rn survey in July 2017, ^{226}Ra samples (40 – 50 L) collected at high and low tides during a 24-hour stationary monitoring event that month were used to correct for in-situ production of ^{222}Rn.

2.2.6 Ra-derived SGD

To estimate SGD from ^{226}Ra observations, we use an estuarine mass balance to determine the excess inventory of ^{226}Ra (attributed to groundwater flux) in the bay. This mass balance includes all sources of radium other than groundwater such as tidal exchange, rivers, and desorption from riverine suspended sediments (Moore 1996). In this study, excess ^{226}Ra ($^{226}Ra_{ex}$ [dpm·d^{-1}]) is expressed mathematically as:

$$^{226}Ra_{ex} = \left(\frac{(^{226}Ra_{NB} - ^{226}Ra_{CCB}) \times V_{NB}}{T_w}\right) - \left(^{226}Ra_R \times Q_R\right) - \left(^{226}Ra_{des} \times TSS \times Q_R\right) \quad (1)$$

where $^{226}Ra_{NB}$ is the average activity in Nueces Bay (dpm·m^{-3}), $^{226}Ra_{CCB}$ is the activity in Corpus Christi Bay waters (i.e., the offshore end-member, dpm·m^{-3}), $^{226}Ra_R$ is the Nueces River activity (i.e., the nearshore end-member, dpm·m^{-3}), Q_R is the integrated Nueces River discharge for the week prior to sample collection (m^3·d^{-1}), $^{226}Ra_{des}$ is the maximum desorption of radium from riverine suspended sediments transported with freshwater (dpm·g^{-1}), V_{NB} is the volume of Nueces Bay (m^3), T_w is the residence time calculated from the apparent radium water mass ages (d), and TSS is the total suspended sediment concentration (g·m^{-3}) in the river (Charette et al. 2001; Swarzenski 2007). After accounting for all possible sources of ^{226}Ra, it is assumed that the excess activity from equation (1) is the result of SGD. Thus, using ^{226}Ra activities from the groundwater wells in the vicinity of Nueces Bay, SGD (m^3·d^{-1}) is calculated as:

$$SGD = \frac{^{226}Ra_{ex}}{^{226}Ra_{GW}} \quad (2)$$

Discrete ^{224}Ra and ^{226}Ra measurements across the bay were used to calculate apparent water mass ages (Moore 2000). To calculate the apparent radium water mass age, or the relative time that has passed since the radium first entered the system (T_W), we used the activity ratios (AR) of the short-lived ^{224}Ra to the long-lived ^{226}Ra (^{224}Ra/^{226}Ra) isotopes (Johnson et al. 2008):

$$T_w = \frac{ln\left(\frac{AR_{obs}}{AR_{gw}}\right)}{(\lambda_{224}-\lambda_{226})} \quad (3)$$

where AR_{obs} is the activity ratio of the samples of interest, AR_{gw} is the initial groundwater source activity ratio, and λ_{224} and λ_{226} are the decay constants for ^{224}Ra and ^{226}Ra, respectively. This equation assumes: 1) surface water Ra activities and ARs will be lower than the Ra source (i.e., groundwater or Ra-bearing sediments) but higher than offshore waters, and 2) the Ra source is constant with respect to ARs (Knee et al. 2011).

Radium desorption experiments were conducted to determine the activity of ^{226}Ra released from riverine suspended sediments upon entering the estuary using representative riverine sediment samples (i.e., 0 – 10 cm depth in the sediment column) from just downstream of the salt-water barrier dam near Calallen, TX. Sediment samples were collected when the river had been overflowing the dam for a week and salinities approximately 50 m downstream of the dam were 0.78. High salinity bay water (31.1) was collected, filtered through Whatman GF/F filters to remove suspended solids, and processed through MnO_2 fibers to remove dissolved radium. Known masses of dried sediments (~15 mg and ~870 mg) were added to a volume of radium-free filtered bay water (3 L) to represent total suspended solid (TSS) concentrations in the study area. Sample solutions were then stirred and placed on a shaker table for 45 minutes before extracting the desorbed radium by passing the solution through MnO_2 fibers and processing as described in section 2.2. Total ^{226}Ra activity was normalized to the sediment mass and then multiplied by the sediment flux from the river. Typical TSS concentrations in Nueces Bay range

from 5 – 292 $mg \cdot L^{-1}$ (Nicolau and Hill 2013). For the most conservative estimates of radium desorption, the experiments were performed for the highest (~290 $mg \cdot L^{-1}$) previously observed TSS concentrations at salinities of approximately 30, 25, 20, 15, 10, and 5. The desorption activities ranged from 1.2 $dpm \cdot g^{-1}$ (salinity 30) to 2.3 $dpm \cdot g^{-1}$ (salinity 20). The maximum desorption activity corresponding to the salinity of each sampling event was applied to the calculation (Eq. 1).

An estimate of total surface inflow to Nueces Bay serves as the streamflow term (Q_R) as the USGS streamflow gauge for Nueces River at Calallen, TX (08211500), being upstream of dams, diversions, and municipal intakes, significantly overestimates river discharge to the bay. Freshwater surface inflow to Nueces Bay was retrieved from the TWDB's Water Data for Texas coastal freshwater inflow estimates for watersheds 21010, 22012, and 20005, shown in **Figure 2.1B and C** (Fernando 2017; TWDB 2018). The region north of the bay encompasses approximately half of the 20005 watershed. Thus, half of the inflow estimates for this watershed were applied to the sum of watersheds 21010 and 22012. **Table 2.4** shows the values of each term used for estimating SGD to Nueces Bay in this study using the ^{226}Ra mass balance.

2.3 Results and Discussion

2.3.1 Continuous Resistivity Profiles (CRP)

2.3.1.1 Preliminary CRPs

Exploratory CRPs conducted in September 2014 for the northern and southern areas of the bay (**Figure 2.1C**) reveal several locations with resistivity anomalies. Average resistivity for freshwater saturated sediments like clay and sandy loam are typically 38 Ω-m and 51 Ω-m, respectively (Nyquist et al. 2008). The range of resistivities measured during the CRPs (0.10 – 10 Ω-m) is suggestive of sediments saturated with high salinity water (Murgulet et al. 2016), an

observation supported by porewater salinities ranging from 23.6 to 40.8 ($\overline{x}$ = 32.9, n = 26) over the study period. Vertically elongated features of very low resistance (0.1 – 0.24 Ω-m) within mostly higher resistance sediments (3.2 – 10 Ω-m) occurred at stations 1, 2, and 4 along the northern transect and station 12 along the southern transect (**Figure 2.4 A-B and E-F**). From CRP image interpretation, these abrupt, small-scale anomalies are not consistent with SGD plumes as outside these locations most of the subsurface within the imaged transect does not change significantly and is comprised of more resistant sediments.

The observed abrupt changes in resistance were found to correspond well with the location of some buried oil and gas pipelines (**Figure 2.2**). The resistivity signature may differ depending on the pipe material (i.e., steel will have lower resistivity), the composition of the product within the pipeline, and the saturation status (i.e., filled or empty). However, these types of bottom sediment disturbances, such as sediment dredging and infill, likely create exchange conduits between aquifers and bay waters by short circuiting confining layers as indicated by these preliminary CRPs. Other changes in resistivity that occur across a broader area and are confined to the shallower portions of transects correspond to oyster reefs (confirmed by field observations; **Figure 2.4 B-C and D-E**), which settle on harder substrates when compared to surrounding softer, more conductive sediments (Twichell et al. 2010) and may influence bay chemistry and circulation patterns (Murgulet et al. 2018). The highest resistivities measured in the subsurface were below the navigation channel crossing between Nueces and Corpus Christi Bays. Emplacement of bridge pilings and cutting deep into or removing the underlying low permeability/confining sediments through dredging of bottom sediments could facilitate the flow of groundwater to the offshore water column (Burnett et al. 2006; Santos et al. 2008b) such as at stations 13 (**Figure 2.4 E-F**).

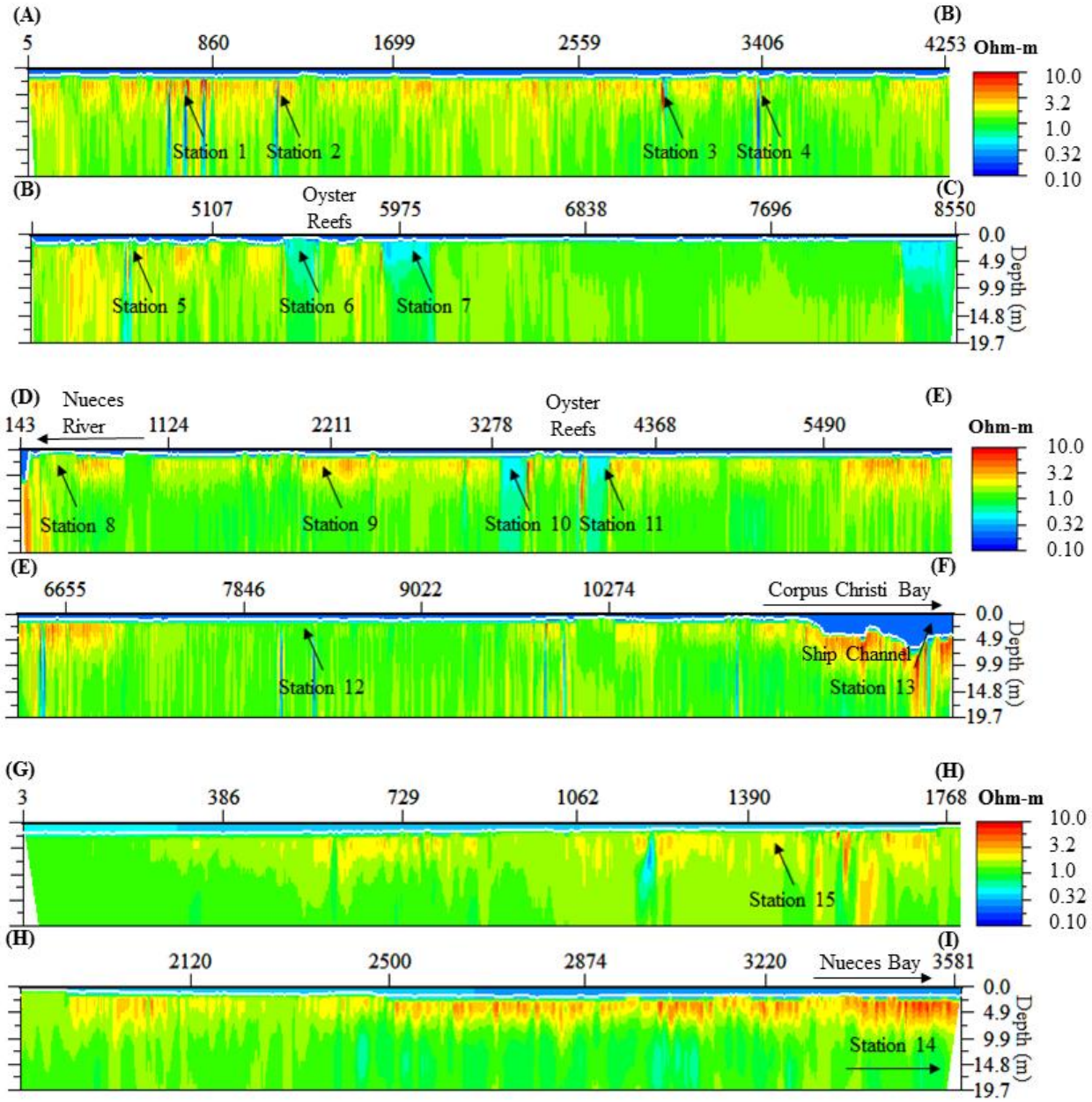

Figure 2.4: Continuous resistivity profile for Transect 1 along the north shore (A-B, B-C), Transect 2 from Nueces River mouth to the ship channel in Corpus Christi Bay (D-E, E-F), and Transect 3 along the lower Nueces River (G-H, H-I). Warm colors indicate areas of higher electrical resistivity (lower electrical conductivity) and cold colors indicate areas of lower electrical resistivity (higher electrical conductivity).

The lower Nueces River is underlain by a few meters of more resistant sediments with increasing thickness toward the bay (**Figure 2.4 G-H and H-I**). Two sampling stations were selected in this region, one upstream where the resistive layer is more continuous (station 15) and one in a slightly more heterogeneous resistivity area downstream (station 14). Laser diffraction sediment grain size analysis shows the percent sand in the sediments decreases downstream from predominantly sand or sand-silt-clay (i.e., more resistive) to clayey silt (i.e., less resistive) in the river mouth (Pena 2017). Thus, the higher resistivity in the downstream stretch is likely not explained by the difference in sediment types but rather by changes in pore fluid salinity toward a fresher condition (station 14 salinity 23.6 – 31.5; station 15 salinity 38.7 – 40.7). This difference has implications related not only to different chemistry of SGD inputs to the river and bay, but a possible indication of more significant fresher groundwater discharge at locations with higher porewater resistivity.

2.3.1.2 North-South CRPs

The north-south transects indicate that the middle of the bay is likely characterized by finer sediments and is not underlain by a more resistant layer (i.e., sand), as are the northern and southern portions of the bay (**Figure 2.5**). This finding is in agreement with Shideler et al. (1981), who show that in this portion of the bay sediments are mainly comprised of silt and clay. The eastern N-S transect, close to stations 1 and 12, shows decreasing resistance from N to S in the deeper (>10 m deep) profile underlying an almost constant low resistivity surface layer (to 5 – 10 m depth). During porewater collection at station 12 and periodically at station 11, we observed soft, unconsolidated, and saturated silty-clay to ~3 m below sediment-water interface. This layer may indicate that the integrity of the bottom clay-rich layer as a reliable confining unit has been altered, favoring vertical advective flow (Barbour and Fredlund 1989; Gerla 1992;

Silliman et al. 2002), similar to terrestrial occurrences of quicksand or soap holes (Toth 1971). The N and S shore transects show vertically elongated anomalies of very low resistivity surrounded by areas of higher resistivity, which are believed to correspond to buried pipelines, as observed in the preliminary CRPs (see section 2.3.1.1).

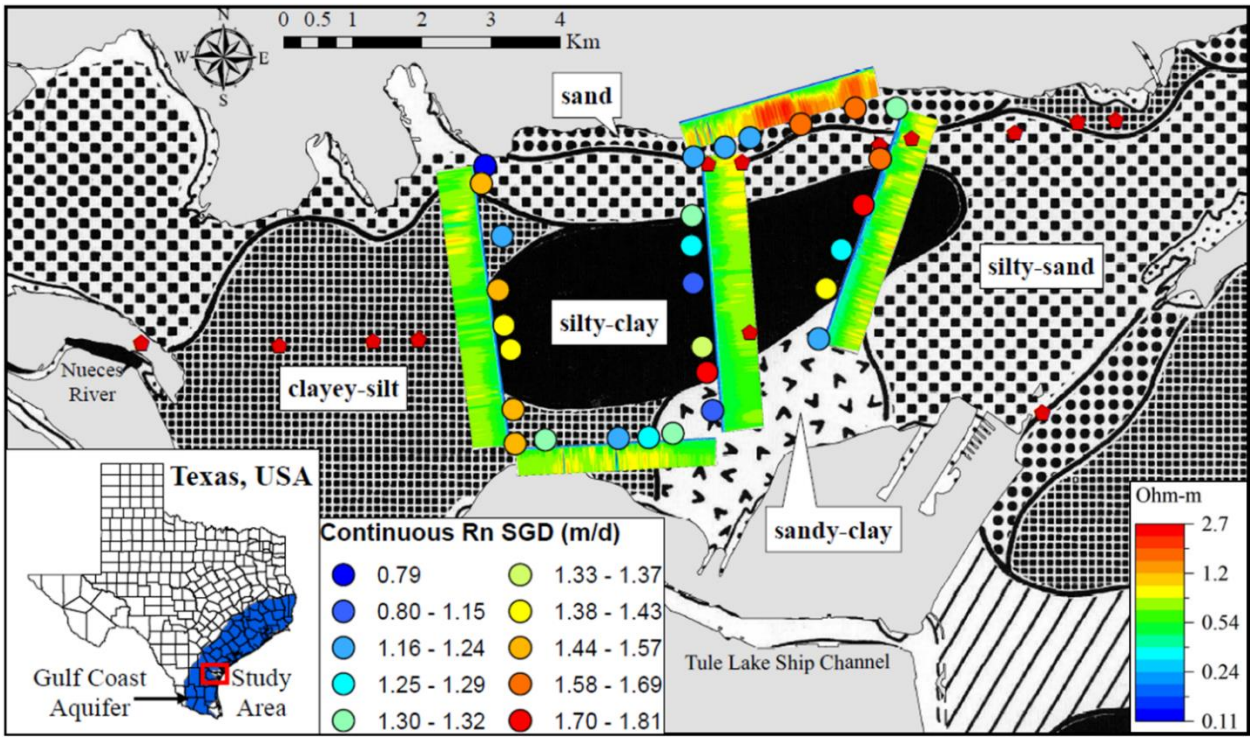

Figure 2.5: CRP and continuous ^{222}Rn-derived SGD survey in spring 2017. Sediment textural class distributions labelled on the map are from Shideler et al. (1981).

The N shore transect contains areas with the highest observed bay resistivity, likely reflecting different depositional environments and a higher sand fraction. The profile reveals a possible infilled paleovalley (Spalt et al. 2018) – a relict fluvial channel incised during a glacial maximum and subsequently filled with finer grained sediments as energy levels within the channel decreased – with much higher resistivity areas confining a shallow valley of lower resistivity sediments (Russoniello et al. 2013). Shallow stratigraphic features like paleovalleys are known to

modify groundwater discharge to coastal waters and geochemical processes across the sediment-water interface (Sawyer et al. 2014).

2.3.2 SGD Characterization

2.3.2.1 Groundwater Endmember Characteristics

Groundwater salinities were brackish in shallow groundwater (salinity: 4.0 – 27.4, $\bar{x}$ = 12.5, n = 4) and ranged from fresh to brackish in deep groundwater (salinity: 0.7 – 4.0, $\bar{x}$ = 1.6, n = 6). In comparison, bay porewater was more saline than terrestrial groundwater (salinity: 25.1 – 40.8, $\bar{x}$ = 32.9, n = 17) throughout the study period. Average ^{224}Ra activities in shallow, brackish groundwater samples (650.4 – 793.6 dpm·100L^{-1}, $\bar{x}$ = 725.9 dpm·100L^{-1}) were 2 – 7 times higher than those in fresher deep groundwater samples (21.0 – 138.6 dpm·100L^{-1}, $\bar{x}$ = 61.6 dpm·100L^{-1}). However, average ^{226}Ra activities in shallow groundwater (22.9 – 97.4 dpm·100L^{-1}, $\bar{x}$ = 69.1 dpm·100L^{-1}) were slightly lower than in deep groundwater (26.5 – 238.9 dpm·100L^{-1}, $\bar{x}$ = 76.9 dpm·100L^{-1}). The range of groundwater ^{226}Ra activities was consistent with those observed in shallow, brackish groundwater (8.5 – 70.3 dpm·100L^{-1}) by Breier and Edmonds (2007). However, because shallow groundwater was sampled following the recession of the late spring 2015 flood waters, these lower ^{226}Ra activities could be a result of flushing of the surficial aquifer leading to an insufficient amount of time for the long-lived ^{226}Ra to regenerate and desorb from the aquifer matrix (Cerdà-Domènech et al. 2017). Consequently, shallow groundwater ARs (8.2 – 31.2; $\bar{x}$ = 14.4 n = 4) were significantly higher than in the deep groundwater (0.4 – 2.6; $\bar{x}$ = 1.1, n = 6).

Porewater radium measured near station 7 in 2017 varied by a factor of 2 – 3 (^{224}Ra: 335.7 – 920.3 dpm·100L^{-1}, $\bar{x}$ = 686.0 dpm·100L^{-1}, n = 10; ^{226}Ra: 73.9 – 171.9 dpm·100L^{-1}, $\bar{x}$ = 113.7 dpm·100L^{-1}, n = 11; **Table 2.1**). The mean porewater ^{224}Ra activity was slightly lower than that

in shallow groundwater and 6-fold greater than that in deep groundwater; mean porewater ^{226}Ra was 1.5-fold greater than both the mean shallow and mean deep groundwater. For comparison, porewater ARs ranged from a minimum of 2.0 in May 2017, similar to the deep groundwater average AR, to a maximum of 10.6 in January 2018, a value near that of average shallow groundwater AR. The annual average porewater AR ($\overline{x}$ = 6.6) is like the average of all groundwater ARs ($\overline{x}$ = 6.4). This large range in porewater ARs and the considerable upward groundwater discharge within the Gulf Coast Aquifer (Chowdhury et al. 2004) suggest that groundwater flowpaths fluctuate throughout the year and that porewater is likely a mixture of deep and shallow groundwater. Thus, an average AR of all groundwater sampled during our study represents the mean porewater endmember for the current study.

Table 2.1: Porewater sampling depth below ground surface (bgs), dissolved oxygen (DO), salinity (Sal), pH, ^{222}Rn, dissolved Ra activity, and ^{224}Ra:^{226}Ra activity ratios for 2017 – 2018 time series sampling near station 7.

Season	ID	Depth (m bgs)	DO (mg·L^{-1})	Sal	pH	^{222}Rn	^{224}Ra	^{226}Ra	224:226
						(dpm·100L^{-1})			
Winter 2017	7-P1	1.35	0.8	27.8	7.71	7,666		121	
	7-P2	1.35	0.7	28.0	7.60	1,646	547	135	4.0
Spring 2017	P1	0.5	1.4	32.9	7.60	27,707	336	172	2.0
	P2	0.5	2.5	33.1	7.58		339	112	3.0
	P3	1.5	2.0	32.8	7.58	17,149	896	96	9.4
Summer 2017	P1	1.9	4.1	33.9	7.39	11,565	790	114	6.9
	P2	0.55	2.2	34.3	7.49	23,128	802	137	5.8
	P3	0.55	1.2	33.9	7.60	14,287	920	106	8.7
Winter 2018	P1	0.5	1.5	27.8	7.13	17,070	616	82	7.5
	P2	0.45	0.7	27.5	7.16	9,193	786	74	10.6
	P3	0.45	0.8	27.7	7.22	15,075	828	110	7.5
Avg. all		**0.9**	**1.6**	**30.9**	**7.5**	**14,449**	**686**	**114**	**6.6**

Salinity has been long recognized as an important factor that controls dissolved Ra activities (Boehm et al. 2006; Moore 1996), as Ra is strongly particle-reactive at low salinities and becomes more soluble with an increase in salinity and ionic strength of the solution, which

enhances ion exchange. However, dissolved oxygen (DO) and pH may also influence Ra solubility in groundwater (Cerdà-Domènech et al. 2017). At DO concentrations less than ~1 $mg \cdot L^{-1}$ or pH less than ~6, Ra adsorption to the aquifer matrix has been shown to decrease, which facilitates its mobility in groundwater (Szabo et al. 2012a; Szabo et al. 2012b). Salinities less than 5 were observed in all deep groundwater and one shallow groundwater sample (salinity: 4.03; **Supplementary Table 2.S1**). We did not observe pH less than 6 in any of the deep groundwater (pH: 6.6 – 8.2) or most of the shallow groundwater samples (pH: 6.4 – 6.9), but pH less than 6 was observed in one shallow groundwater sample (pH: 5.9) which corresponds to the sample with the greatest AR observed (31.2). DO concentrations less than 1 $mg \cdot L^{-1}$ were observed in one shallow groundwater sample (0.95 $mg \cdot L^{-1}$), three deep groundwater wells (0.3 – 0.7 $mg \cdot L^{-1}$), and four of five wells screened deeper than 80 m (0.2 – 0.5 $mg \cdot L^{-1}$).

All porewater (n = 24) (**Supplementary Table 2.S2)** and groundwater (**Table 2.S1**) ^{222}Rn activities were 1 to 3 orders of magnitude higher than surface waters (**Table 2.2**). Average ^{222}Rn activities in shallow groundwater ($34.3x10^3$ – $48.4x10^3$ $dpm \cdot 100L^{-1}$, $\bar{x} = 39.1x10^3$ $dpm \cdot 100L^{-1}$) were similar to the lower range of deep groundwater activities ($27.3x10^3$ – $143.4x10^3$ $dpm \cdot 100L^{-1}$, $\bar{x} = 52.1x10^3$ $dpm \cdot 100L^{-1}$). All groundwater ^{222}Rn activities exceeded the dissolved ^{226}Ra activities by two to three orders of magnitude, indicating an enrichment of particle-bound ^{226}Ra within the aquifer. Porewater ^{222}Rn activities ($0.2x10^3$ – $82.7x10^3$ $dpm \cdot 100L^{-1}$, $\bar{x} = 20.1x10^3$ $dpm \cdot 100L^{-1}$) were variable across the system. Sediment supported ^{222}Rn activities determined from sediment incubation experiments ranged from $1.6x10^3$ to $17.4x10^3$ $dpm \cdot 100L^{-1}$ ($\bar{x} = 7.9x10^3$ $dpm \cdot 100L^{-1}$) across four stations (7, 8, 12, and 14). Any porewater ^{222}Rn activities derived from field measurements below the minimum activity supported by the sediment ($1.6x10^3$ $dpm \cdot 100L^{-1}$) were deemed compromised, due to loss of radon during sampling, handling, or analysis (Lambert

and Burnett 2003), and disregarded from further analysis. The average porewater ^{222}Rn activity ($\bar{x}$ = 24.0x10^3 dpm·100L^{-1}) is similar to the lowest deep groundwater and the maximum activity is greater than the shallow groundwater. No significant difference ($p = 0.36$) was observed in average porewater ^{222}Rn activities by sampling event; however, average porewater in the river (48.3 x10^3 dpm·100L^{-1}) was significantly ($p < 0.004$) more enriched in ^{222}Rn than the porewater in the bay (12.3 x10^3 dpm·100L^{-1}). This ^{222}Rn enrichment in the river porewater may result from less surface water recirculation (i.e., less dilution) given the deeper collection points (i.e., 1.5 to 2 m into the sediment), closer proximity to the bank and source of groundwater, and/or legacy of ^{226}Ra sequestered in the sediment from direct discharges of oil-field brines into the river (**Figure 2.1C**). In the river, sediment supported ^{222}Rn increased with depth into the sediments with the highest activities at 100-102 cm and 125-127 cm (11.2x10^3 dpm·100L^{-1} and 17.4x10^3 dpm·100L^{-1}, respectively) and the lowest at 10 – 12 cm and 22 – 24 cm (1.6x10^3 dpm·100L^{-1} and 1.8x10^3 dpm·100L^{-1}, respectively), following the trend expected in oxic sediments (Kadko et al. 1987). This increasing supported ^{222}Rn with depth was not observed in the middle of the bay, likely reflecting the different sedimentary environments and depositional rates (Hill and Nicolau 2014), oxidation-reduction conditions (Kadko et al. 1987), and history of bay bottom disturbance (RRC 2018).

2.3.2.2 Radium Activity Characterization

2.3.2.2.1 Surface Water ^{224}Ra and ^{226}Ra Activities and Salinity

Similar to our study **(Table 2.2)**, (Breier et al. 2005; Breier et al. 2010; Breier and Edmonds 2007) report elevated ^{224}Ra (approximately 10.0 – 120.0 dpm·100L^{-1}) and ^{226}Ra (13.8 – 112.2 dpm·100L^{-1}) activities for Nueces Bay. Overall, ^{224}Ra varied by 2- to 4.5-fold while ^{226}Ra was more consistent and varied by 1.5- to 2.5-fold during each event. The CCB seawater endmember

experienced the least variation in both radium activities across the study period (^{224}Ra: 40.9 – 73.7 dpm·100L^{-1}, $\overline{x}$ = 56.3 dpm·100L^{-1}; ^{226}Ra: 42.8 – 72.4 dpm·100L^{-1}, $\overline{x}$ = 48.7 dpm·100L^{-1}), likely due to the distance from terrestrial Ra sources and consistently high salinity (17.2 – 38.8) at this location. The Nueces River ^{224}Ra and ^{226}Ra endmembers varied by 1.6- to 4.5-fold and by 2.1- to 6.2-fold, respectively (^{224}Ra: 20.0 – 90.2 dpm·100L^{-1}, $\overline{x}$ = 53.0 dpm·100L^{-1}; ^{226}Ra: 16.4 – 101.8 dpm·100L^{-1}, $\overline{x}$ = 57.3 dpm·100L^{-1}), with consistently the lowest activities during summer for both isotopes.

The most significant differences in bay Ra activities between sampling periods are closely associated with flooding of the Nueces River in summer 2015 (**Table 2.2, Figure 2.3**). Within the bay, the lowest salinity (min = 0.2, max = 6.5, $\overline{x}$ = 3.3) and Ra activities (^{224}Ra: 21.8 – 61.2 dpm·100L^{-1}, $\overline{x}$ = 43.0 dpm·100L^{-1}; ^{226}Ra: 19.3 – 36.6 dpm·100L^{-1}, $\overline{x}$ = 27.9 dpm·100L^{-1}) occur in summer 2015 as a result of nearly complete flushing of the bay by Nueces River floodwaters, which first peaked three weeks prior to sample collection followed by lesser peaks 9 days prior to sample collection and one day before subsequent sample collection days (**Figure 2.3**). Between spring and summer 2015 sampling, salinities decreased from 15.1 – 31.7 ($\overline{x}$ = 27.1) to 0.2 – 6.5 ($\overline{x}$ = 2.5). Because of these low salinities and flushing of the bay, summer 2015 radium activities were lowest in the river and increased with distance from the river mouth. Consequently, Ra activities are greater in offshore waters (i.e., CCB) so radium isotopes are not suitable tracers of SGD during the summer 2015 sampling event as the assumption of decreasing activities with distance from shore does not hold.

Highest ^{224}Ra activities were observed near the Nueces River mouth (station 8, ^{224}Ra: 21.8 – 147.0 dpm·100L^{-1}, $\overline{x}$ = 85.6 dpm·100L^{-1}) and in close proximity to Gum Hollow Creek in the north-bay (station 7, ^{224}Ra: 53.0 – 190.9 dpm·100L^{-1}, $\overline{x}$ = 106.8 dpm·100L^{-1}). Station 7 had the

highest ^{224}Ra activity in each season apart from fall and winter 2015 when the river mouth had the highest activity. This finding suggests the river and creek are persistent sources of radium to the bay. However, the ^{224}Ra mixing model and results from Murgulet et al. (2018) indicate minimal riverine influence/input across the south-bay (**Figure 2.6 A-D and F-I**), except for in fall 2015 (**Figure 2.6E**). Furthermore, during the drought, the Nueces Estuary was hypersaline with mean salinities ($\overline{x}$ = 37.0 in fall 2014 and $\overline{x}$ = 35.5 in winter 2014) slightly greater than typical seawater (i.e., 35) and the lower river salinities as high as 15 (**Figure 2.3B**). Under these conditions, maximum desorption from riverine suspended sediments likely occurred near the river mouth, as there does not appear to be any riverine influence beyond station 8 (**Figure 2.6 F-H**). Thus, elevated Ra activities across the bay are likely due to inputs from groundwater and bay sediment sources alone rather than riverine inputs.

Ra-224 was elevated in spring 2015 and 2016 compared to all other sampling events, particularly at northern stations. These increased ^{224}Ra activities in spring likely result from increased runoff and shallow groundwater discharge following the onset of the spring rains, further supporting the link between the inland hydrologic cycle and SGD. Recall that shallow groundwater is more enriched in ^{224}Ra than ^{226}Ra compared to deeper groundwater. These findings likely result from decreased contact time of waters with aquifer solids (Lamontagne et al. 2008), changes in redox conditions, or chemical characteristics of the aquifer matrix (Gonneea et al. 2008).

2.3.2.2.2 Radium Activity Ratios and Radium Ages

Overall, ^{224}Ra and ^{226}Ra activities in surface water do not have a significant correlation ($r = 0.13$, $p = 0.3$); however, three distinct trends separate samples into two strongly correlated clusters by ARs <1 and ARs >1 ($r = 0.80$, $p < 0.0001$ and $r = 0.78$, $p < 0.0001$, respectively;

Figure 2.7) and a riverine mixing line that only occurs in fall 2015 (**Figure 2.6E**). These distinct trends suggest that there are likely two or more sources of radium in the study area (Charette et al. 2001): one enriched in ^{224}Ra (high AR) and one deficient in ^{224}Ra (low AR) relative to ^{226}Ra. These sources could reflect more deep groundwater input with its relatively low ARs (0.4 – 2.6) or shallow groundwater with its much higher ARs (8.2 – 31.2).

Bay ARs <1 were observed during fall 2014, fall 2015, and winter 2015 and in the river in summer, fall, and winter 2015 and summer 2016. These sampling events occur in fall 2014 towards the end of a multi-year drought (2011 – 2015) and 3 – 6 months after heavy precipitation and flooding (fall and winter 2015). Following long-term droughts, groundwater discharge from shallower aquifers is expected to diminish due to reduced recharge and the consequent lowering of the water table. Meanwhile, deeper groundwater discharge may become more significant in the overall bay water budget due to a lag between climatic changes and deeper groundwater systems. In addition, deeper groundwater gradients may be enhanced as the surface water level is lowered due to large effects of evaporation and almost absent surface runoff inputs. Following the flooding event, although the water table is recovering, discharge from the shallow aquifer could potentially be accompanied by deeper formation groundwater input.

Another possible cause of low surface water ARs (i.e., <1) could be scavenging of dissolved radium from surface waters and regeneration in the sediments. It has been shown that radium may be scavenged during the biogenic formation of barite or opal (Bishop 1988; Krest et al. 1999) or through oxidation-reduction reactions (Kadko et al. 1987), see section 2.3.3., remineralized under hypoxic conditions, and then could be released into the porewater and bottom waters. Storage of scavenged radium for just a few days would produce a distinct decrease of short-lived ^{224}Ra activities compared to the much longer-lived ^{226}Ra activities over

time leading to lower $^{224}Ra/^{226}Ra$ activity ratios. The ARs <1 demonstrate a ^{224}Ra deficiency within the bay during fall and winter 2015, 3 – 6 months following the occurrence of hypoxic conditions (summer 2015 DO: 1.43 – 3.22 $mg \cdot L^{-1}$) within the river and bay, which indicates radium scavenging may have occurred. Additionally, hypoxic to anoxic conditions are common in the bay porewater across all seasons (0.32 – 4.47 $mg \cdot L^{-1}$, $\bar{x}$ = 1.44 $mg \cdot L^{-1}$; n = 21), so the scavenging and release cycle may be taking place entirely within the sediment resulting in higher AR shallow groundwater losing a portion of its ^{224}Ra and discharging with lower ARs.

We calculated a water-mass age from radium ARs for each season assuming the following groundwater endmembers: 1) average AR of deep groundwater ($\bar{x}$ = 1.27); 2) average AR of all groundwater ($\bar{x}$ = 6.5); and 3) average AR of shallow groundwater ($\bar{x}$ = 14.4; **Table 2.2**). Radium ages calculated from the average deep groundwater AR suggest a deep groundwater signature (i.e., ^{224}Ra deficient) or that geochemical processes occurring within the sediment may influence ARs by facilitating a ^{224}Ra deficiency bay-wide in fall (2.5 – 8.6 days) and winter 2015 (0.3 – 5.0 days) and only in certain regions of the bay during other sampling events. In contrast, radium ages utilizing the shallow groundwater (8.6 – 21.2 days) and the average of all groundwater (4.5 – 17.2 days) suggest shallow groundwater is the dominant source to the bay during most seasons. The ^{224}Ra deficient signature seen in fall and winter 2015 likely reflects the freshening of the bay sediments which increased sorption of radium to aquifer materials. The increase in salinity with time is expected to be accompanied by increased radium desorption and input of ^{224}Ra deficient signature due to decay (see section 2.3.3.). Nevertheless, the deep groundwater input should not be ignored in this system. Recall the Gulf Coast Aquifer is described as a leaky artesian aquifer composed of discontinuous sand, silt, clay, and gravel beds, thus the small-scale heterogeneities and interconnections between the surficial unconfined aquifer and the deeper confined aquifers

are not well constrained and it is likely that source mixing is occurring within the aquifer prior to discharge. Due to these limited constraints on aquifer heterogeneity and the close agreement with average porewater ARs, the average groundwater AR radium ages were applied to all stations.

Table 2.2: Surface water dissolved oxygen (DO), pH, salinity, dissolved Ra activity, ^{224}Ra:^{226}Ra activity ratios and radium ages (RA) for each station and event. Radium ages using the average ARs of: all groundwater (All GW, 6.5), shallow groundwater (shallow GW, 14.4), deep groundwater (deep GW, 1.3), and porewater (Avg. PW, 6.6) from the 2017 follow-up study as endmembers are provided.

Event	Station	DO ($mg \cdot L^{-1}$)	pH	Sal	^{224}Ra	^{226}Ra	224:226	RA All GW	RA Shallow GW	RA Deep GW	RA PW
					($dpm \cdot 100L^{-1}$)			(days)			
Fall 2014	1	5.27	7.95	38.24	36.7	70.2	0.5	13.1	17.2	4.6	13.2
	4	5.89	8.01	38.18	32.0	66.9	0.5	13.6	17.7	5.1	13.6
	7	6.27	8.13	36.63	111.6	67.0	1.7	7.1	11.2	*-1.4*	7.1
	8	5.29	8.21	34.45	47.6	82.5	0.6	12.6	16.7	4.1	12.7
	11	6.03	8.18	36.43	45.6	74.1	0.6	12.2	16.4	3.8	12.3
	12	5.92	8.20	38.19	85.5	47.4	1.8	6.7	10.8	*-1.8*	6.7
	13	6.08	8.24	38.72	67.8	49.3	1.4	8.1	12.2	*-0.4*	8.2
Winter 2014	1	6.57	7.91	35.79	74.1	50.7	1.5	7.7	11.9	*-0.7*	7.8
	4	6.29	8.09	35.85	77.2	48.0	1.6	7.2	11.4	*-1.2*	7.3
	7	6.94	8.11	35.82	102.7	60.7	1.7	7.0	11.1	*-1.5*	7.1
	8	7.32	8.04	34.51	88.1	62.6	1.4	7.9	12.1	*-0.5*	8.0
	11	7.46	7.98	35.70	73.4	63.8	1.2	9.0	13.1	0.5	9.1
	12	7.49	8.12	35.67	61.4	49.8	1.2	8.6	12.7	0.2	8.7
	13	7.34	8.10	35.17	52.3	43.4	1.2	8.8	12.9	0.3	8.8
Spring 2015	1	4.50	7.87	30.49	139.4	51.0	2.7	4.5	8.6	*-4.0*	4.6
	4	3.72	7.88	31.60	126.7	46.0	2.8	4.5	8.6	*-4.0*	4.5
	7	4.01	7.95	31.73	190.9	105.9	1.8	6.7	10.8	*-1.8*	6.7
	8	5.33	7.93	25.92	107.7	58.1	1.9	6.5	10.6	*-2.0*	6.6
	11	4.70	7.92	26.65	111.5	53.3	2.1	5.9	10.0	*-2.6*	6.0
	12	5.42	7.90	30.16	99.5	44.4	2.2	5.5	9.6	*-2.9*	5.6
	13	5.39	8.04	31.75	48.6	43.4	1.1	9.1	13.3	0.7	9.2
	14	4.77	8.02	24.86	128.0	50.2	2.5	4.9	9.0	*-3.6*	4.9
	15	4.46	8.71	14.88	75.4	51.5	1.5	7.7	11.9	*-0.7*	7.8
Summer 2015	1	3.27	8.49	3.71	47.9	30.4	1.6	7.4	11.5	*-1.1*	7.4
	4	1.36	8.29	5.51	56.9	36.6	1.6	7.4	11.5	*-1.1*	7.5
	7	1.61	8.35	6.18	61.2	31.1	2.0	6.2	10.3	*-2.3*	6.3
	8	1.72	7.32	0.23	21.8	19.3	1.1	9.1	13.2	0.6	9.2

	11	2.03	8.18	0.61	23.5	19.9	1.2	8.8	13.0	0.4	8.9
	12	2.89	8.48	3.27	46.5	30.4	1.5	7.5	11.6	*-1.0*	7.6
	13	2.90	8.18	16.56	55.4	42.8	1.3	8.4	12.5	*-0.1*	8.5
	14	1.82	7.21	0.22	13.5	16.5	0.8	10.8	14.9	2.3	10.8
	15	1.12	7.43	0.22	20.0	16.4	1.2	8.7	12.8	0.2	8.8
Fall 2015	1	4.68	8.23	31.67	47.6	74.7	0.6	12.1	16.2	3.6	12.1
	4	4.66	8.16	30.89	49.7	69.1	0.7	11.4	15.5	3.0	11.5
	7	6.21	8.28	31.45	55.8	71.3	0.8	11.0	15.1	2.5	11.1
	8	5.97	8.24	22.44	81.6	161.2	0.5	13.3	17.4	4.8	13.3
	11	4.63	8.23	26.19	31.0	128.4	0.2	17.1	21.2	8.6	17.2
	12	4.57	8.22	27.58	53.2	84.9	0.6	12.1	16.3	3.7	12.2
	13	4.49	8.25	31.05	40.9	72.4	0.6	12.7	16.8	4.2	12.8
	14	6.60	8.81	12.07	52.4	124.3	0.4	14.2	18.3	5.7	14.3
	15	7.71	8.96	5.96	42.2	101.8	0.4	14.3	18.4	5.8	14.4
Winter 2015	1	--	8.31	31.80	34.2	70.8	0.5	13.5	17.6	5.0	13.6
	4	--	8.14	31.41	40.3	76.7	0.5	13.1	17.2	4.6	13.1
	7	--	8.24	32.39	53.0	78.2	0.7	11.7	15.9	3.3	11.8
	8	--	8.36	25.76	74.2	87.4	0.8	10.6	14.7	2.1	10.7
	11	--	8.17	29.03	53.0	75.3	0.7	11.5	15.7	3.1	11.6
	12	--	8.29	30.42	50.7	67.0	0.8	11.2	15.3	2.7	11.2
	13	--	8.12	30.74	53.5	44.7	1.2	8.8	12.9	0.3	8.9
	14	--	8.41	20.80	70.7	90.8	0.8	11.0	15.1	2.5	11.1
	15	--	8.59	14.77	57.9	86.1	0.7	11.8	15.9	3.3	11.9
Spring 2016	1	8.37	8.10	26.48	117.1	55.5	2.1	5.8	10.0	*-2.6*	5.9
	4	8.00	7.81	26.64	128.6	46.9	2.7	4.5	8.6	*-4.0*	4.6
	7	8.28	8.29	25.75	153.3	67.0	2.3	5.4	9.5	*-3.1*	5.5
	8	8.24	7.96	20.12	147.0	69.4	2.1	5.8	9.9	*-2.7*	5.9
	11	10.35	8.33	24.46	91.7	70.7	1.3	8.4	12.5	*-0.1*	8.5
	12	8.63	8.23	27.48	86.8	46.2	1.9	6.4	10.6	*-2.0*	6.5
	13	7.90	8.10	28.56	73.7	48.7	1.5	7.6	11.7	*-0.9*	7.7
	14	8.27	8.32	14.39	138.1	75.8	1.8	6.6	10.7	*-1.9*	6.7
	15	8.33	8.47	12.00	90.2	53.1	1.7	7.0	11.1	*-1.5*	7.1
Summer 2016	1	7.05	8.12	25.34	69.6	66.0	1.1	9.4	13.6	1.0	9.5
	4	7.09	8.02	25.20	95.7	54.2	1.8	6.8	10.9	*-1.7*	6.8
	7	5.30	7.94	24.35	126.0	46.2	2.7	4.5	8.6	*-4.0*	4.6
	8	5.79	7.96	22.96	116.7	68.0	1.7	6.9	11.0	*-1.6*	7.0
	11	6.75	8.14	24.09	109.1	69.8	1.6	7.4	11.5	*-1.1*	7.5
	12	6.99	8.09	24.96	80.6	58.0	1.4	8.0	12.1	*-0.5*	8.1
	13	6.41	8.03	24.67	69.9	45.3	1.5	7.5	11.6	*-1.0*	7.6
	14	10.16	8.19	7.41	49.8	37.0	1.3	8.2	12.3	*-0.3*	8.3
	15	10.47	8.41	0.91	32.5	35.1	0.9	10.1	14.2	1.6	10.2

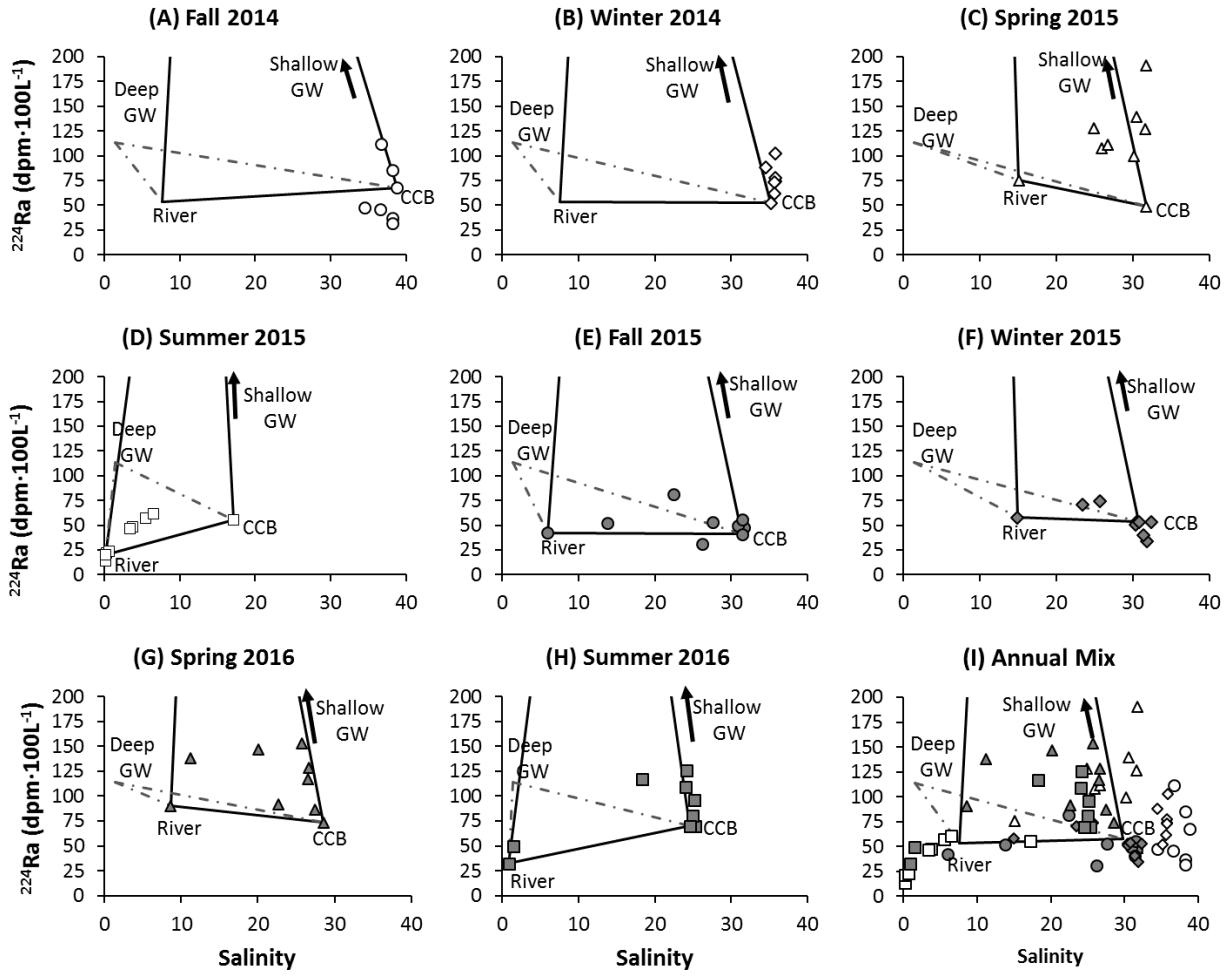

Figure 2.6: Seasonal and annual mixing models for Nueces Bay using three endmembers (Nueces River, Corpus Christi Bay, and average shallow groundwater). Solid lines indicate the shallow GW-river, river-CCB, and shallow GW-CCB mixing lines. Note dotted triangles include average deep groundwater. Since river data were not available for fall and winter 2014, the average river salinity and ^{224}Ra activities for station 15 were used (excluding summer 2015).

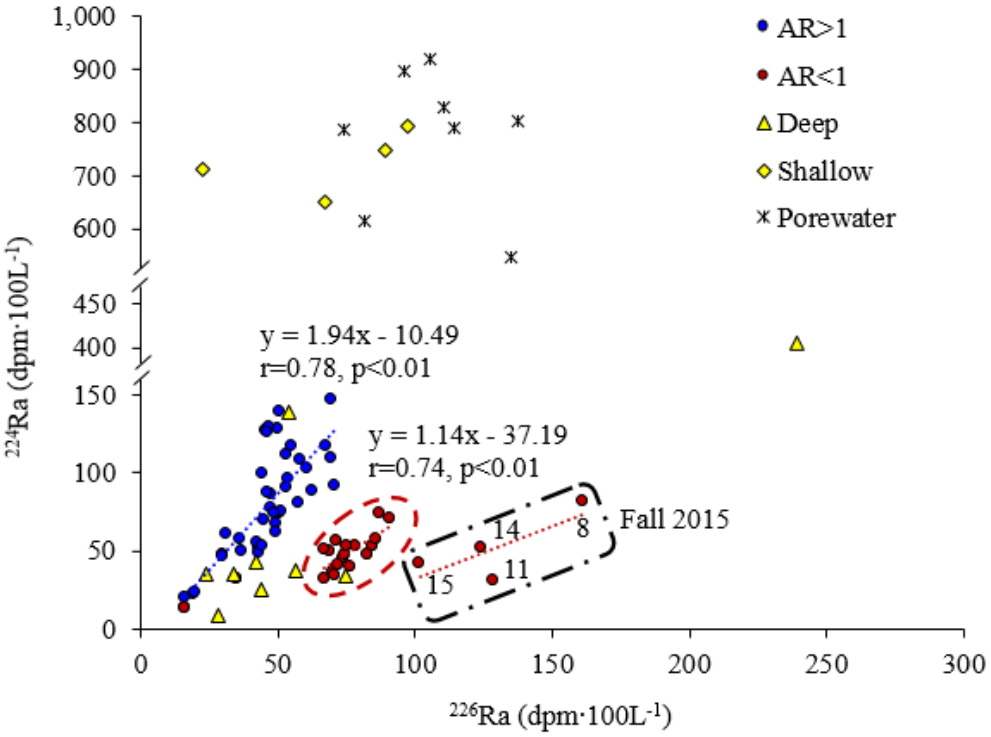

Figure 2.7: Correlation of ^{224}Ra and ^{226}Ra activities (dpm·100L^{-1}). Activity ratios (ARs) >1 (i.e., more ^{224}Ra than ^{226}Ra; blue circle) and <1 (i.e., more ^{226}Ra than ^{224}Ra; red circle) are represented. Activities of deep groundwater (yellow triangle), shallow groundwater (yellow diamond), and porewater (star) are also represented.

2.3.2.3 SGD Rates

2.3.2.3.1 Theoretical Groundwater Discharge Rate Estimates

Regional groundwater elevation data reveal hydraulic gradients toward the lower Nueces River and the bay in the north, but toward the Kingsville drawdown (Chowdhury et al. 2004; Rettman 1983; Shafer and Baker Jr 1973; Uddameri et al. 2014) and away from the river and bay in the south (**Figure 2.1B**). For this study, all shallow groundwater velocities were determined using hydraulic conductivities measured from slug tests performed on four piezometers near the

lower Nueces River (**Figure 2.1C**). Measured hydraulic conductivities ranged from 1.21 – 5.8 $m \cdot d^{-1}$, which are an order of magnitude greater than the 0.86 $m \cdot d^{-1}$ reported by Capuano and Jan (1996) for similar clay and silty-clay fluvial-deltaic sediments in the upper 7.5 m of the Beaumont formation along the Texas Gulf Coast. These hydraulic conductivities are 3 – 4 orders of magnitude greater than would be expected for silts and 5 – 6 orders of magnitude greater than expected for clays, which may be attributable to macroporosity rather than matrix porosity (Capuano and Jan 1996). Shallow groundwater levels were measured in October 2015 following the recession of flood waters. Given that flood waters have pooled at the ground surface in the area with piezometers, we expect that these measured water levels are likely more elevated than would be expected during a dry or normal year and would thus represent a maximum estimate for hydraulic gradients and discharge rates. For comparison, we revisited the piezometers in June 2018 after a moderately wet winter and a very dry spring when conditions reflected more normal conditions. Freshwater heads were on average 0.79 m greater under wet conditions in the piezometers with higher salinity groundwater (n = 2) but were similar between the wet and normal conditions in the lower salinity ones (n = 2) (**Table 2.3**).

True groundwater/pore velocities (v_p) were estimated as the ratio of specific groundwater discharge rates (q) to the effective porosity (n_e). An effective porosity of 0.05 for the Chicot Aquifer (Young et al. 2016) was applied to Darcy estimates to convert from specific discharge to groundwater velocity. The groundwater seepage velocities ranged from -0.02 – 7.84 $m \cdot d^{-1}$ during normal conditions and 0.09 – 8.28 $m \cdot d^{-1}$ during wet conditions.

Table 2.3: Darcy estimates of pore velocity (v_p) calculated from freshwater heads (h_f), flowpath length (l), hydraulic gradient (i), hydraulic conductivity (K), specific (Darcy) velocity (q), and effective porosity (n_e) for shallow local groundwater collected in October 2015 (1015) and June 2018 (0618).

		h_f (m)	l (m)	i	K ($m \cdot d^{-1}$)	q ($m \cdot d^{-1}$)	n_e	v_p ($m \cdot d^{-1}$)
1015	W1	2.28	200	0.004	5.80	0.02	0.05	0.44
	W2	2.24	200	0.004	1.21	0.004	0.05	0.09
	W3	3.26	24	0.073	5.71	0.41	0.05	8.28
	W4	3.43	24	0.080	2.48	0.20	0.05	3.95
0618	W1	1.55	200	0.000	5.80	0.001	0.05	0.02
	W2	1.39	200	-0.001	1.21	-0.001	0.05	-0.02
	W3	3.17	24	0.069	5.71	0.39	0.05	7.84
	W4	3.41	24	0.079	2.48	0.20	0.05	3.91

2.3.2.3.2 Radon SGD Estimates

Time-series ^{222}Rn SGD estimates presented by Murgulet et al. (2018) show large seasonal and spatial variability with discharge rates that range over 2 orders of magnitude with time and 3 orders of magnitude depending on the groundwater endmember (**Supplementary Figure S1**). The 2017 continuous, mobile ^{222}Rn survey supports the occurrence of generally high SGD rates (0.79 – 1.81 $m \cdot d^{-1}$) throughout the bay (**Figure 2.5**). An increase in ^{222}Rn activity (from 3.8 – 4 $dpm \cdot L^{-1}$ to 5.1 – 7.3 $dpm \cdot L^{-1}$) and SGD (from 1.16 – 1.24 $m \cdot d^{-1}$ to 1.58 − 1.69 $m \cdot d^{-1}$) was observed across the north-bay in conjunction with the highest resistivities observed in the CRP (see section 2.3.1.2; **Figure 2.5**). Other studies that continuously surveyed ^{222}Rn along coastal transects and rivers found that ^{222}Rn ranged around a low background value (Santos et al. 2008b; Swarzenski et al. 2006b), but reached an order of magnitude higher where groundwater inputs were the highest. While we did not observe an order of magnitude increase, ^{222}Rn activities and

SGD rates were twofold higher along a portion of the north-bay near the highest observed resistivities and near the transitions from finer grain sediments to sandier sediments (**Figure 2.5**). For instance, the highest ^{222}Rn activities (6.2 to 7.3 dpm·L^{-1}) and SGD rates (1.70 – 1.81 m·d^{-1}) were observed farther from shore near these sediment transition zones, from predominantly silty-clay mid-bay sediments to more silty-sand and sandy-clay sediments in the north- and south-bay, respectively (Shideler et al. 1981). A lesser increase in ^{222}Rn activity (5 to 5.4 dpm·L^{-1}) and SGD rates (1.38 – 1.43 m·d^{-1}) was observed at the silty-clay to clayey-silt transition along the western most survey line (**Figure 2.5**). Though not acting as a barrier to flow (see section 2.3.1.2.), these low permeability sediments may redirect some of the groundwater toward the more permeable sediment transition areas mentioned above. This survey further confirms the ^{222}Rn activity variability and demonstrates that SGD rates may vary by an order of magnitude across the system, as also observed with the time-series stations (Murgulet et al. 2018).

2.3.2.3.3 Radium Budget

Bay-wide ^{226}Ra-derived SGD rates ranged from 2.9x10^{4} m^{3}·d^{-1} (4x10^{-4} m^{3}·m^{-2}d^{-1}; fall 2015) to 1.2x10^{6} m^{3}·d^{-1} (0.04 m^{3}·m^{-2}d^{-1}; spring 2015) using the average terrestrial groundwater endmember (**Table 2.4**). In contrast, applying the average deep terrestrial groundwater endmember to fall and winter 2014 and 2015 seasons results in bay-wide SGD rates ranging from 2.3x10^{6} m^{3}·d^{-1} (0.04 m^{3}·m^{-2}d^{-1}) to 8.8x10^{7} m^{3}·d^{-1} (1.2 m^{3}·m^{-2}d^{-1}), respectively. These deep SGD rates are 1 – 2 orders of magnitude greater than those derived with the average terrestrial groundwater. While it is unlikely the deeper groundwater is discharging bay-wide due to subsurface heterogeneity, this study strongly suggests that sources of SGD to Nueces Bay are from both shallow/shorter (i.e., nearby water table aquifer) and deeper/longer flowpaths (i.e., confined/semiconfined aquifers). The influence of one groundwater source over the other is

likely determined by the impact of local and inland climatic conditions on hydraulic gradients (i.e., drought versus flood conditions), disturbance of the bay sediments (Santos et al. 2008b), and the clay sediments failing to restrict flow, but instead enhancing flow (Barbour and Fredlund 1989; Bighash and Murgulet 2015; Toth 1971). It should be noted that this method could not be applied to calculate a bay-wide SGD rate for the summer 2015 flood event when the ^{226}Ra activity increased with distance from shore (see section 2.3.2.2) and thus violates the necessary assumptions for this model (see section 2.2.6).

Breier and Edmonds (2007) found that ^{226}Ra-derived SGD rates in Nueces Bay were $3.1x10^{5}$ $m^{3}{\cdot}d^{-1}$ ($4x10^{-3}$ $m^{3}{\cdot}m^{-2}d^{-1}$) in Nueces Bay, which was deemed too high for such a clay-rich semi-arid environment and in comparison to riverine inflows, so the authors attributed this excess ^{226}Ra to oil-field brine leakage from pipelines throughout the bay. The current study found similar ^{226}Ra-derived SGD rates, which we believe to be likely due to groundwater discharge directly to the lower Nueces River and the bay. In fact, even higher SGD fluxes are expected based on the ^{222}Rn mass balance (Murgulet et al. 2018), see section 2.3.2.3.2. Any excess ^{226}Ra derived from leaking oil-field brines is accounted for in the ^{222}Rn mass balance as part of the ^{226}Ra supported radon step where supported ^{226}Ra is subtracted from the total ^{222}Rn measurements to calculate an excess ^{222}Rn (Burnett and Dulaiova 2003).

Table 2.4: Summary of ^{226}Ra-derived groundwater flux components. Groundwater endmembers represented are average ($\bar{x}$) of all terrestrial groundwater and $\bar{x}$ of deep terrestrial groundwater (in parenthesis). ‡Freshwater surface inflow for spring 2016 and summer 2016 are provisional data and do not account for diversions and return flows. Total suspended solids (TSS) represent the maximum previously observed TSS concentrations for Nueces Bay (Nicolau and Hill 2013). Most conservative and least conservative average bay SGD from Murgulet et. al. (2018) are provided for comparison. Darcy estimates during the study period are shown for comparison.

		Fall 2014	Winter 2014	Spring 2015	Summer 2015	Fall 2015	Winter 2015	Spring 2016	Summer 2016	Units
$^{226}Ra_{NB}$	$\bar{x}$ ^{226}Ra in surface bay water	680.1	559.3	597.8	279.3	982.6	759.1	592.9	603.7	dpm·m^{-3}
$^{226}Ra_{CCB}$	$\bar{x}$ ^{226}Ra in CCB	493.3	434.4	434.5	427.8	723.7	447.1	487.2	453.1	dpm·m^{-3}
V_{NB}	Bay volume	5.5x10^{7}	5.5x10^{7}	5.5x10^{7}	5.5x10^{7}	5.5x10^{7}	5.5x10^{7}	5.5x10^{7}	5.5x10^{7}	m^{3}
T_w	Residence time of bay water from radium ages	33.2 (6.9)	18.6 (0.3)	10.4	16.8 (0.5)	57.2 (7.9)	45.2 (5.1)	11.4	15.3	days
$^{226}Ra_{NR}$	$\bar{x}$ ^{226}Ra in NR	884.6	884.6	508.8	164.5	1,130.2	884.6	644.5	360.3	dpm·m^{-3}
Q_R	Freshwater surface inflow	139,236	9,190	16,035	17,015,215	152,026	5,962	*70,000*‡	*520,066*‡	m^{3}·d^{-1}
$^{226}Ra_{des}$	Max. desorption ^{226}Ra from TSS	1.2	1.2	1.8	1.7	1.8	1.4	1.8	1.8	dpm·g^{-1}
TSS	Max. TSS in NB	290	290	290	290	290	290	290	290	g·m^{-3}
$^{226}Ra_{GW}$	$\bar{x}$ ^{226}Ra in terrestrial groundwater	745.2 (781.3)	745.2 (781.3)	745.2	745.2	745.2 (781.3)	745.2 (781.3)	745.2	745.2	dpm·m^{-3}
A	Bay area	7.5x10^{7}	7.5x10^{7}	7.5x10^{7}	7.5x10^{7}	7.5x10^{7}	7.5x10^{7}	7.5x10^{7}	7.5x10^{7}	m^{2}
^{226}Ra-derived SGD		1.3x10^{6} (3.0x10^{6})	1.2x10^{6} (2.9x10^{7})	2.0x10^{6}	---	1.3x10^{6} (4.0x10^{6})	1.9x10^{6} (6.6x10^{6})	1.2x10^{6}	9.5x10^{5}	m^{3}·d^{-1}
		0.017 (0.04)	0.016 (0.39)	0.03	---	0.018 (0.05)	0.026 (0.09)	0.016	0.013	m^{3}·m^{-2}d^{-1}
^{222}Rn-derived Bay SGD (Murgulet et. al. 2018)		---	0.66 - 9.49	0.23 - 3.29	0.07 - 1.02	0.11 - 1.62	0.19 - 2.71	0.26 - 3.61	0.28 - 3.90	m^{3}·m^{-2}d^{-1}
Darcy estimate						0.09 – 8.28				m·d^{-1}

2.3.3 SGD Intercomparison

Semi-arid regions experience intra-annual and inter-annual fluctuations between dry and wet periods. During wet periods, precipitation exceeds evaporation so SGD is expected to be greater nearshore as the surficial aquifer is recharged and the hydraulic gradient increased; however, during dry periods, evaporation far exceeds precipitation so SGD is expected to decline at the shoreline as the hydraulic gradient in the surficial aquifer decreases slowly due to reduced aquifer recharge. Furthermore, SGD away from shore resulting from longer/deeper flow paths may increase on a time scale of weeks to months following precipitation events due to a lag time and/or as the hydraulic gradient increases due to greater evaporation rates lowering the surface water level more quickly than the water table. The ^{222}Rn-derived SGD fluxes reported here seem high for a semi-arid region rebounding from a multi-year drought compared to results from other regions and other south Texas bays (**Table 2.5**). These ^{222}Rn-derived SGD fluxes are even greater than those measured in the slightly less disturbed similar semi-arid, clay-rich environments of Baffin Bay (Lopez et al. 2018) and Mission-Aransas estuary (Douglas et al. 2017; Spalt et al. 2018) to the north and south, respectively, of Nueces Bay during overlapping sampling periods.

Urquidi-Gaume et al. (2016) used radon to investigate SGD in semi-arid southeastern La Paz Bay, Mexico, and found elevated SGD rates (0.10 – 0.18 $m \cdot d^{-1}$) and nutrient concentrations in winter lagging precipitation by 3 – 4 months. Using radium, Shellenbarger et al. (2006) reported higher than expected SGD fluxes, ranging from 0.06 – 0.26 $m \cdot d^{-1}$, in arid Eilat, Israel, after a 4-year drought and Boehm et al. (2006) reported 0.06 – 0.92 $m \cdot d^{-1}$ in semi-arid Huntington Beach, California. El-Gamal et al. (2012) found low SGD rates (0.02 – 0.06 $m \cdot d^{-1}$) in both wet and dry seasons in the arid Marina Lagoon, Egypt. This lack of a seasonal pattern was attributed to either

SGD-derived from regional aquifers not influenced by recharge from local rainfall or artificial recharge to the surficial aquifer from anthropogenic activities. While these studies demonstrate that elevated groundwater discharge occurs in arid and semi-arid regions following drought conditions, the ^{222}Rn-derived SGD fluxes shown here and in Murgulet et al. (2018) exceed these previous investigations by an order of magnitude in some seasons and are more variable. The large seasonal and spatial SGD variabilities observed with the time-series measurements likely reflect different groundwater inputs (i.e., regional and local), responses to hydroclimatic changes (i.e., recharge to the aquifer following rain events), and anthropogenic influences (i.e., oil/gas activities, dredging). This is also supported by seasonally variable radium ARs, which, as discussed earlier, indicate either the occurrence of deep and shallow groundwater mixing within bay sediments (fall and winter 2014) or responses to heavy precipitation events (fall and winter 2015).

In contrast to ^{222}Rn, ^{226}Ra-derived fluxes generally fall below rates from the above-mentioned investigations, but match the Boehm et al. (2006) range fairly well for rates calculated with the deeper terrestrial groundwater endmember (i.e., the most conservative SGD estimates). However, deeper groundwater input, as suggested by this current study, although likely to occur, is not expected to be predominant or the sole source. Thus, next we are evaluating potential factors leading to these discrepancies, both between methods of measurements and other areas similar in nature. An intercomparison of submarine groundwater discharge estimates using ^{222}Rn, ^{226}Ra, and Darcy estimates in Waquoit Bay, MA, by Mulligan and Charette (2006) found the difference between the total (i.e., ^{222}Rn) and fresh/terrestrial (i.e., Darcy estimates) SGD estimates to be in good agreement with the saline recirculated SGD (i.e., ^{226}Ra) in an unconfined sandy coastal aquifer. However, in the current study, the difference between the average total

and fresh/terrestrial SGD estimates exceeds the saline recirculated SGD estimates by one or two orders of magnitude in all events. Possible causes of discrepancy are overestimation of ^{222}Rn-derived SGD estimates, underestimation of the freshwater terrestrial SGD component by Darcy calculations, or underestimation of the saline SGD component by the ^{226}Ra mass balance. Average ^{222}Rn-derived SGD from stationary measurements are likely overestimated when scaled bay-wide. This overestimation may occur because stationary continuous ^{222}Rn measurements were performed at locations where SGD was expected based on CRP analysis. Nevertheless, the follow-up continuous/mobile ^{222}Rn survey indicates that high ^{222}Rn-derived SGD (0.79 to 1.81 $m \cdot d^{-1}$, $\bar{x}$ = 1.36 $m \cdot d^{-1}$) occurs bay-wide (**Figure 2.5**).

Table 2.5: SGD rates compared to other arid and semi-arid locations. The data range for this study is from the minimum and maximum of all measurements. For the radium SGD for this study, results from the deep groundwater endmember are provided in parenthesis. The year(s) in which the studies were conducted in the south Texas estuaries are included in parentheses.

Site	Method	SGD (m/d)	References
Eilat, Israel	^{223,224}Ra mass balance	0.06 - 0.26	Shellenbarger et al. (2006)
Marina Lagoon, Egypt	^{222}Rn	0.02 - 0.06	El-Gamal et al. (2012)
Huntington Beach, USA	Ra mass balance	0.06 - 0.92	Boehm et al. (2006)
La Paz Bay, Mexico	^{222}Rn	0.02 - 0.18	Urquidi-Gaume et al. (2016)
Ubatuba, Brazil	^{222}Rn	0.01 - 0.29	Burnett et al. (2008)
Yellow River delta, China	^{222}Rn Ra mass balance	0.08 - 0.14 0.05 - 0.14	Peterson et al. (2008)
Nueces Bay, USA	^{226}Ra mass balance	0.004	Breier and Edmonds (2007)
Mission-Aransas Estuary, USA (2015)	^{222}Rn	0.005 - 0.88	Douglas et al. (2017)
Copano Bay, USA (2017)	^{222}Rn	0.07 - 0.83	Spalt et al. (2018)
Baffin Bay, USA (2016)	^{222}Rn ^{226}Ra mass balance	0.23 - 0.27 0.13 - 0.16	Lopez et al. (2018)
Nueces Bay, USA (2014-2016)	**^{222}Rn** **^{226}Ra mass balance** **Darcy estimate**	**0.13 - 3.85** **0.01 - 0.03** **(0.04 – 0.39)** **0.02 - 8.28**	Murgulet et al. (2018) **This study** **This study**

Darcy calculations rely on hydraulic gradients and hydraulic conductivities from monitoring wells to the bay, but this method is limited by the number of wells with water level data and these calculations do not account for unique geologic features like growth faults that may enhance groundwater discharge. Studies have identified at least three growth faults that transect Nueces Bay (Brown Jr et al. 2005; Hammes et al. 2004) and if these faults are active and extend to the surface within the bay, vertical fluid flow may be enhanced along the fault (Hooper 1991). Furthermore, anecdotal evidence (personal communications with Rick Hay) suggests that growth faults may surface in Nueces County in areas of active oil and gas extraction (**Figure 2.2**). Incised creeks occur in the approximate locations of two of the identified growth faults north of the bay, potentially indicating surfacing of these faults within close proximity to the bay. Additional geophysical investigations are necessary to determine what role, if any, growth faults may play in SGD to Nueces Bay.

Given that porewater throughout the system was always found to be saline, we consider other factors that may influence radium activity, such as the rock source and reactivity of radium within the sediment, all of which can influence the resulting radium ages and ^{226}Ra-derived SGD. Epigenetic, roll-type, uranium deposits occur heterogeneously throughout the regional aquifer system and preferentially leach ^{238}U, the parent of ^{226}Ra, over ^{232}Th, the precursor of ^{224}Ra, from the aquifer, which may then precipitate and concentrate at mineralizing fronts within the aquifer (Hobday and Galloway 1999). Consequently, dissolved ^{226}Ra would be locally concentrated around these uranium deposits, while ^{224}Ra would not, which could contribute to the lower ARs we measure in deep groundwater. Additionally, fault zones may distort the ideal roll geometry of mineralization fronts, which may lead to syndiagenetic uranium formation (the product of circulating, semi-confined groundwater within sediments subject to extreme variations in Eh and

pH) in shallow, reduced, or evaporative facies, such as lakes, ponds, and marshes (Hobday and Galloway 1999). Consequently, more radium may be generated in the shallower aquifers near the growth faults.

Oxidation-reduction reactions accompanying early diagenesis of organic matter can greatly influence the chemical nature of estuarine sediments (Kadko et al. 1987). The rate of organic carbon accumulation influences the depth into the sediment where reduction processes occur (i.e., rapid carbon accumulation results in the accumulation of manganese oxides within centimeters of the sediment-water interface). As sediments accumulate and are buried, manganese may be mobilized in sediment porewater where it becomes oxidized and precipitates within the shallow oxic zone, thus creating a highly Mn-rich layer. The depth of this layer is principally governed by the balance between downward O_2 diffusion and upward Mn^{2+} diffusion. The discharge of oil-field brines, between 1920s until 1993 into Nueces Bay (D'Unger et al. 1996) is an indication that the presence of a Mn-rich layer may be significant in our study area, as manganese is present in many oil-field brines (Collins 1975). Manganese oxides are important scavengers of radium and other trace elements in marine environments, and the adsorptive properties of the upper sediment column can be significantly altered by the redistribution and concentration of manganese oxides (Kadko et al. 1987). Consequently, dissolved radium in the upwelling groundwater may be sequestered in the bottom sediments as the water passes through reducing fronts or the Mn-rich layer in the upper 1 – 2 m of bay sediments, which leads to lower ^{226}Ra-derived SGD estimates compared to ^{222}Rn-based estimates. Further investigation into the redox chemistry and radium activities within the sediment are needed to elucidate the impact of these processes.

The discharge of oil-field brines may have major effects on SGD estimates, not only related to the possible scavenging of radium (i.e., the Mn-rich layer) and underestimation of discharge rates, but as an unaccounted for source of ^{222}Rn and overestimation of discharge rates. Typical oil-field produced waters from the Corpus Christi area had salinities from 17.5 – 36.3 and ^{226}Ra activities from 240 – 3,470 dpm·100L^{-1} (Kraemer and Reid 1984). Given the density of these produced waters, they would likely have downwelled into the sediments where, depending on the redox conditions, organic matter concentrations, salinity, and temperature, the dissolved ^{226}Ra and other contaminants may have become sediment bound (Warner et al. 2013), thus potentially contributing to the higher observed ^{222}Rn activities and lower dissolved ^{226}Ra activities in porewater. The greatest density of historic discharge locations occurs around White Point, in the north-western portion of the bay (**Figure 2.1C**), which also coincides with the region of greatest hydraulic gradients (**Figure 2.1B**).

Findings here indicate that to select the most appropriate SGD tracer in any given system, several factors must be considered: tracer enrichment in the groundwater/porewater relative to surface water, tracer reactivity in the environment, and the ability to quantify the sources and sinks of naturally occurring tracers (Santos et al. 2008b). As discussed above there are many processes that may influence the activities of dissolved radium within a system, whereas ^{222}Rn is conservative which simplifies analysis of its sources and sinks. On all accounts, ^{222}Rn appears to be the preferred groundwater tracer in this system.

2.4 Conclusions

The objectives of this study were to examine the spatial and temporal variability of SGD in a semi-arid, micro-tidal, highly anthropogenically disturbed bay dominated by low hydraulic conductivity sediments through the application of several techniques to account for all

components of SGD. In this study: 1) continuous resistivity surveys showed resistivity anomalies that were identified as buried oil/gas pipelines and potentially significant groundwater seepage faces in the lower Nueces River, near the river mouth, and in the middle and along the northern shore of Nueces Bay; 2) a CRP in conjunction with a continuous ^{222}Rn survey highlighted the influence of different lithologies on SGD rates with the greatest SGD rates observed in higher hydraulic conductivity sediments and at transitions from low hydraulic conductivity mid-bay sediments to higher hydraulic conductivity north- and south-bay sediments; 3) radium activity ratios reveal useful information for groundwater source identification with surface water ratios following two distinct trends that suggest a high AR shallow groundwater source or a low AR deep groundwater source; porewater AR align very well with the average AR of all groundwater, an indication that source mixing occurs in the subsurface beneath the bay; and 4) ^{226}Ra-derived (saline/recirculated) estimates fall short of ^{222}Rn-derived (total) SGD due to inability to account for radium tracer reactivity within the sediment; however, local Darcy (fresh/terrestrial) estimates agree well with the range of ^{222}Rn-derived SGD estimates, likely due to the steeper gradients near shore. Results of this study indicate that semi-arid systems receive significant SGD and that highly anthropogenically disturbed systems may experience SGD from both shallower/shorter and deeper/longer groundwater flowpaths, and potentially lag the climatic conditions by weeks (surficial aquifers) and months or longer (deeper aquifers). This study demonstrates the importance of characterizing natural heterogeneities (i.e., sediment type, depositional environment, growth faults) and anthropogenic disturbances (i.e., oil/gas drilling, dredging, oil-field brine discharges) within a system to improve understanding of spatial and temporal variations in SGD rates.

This investigation demonstrated that ^{222}Rn is the preferred groundwater tracer in Nueces Bay because it is enriched in groundwater and porewater compared to bay waters and is non-reactive compared to radium. To further understand the processes controlling radium cycling in this system, a detailed study of bay sediment and porewater composition/chemistry is necessary to address: 1) any legacy radionuclide deposits from historic oil-field brine discharges that may not be accounted for in the ^{222}Rn mass balance and thus contribute to the high ^{222}Rn-derived SGD rates; 2) the redox conditions within the sediment that influence the cycling of Ra in the subsurface and may contribute to changing activity ratios as Ra isotopes cycle through adsorption/desorption from sediment particles; and 3) the depth and thickness of the Fe and Mn (hydr)oxide-rich layer that may sequester Ra from the upwelling groundwater. Additionally, further geophysical investigations (i.e., seismic surveys) of the bay are needed to reveal the location(s) of growth faults throughout the bay where future SGD studies could focus to determine whether the faults contribute to SGD. Future studies in regions with active oil/gas extraction should consider the linkage between anthropogenic disturbances (i.e., oil/gas extraction, drilling, dredging) and natural subsurface heterogeneities (i.e., hydroclimatic and hydrogeologic setting, growth faults) as they could alter groundwater flowpaths and create conduits for deeper groundwater and nutrient inputs via SGD.

Acknowledgements

Texas Sea Grant (award number: NA14OAR4170102), Texas General Land Office (award number: NA13NOS4190113), and the Center for Water Supply Studies at Texas A&M University-Corpus Christi financially supported this research and ARD's dissertation from which this paper has been derived. The authors thank all those who assisted in the lab and/or in the

field, namely: Nicholas Spalt and Melissa Treviño. We would like to thank Dr. Paula Rose for her advice and help in developing our radium methodology. The authors would also like to thank Dr. Nelun Fernando and the Texas Water Development Board for their assistance with retrieving freshwater inflow data and processing groundwater samples, respectively. Finally, the authors thank the reviewers for their comments. All views, opinions, findings, conclusions, and recommendations expressed in this material are those of the authors and do not necessarily reflect the opinions of the Texas Sea Grant College Program or the National Oceanic and Atmospheric Administration.

Supplementary Material

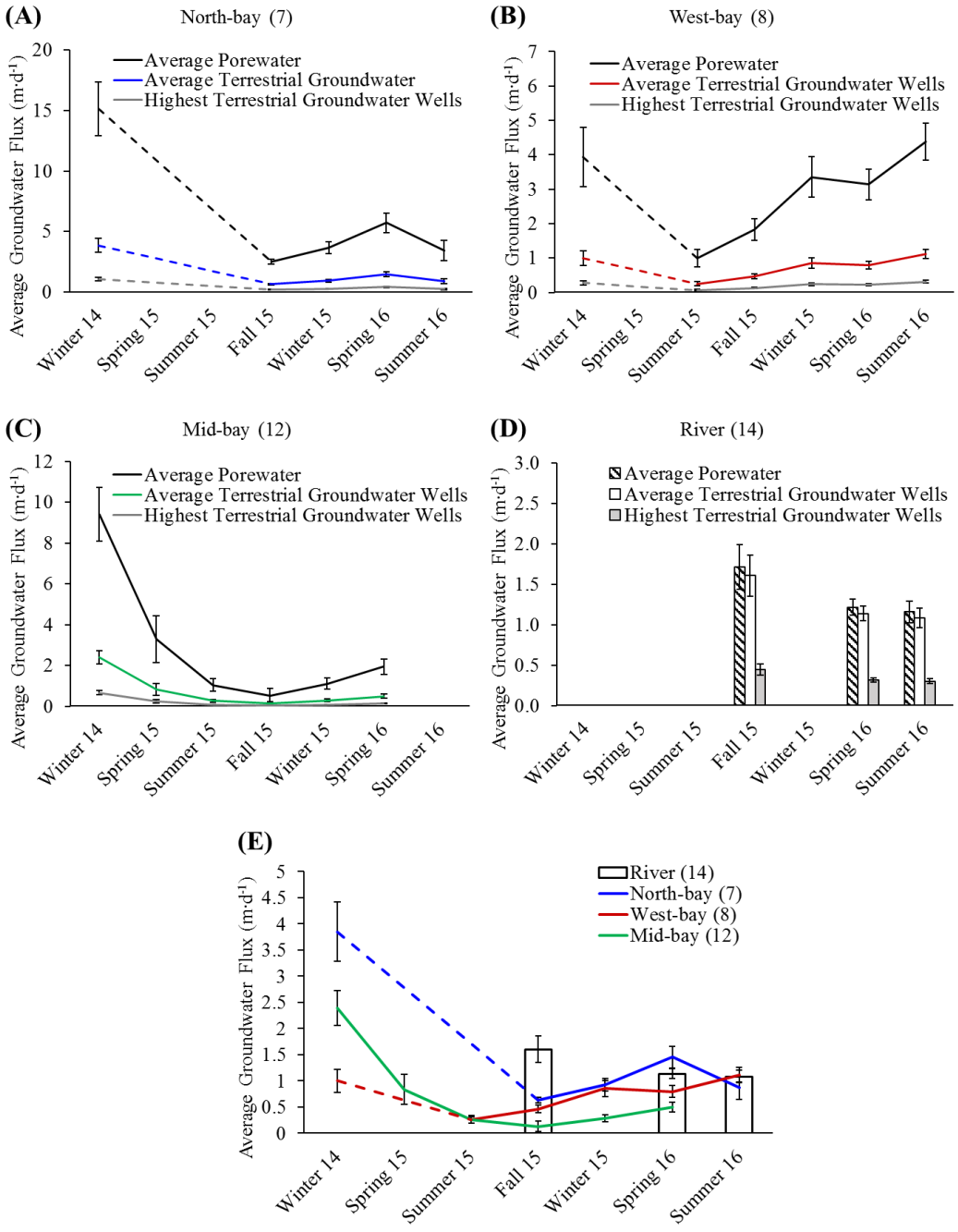

Figure 2.S1: Seasonal average groundwater fluxes ($m \cdot d^{-1}$) derived from radon mass balance model for North-bay (A, blue), West-bay (B, red), Mid-bay (C, green), the river (D, no fill), and comparison of all four stations utilizing most representative ^{222}Rn endmember (E). Three ^{222}Rn

endmembers are represented: average porewater (black line or black slash), average terrestrial groundwater (color line or no fill), and highest terrestrial groundwater (grey line or grey fill). Error bars show 1σ standard deviations.

Table 2.S1: Terrestrial groundwater sampling depth below ground surface (bgs), dissolved oxygen (DO), salinity (Sal), pH, ^{222}Rn, ^{224}Ra, ^{226}Ra, and ^{224}Ra/^{226}Ra activity ratios.

ID	Date	Latitude	Longitude	Depth (m)	DO (mg·L^{-1})	Sal	pH	^{222}Rn (dpm·100L^{-1})	^{224}Ra (dpm·100L^{-1})	^{226}Ra (dpm·100L^{-1})	224:226
8311101	5/19/2015	27.87361	-97.716388	68	1.9	1.9	7.86	27,282	35	26	1.3
7958108	5/23/2015	28.12203	-97.86046	82	0.7	4.0	6.57	143,359	96	239	0.4
7958107	5/23/2015	28.12361	-97.861111	82	0.5	0.7	7.50	---	38	57	0.7
7957605	5/26/2015	28.070277	-97.883054	60	2.8	1.1	7.07	30,706	139	54	2.6
8301901	5/26/2015	27.88111	-97.904444	88	2.2	0.9	7.32	43,755	43	42	1.0
7960616	5/27/2015	28.071943	-97.534166	177	0.3	0.7	7.89	66,973	21	44	0.5
Avg.				92.8	1.4	1.6	7.37	62,415	62	77	1.1
W1-HBP	10/26/2015	27.870091	-97.644143	7	2.5	12.3	6.39	36,058	650	67	9.7
W2-HBP	10/26/2015	27.870079	-97.644137	3	2.1	27.4	5.93	48,453	713	23	31.2
W3-HBP	10/7/2015	27.865682	-97.639244	3	1.0	4.0	6.92	37,499	794	97	8.2
W4-HBP	10/7/2015	27.86569	-97.639268	7	2.9	6.1	6.82	34,302	747	89	8.4
Avg.				5	2.1	12.5	6.52	39,078	726	69	14.3

Table 2.S2: Porewater sampling depth below ground surface (bgs), dissolved oxygen (DO), salinity (Sal), pH, and ^{222}Rn for spatial sampling.

Season	Station	Depth (m bgs)	DO ($mg \cdot L^{-1}$)	Sal	pH	^{222}Rn ($dpm \cdot 100L^{-1}$)
Fall 2014	1	0.7	0.3	38.6	7.49	43,322
Winter 2014	8	1.2	0.4	25.4	6.92	1,980
	9	1.5	4.5	34.9	7.82	13,434
Spring 2015	3	1.6	1	36.7	7.32	14,268
	11	2	0.9	33.1	7.07	2,334
	14	1.8	1.4	31.5	7.33	53,568
	15	1.6	0.8	40.7	6.79	35,178
Summer 2015	1	2	0.4	30.5	7.44	15,666
	3	1	0.5	31.9	7.25	
	9	2.25	0.7	25.1	7.06	5,094
	15	1.5	1.2	39.7	6.73	68,364
Fall 2015	7	2	1.1	32.1	7.73	3,024
	14	1	2.7	23.6	7.66	30,720
Winter 2015	3	0.5	---	37.7	7.35	4,764
	11	0.25	---	35.8	---	29,928
	14	0.5	---	28.9	7.55	19,476
	15	1	---		7.45	21,780
Spring 2016	3	1.5	2.7	31.4	7.13	---
	4	1.4	2.4	31.6	6.99	---
	8	2.3	2.6	27.3	7.21	---
	14	1.9	2.2	27.2	6.56	30,516
	15	1.7	2.3	38.7	7.07	82,740
Summer 2016	1	2	1	35.5	7.42	20,580
	3	1.9	0.7	30.3	7.11	2,790
	11	3.4	0.7	40.8	7.22	2,292
Avg. all		**1.3**	**1.5**	**32.6**	**6.92**	**23,896**

CHAPTER III: HYDROCLIMATIC VARIABILITY DRIVEN SUBMARINE GROUNDWATER DISCHARGE AND NUTRIENT FLUXES IN AN ANTHROPOGENICALLY DISTURBED, SEMI-ARID ESTUARY

Published as: Douglas, A. R., D. Murgulet, P.A. Montagna (2020). "Hydroclimatic variability drives submarine groundwater discharge and nutrient fluxes in an anthropogenically disturbed, semi-arid estuary." Science of The Total Environment **755**.

Figure 3.1: Graphical Abstract

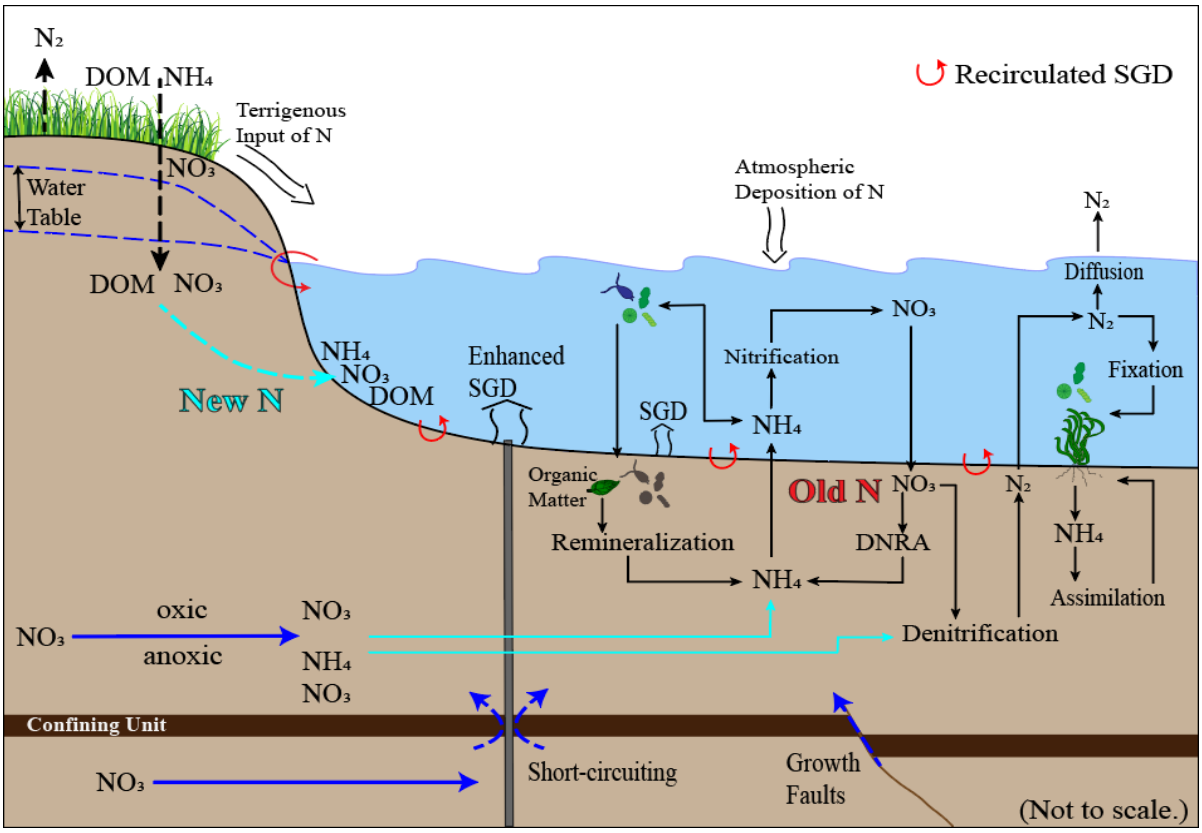

Abstract

Nutrient budgets in semi-arid estuaries, with ephemeral freshwater inflows and limited nutrient sources, are likely incomplete if contributions from submarine groundwater discharge (SGD) are not included. Here, the relative importance of saline/recirculated SGD-derived nutrient fluxes spatiotemporal variability to the overall nutrient budget is quantified for Nueces

Bay, Texas, U.S.A., across hydroclimatic conditions ranging from drought to normal, to flood. On average, 67% of the variance in water quality is due to temporal differences while 16% is explained by spatial differences. Principal component analysis (PCA) reveals three principal components: freshwater inflow (PC1 28.8%), saline/recirculated SGD and recycled nitrogen (PC2 15.6%), and total SGD and "new" nitrogen (PC3 11.2%). Total SGD porewater fluxes ranged from 29.9-690.3 $mmol \cdot m^{-2}d^{-1}$ for ammonium, 0.21-18.7 $mmol \cdot m^{-2}d^{-1}$ for nitrite+nitrate, 3.1-51.3 $mmol \cdot m^{-2}d^{-1}$ for phosphate, 57.1-719.7 $mmol \cdot m^{-2}d^{-1}$ for silicate, and 95.9-36,838.5 $mmol \cdot m^{-2}d^{-1}$ for dissolved organic carbon. Total and saline/recirculated SGD fluxes were on average 150 - 26,000 and 5.8 - 466 times, respectively, greater than surface runoff fluxes across all seasons. Nitrogen (N) enrichment in porewater occurs near the agricultural fields because of soil N flushing and percolation to groundwater, which facilitates N-rich groundwater fluxes. There were substantial "new" N inputs from terrestrial groundwater following precipitation while saline/recirculated SGD of recycled N accounts for only <4 % of total SGD inputs. The "new" N inputs occur in the river and river mouth during flooding, and near the north shore where topography and hydraulic gradients are steeper during drought. Thus, while significant inputs of N may be associated with atmospheric deposition, or remineralization in the porewater, groundwater is the highest contributor to the nutrient budget in Nueces Bay. This result implies that nutrient management strategies should focus on land-use practices to reduce N contamination of shallow groundwater and subsequent contamination of estuaries.

3.1 Introduction

Estuarine eutrophication and hypoxia events have increased as a result of nutrient loading to coastal catchments from human population growth, urbanization, and agricultural and industrial

expansion (Bruesewitz et al. 2015; Kennish 2002; Paerl 2009; Scavia and Bricker 2006). As development of coastal regions continues to grow, understanding nutrient inputs and cycling along freshwater-marine gradients is essential to inform nutrient management strategies (Paerl 2009). Along with changing land use, estuaries are influenced by variable hydrological patterns. The patterns of surface runoff and submarine groundwater discharge (SGD) play a critical role in the timing and amount of freshwater, nutrients, organic matter, and sediments delivered to estuaries (Bruesewitz et al. 2015; Mooney and McClelland 2012; Paudel and Montagna 2014; Santos et al. 2013; Urquidi-Gaume et al. 2016). Estuaries in semi-arid regions are subject to sporadic precipitation events that result in generally low riverine inflows and episodic flood events (Montagna and Kalke 1992; Murgulet et al. 2016). Climate projections indicate intensification of periods of drought and episodes of flooding (Stocker 2014; Trenberth et al. 2003). Significant changes in hydrologic conditions are expected with the predicted increase in frequency and intensity of storms as a result of climate change (Rabalais et al. 2009; Stocker 2014), thereby altering patterns of nutrient transport between terrestrial and marine environments.

SGD has been recognized as an important pathway that transports water and solutes from terrestrial to marine environments (Burnett et al. 2003; Moore 2010; Taniguchi et al. 2002). Nutrient input via SGD rivals riverine inputs in some regions and may contribute significantly to nutrient cycling and primary productivity in coastal oceans (Peterson et al. 2008; Slomp and Van Cappellen 2004; Valiela et al. 1990). The potential impact of even a small volume of SGD may be equal to, or greater than, riverine inputs because the concentrations of nitrogen (N) in coastal groundwater is often much more enriched comparable to surface waters (Valiela et al. 1990). In addition, SGD may play a significant role in nutrient cycling and primary productivity in coastal

oceans (Peterson et al. 2008; Slomp and Van Cappellen 2004; Valiela et al. 1990). While additional inputs of nutrients from SGD may be beneficial to the coastal ecology in some areas (Peterson et al. 2008), they were also found to be detrimental when the extent and timing of inputs coincided with harmful algae bloom events (i.e., eutrophication). When in excess, the SGD-derived nutrients can lead to regional increases in primary production, decreases in seagrass beds, and play a role in the extent of coastal hypoxia.

Many studies have assessed the quantity of SGD and the corresponding nutrient fluxes to coastal waters (Charette et al. 2001; Hwang et al. 2016; Luo et al. 2014; Rodellas et al. 2014; Santos et al. 2013; Spalt et al. 2020; Swarzenski et al. 2007a; Urquidi-Gaume et al. 2016) or the processes influencing nutrient levels and distributions in surface water (Bruesewitz et al. 2015; Paudel et al. 2019). However, it is likely that groundwater inputs and changes of these fluxes vary at seasonal scales (Charette 2007; Sugimoto et al. 2016; Szymczycha et al. 2020) and with extreme hydroclimatic conditions, such as drought and flooding (Majidzadeh et al. 2017). This research investigated the spatial and temporal changes of inorganic and organic nutrients in a semi-arid estuary relative to the role of SGD-derived nutrients. This study is unique in that it estimated SGD-derived nutrient fluxes based on SGD rates and porewater and groundwater concentrations for a semi-arid estuary across hydroclimatic conditions ranging from drought to flood to "normal" semi-wet conditions. The specific objectives of the present study were to: 1) identify the spatial and temporal changes in inorganic and organic nutrients in semi-arid estuaries across variable hydroclimatic conditions, 2) assess temporal changes in nutrient fluxes to the bay in response to drought, flooding, and typical conditions, and 3) assess the role of SGD-derived nutrients to nutrient budgets under changing hydroclimatic conditions. In addition to a dense spatial sampling of bay waters, to better constrain the nutrient inputs to the estuary, both river

and benthic endmembers were evaluated. The influence of SGD-derived nutrients on the system was evaluated through the application of multivariate statistics.

3.2 Methods

3.2.1 Study Area

Nueces Bay (NB), located on the south Texas Gulf of Mexico coast, is a semi-arid, microtidal, secondary bay in the Nueces Estuary system (**Figure 3.1**). Nueces Bay is ~75 km^2 in area with an average depth of 0.7 m and no direct connection to the Gulf of Mexico. (Diener 1975; NBBEST 2011). The area is characterized by dry to sub-humid climate with annual precipitation averaging around 76.2 cm and an average evaporation rate of 145 cm (Ockerman 2001; Shafer 1968). Persistent winds (17-18 $km \cdot h^{-1}$) result in a generally well-mixed water column and increased turbidity due to sediment resuspension (Ockerman 2001). The primary source of surface water to Nueces Bay comes from Nueces River; however, low precipitation in the watershed and dams and diversions on the river limit riverine discharge. Thus, the lower Nueces River, below the saltwater barrier dam at Labonte Park (**Figure 3.1**), received little freshwater inflows throughout most of the year and is tidally influenced. These conditions result in high average salinities and often low nutrient levels (Longley et al. 1994). Entering the study period (December 2014 through August 2016), the southern United States and Mexico were experiencing one of the strongest multi-year (4 - 5 years) droughts on record, which ended in spring 2015 (Murgulet et al. 2017; TWDB 2017). Murgulet et al. (2016) and Douglas et al. (2020b) provide more detailed information on hydroclimatic variability and freshwater inflows, and the impact of hydrological alterations on stream and groundwater flow in Nueces River.

Nueces Bay falls within the Gulf Coast Aquifer (**Fig. 3.1A**), a leaky artesian aquifer with a layered stratigraphy of alternating and intermixed silt, clay, sand, and gravel lenses forming the

Chicot, Evangeline, and Jasper aquifers (Ashworth and Hopkins 1995; Shafer 1968; Waterstone and Parsons 2003). Nueces Bay and the surrounding systems are generally in direct contact with the Chicot aquifer, which extends 366 m below ground surface (bgs) (Chowdhury et al. 2004; Mace et al. 2006). Additionally, a considerable amount of water discharges upward from the Evangeline, which extends 793 m bgs, into the Chicot aquifer in southern Texas. Most shallow groundwater, i.e., <150 m bgs, in south Texas is brackish to saline with areas of high salinity occurring locally (Kreitler 1993). Generally, hydraulic conditions drive groundwater flows toward the river and the north shore to eventually discharge into the bays and estuaries (Bighash and Murgulet 2015; Breier et al. 2010; Nyquist et al. 2008). Bay surface sediments are predominantly sandy to silty-sand across the north-bay, silty-sand at the Nueces River mouth, clayey-sand to clayey-silt throughout the west-bay and across the south-bay, and silty-clay in the middle of the bay and the lower Nueces River (Shideler et al. 1981). More detailed information about aquifer characteristics are provided elsewhere (Douglas et al. 2020b; Waterstone and Parsons 2003; Young et al. 2016).

Previous studies of SGD in this bay by Breier et al. (2010) and Douglas et al. (2020b), found similar SGD rates from excess ^{226}Ra but Douglas et al. (2020b) found 1-2 orders of magnitude greater SGD rates from excess ^{222}Rn. Further, previous nitrogen budgets for Nueces Estuary and Nueces Bay generated net negative balances (Anchor QEA 2017; Brock 2001); however, these budgets did not account for SGD-derived nitrogen (Brock 2001), nor total nitrogen (Anchor QEA 2017). Thus, the SGD-derived solute fluxes are potentially substantial in semi-arid Nueces Bay.

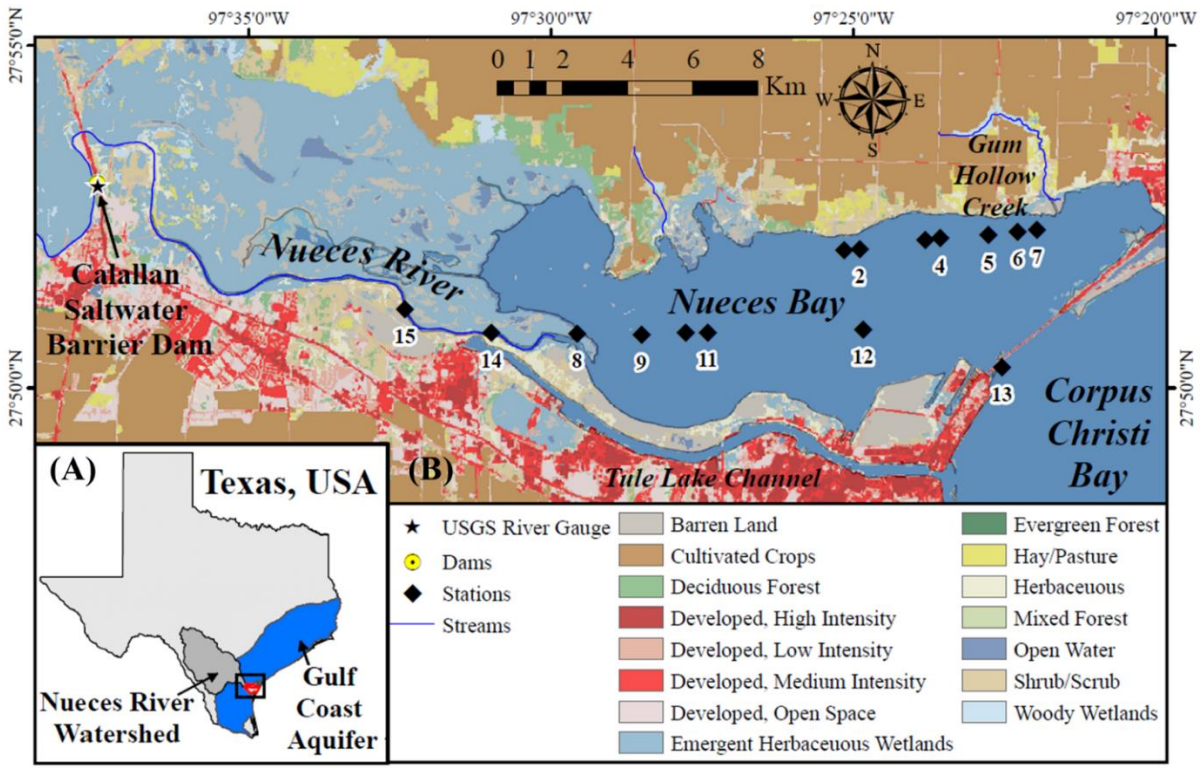

Figure 3.1: Study Area. A) Inset of Texas, USA with location of the aquifer and watershed. B) Location of sample stations in Nueces Bay, Texas.

3.2.2 Sample Collection and Analysis

This study was conducted from September 2014 through July 2016. Surface water and porewater were sampled quarterly according to the Van Dorn and push-point piezometer methods previously outlined in Murgulet et al. (2018) and Douglas et al. (2020b). Water quality variables used for the present study were temperature (temp), salinity (sal, practical salinity scale; the averaged salinity in the global ocean of 35 is used as the reference (Millero 1993)), pH, secchi depth, chlorophyll-α (chl-α), dissolved organic carbon (DOC), total dissolved nitrogen (TDN), ammonium (NH_4^+), nitrate+nitrite ($NO_{2\text{-}3}^-$), orthophosphate (PO_4^{3-}), silicate (SiO_4^{4-}), stable isotopes of nitrate ($\delta^{15}N$ and $\delta^{18}O$), and radioisotopes of radon (^{222}Rn) and radium (^{224}Ra and ^{226}Ra). Details of radioisotope sample collection, sampling stations, water quality

parameters, and procedures to measure radioisotopes and water quality parameters are presented in detail elsewhere (Douglas et al. 2020b; Murgulet et al. 2018; Nelson and Montagna 2009).

3.2.2.1 Chlorophyll-α and Nutrients

Surface water samples were filtered (GF/F filter paper) on site and then stored frozen until analysis. Chlorophyll-α was measured with a Turner Design Trilogy fluorometer within 12-16 hours of methanol addition using a methanol extraction method (Krauk et al. 2006; Montagna et al. 2018; Paudel et al. 2019).

Inorganic nutrient measurements were carried out using an OIA Flow Solution autoanalyzer with computer-controlled sample selection and peak processing. The ranges of detection are 0.25-10.0 μM for $NO_{2\text{-}3}^-$, 0.25-10.0 μM for NH_4^+, 0.10-10.0 μM for PO_4^{3-}, and 10.0-300.0 μM for SiO_4^{4-} (Paudel et al. 2019 and references therein). Concentrations in samples exceeding detection limits (i.e., porewaters) were determined through dilution, whereas samples below detection limit were considered as half of the detection limit. DOC and TDN measurements were conducted using a Shimadzu TOC-V analyzer with nitrogen module. Dissolved organic nitrogen (DON) was estimated as the difference between TDN and dissolved inorganic nitrogen ($DIN=NO_2^-+NO_3^-+NH_4^+$). Ammonium was not removed from TDN samples prior to measurement, thus, only surface water samples, in which ammonium is expected to be relatively low, are used for calculating DON and included in analysis. Only samples with N content ≥0.07 $mg \cdot L^{-1}$ as N were sent for measurement of stable isotopes of nitrate ($\delta^{15}N$ and $\delta^{18}O$). Nitrogen and oxygen isotope ratios of NO_3^- were measured at Colorado Plateau Stable Isotope Laboratory, Northern Arizona University, using the denitrifier method. Nitrite was not removed from these samples; however, NO_3^- and NO_2^- data from this system (Murgulet et al. 2019) shows that NO_2^- accounts for less than 21% of $NO_2^-+NO_3^-$ in surface water and less than 14% in porewater. Thus,

NO_2^- was interpreted as NO_3^-. Typical standard deviations (1σ) for isotopic measurements are 0.2‰ for $\delta^{15}N$ and 0.5‰ for $\delta^{18}O$ (Murgulet and Tick 2013 and references therein).

3.2.2.2 SGD-derived Nutrient Fluxes

SGD rates, determined from radon and radium mass balances from companion studies Murgulet et al. (2018) and Douglas et al. (2020b), were used to calculate the nutrient inputs from total and recirculated/saline SGD. Event average porewater nutrient concentrations ($\mu mol \cdot L^{-1}$) were multiplied by the SGD rate ($m^3 \cdot d^{-1}$) for each season. Other studies have shown that samples high in ammonium, as expected in porewater (Burdige and Zheng 1998; Murgulet et al. 2019), may create interference during the TDN analysis (Burdige and Zheng 1998). Thus, for assessment of the influence of groundwater fluxes on the nitrogen budget of Nueces Bay, porewater samples from June 2015 through March 2016 were processed to remove NH_4^+. Ammonium was removed from these porewater samples prior to DOC/TDN analysis by: 1) raising the pH of each sample to ~12 with a 10 M NaOH solution, 2) sparging the sample with N_2 gas, and 3) lowering the pH to ~2 with 10 M phosphoric acid for analysis (Burdige and Zheng 1998).

3.2.3 Statistical Analyses

The goal was to test for spatial differences within the study area over time and different hydroclimatic conditions. Region classifications were predetermined to separate mixing endmembers (i.e., Nueces River [NR], Nueces River mouth [RM], Corpus Christi Bay [CCB]) and spatial variability of sediment types (i.e., north bay silty-sand [NB], mid-bay silty-clay [MB], and west-bay sandy-silt [WB]). Surface water and porewater samples were assessed separately due to an unbalanced number of samples collected for porewater compared to surface water.

3.2.3.1 Principal Components Analysis (PCA)

Principal components analysis (PCA) was performed to analyze the relationship between inorganic and organic nutrients, SGD tracers, and other water quality parameters. PCA allows for the reduction of complex multivariate datasets into smaller more manageable datasets by analyzing inter-correlations among observed variables, or scores, and extracting latent factors that better explain the underlying processes responsible for the variations observed (Bighash and Murgulet 2015; Murgulet et al. 2015). Factors are extracted in the order of importance based on the weight, or eigen-value, of each factor on the overall model. Generally, only factors with eigen-values greater than 1 are considered. The results are presented graphically as vector plots in which the position and length of each vector represents the relationship and weight of that variable to the defined latent factor. The closer the vectors are aligned to an axis, the more that vector's variable is correlated with the factor represented on that axis (Murgulet et al. 2015). Most statistical analyses were run using SAS software suite (SAS 2017). Before the analysis, data were standardized to a normal distribution using PROC STANDARD so that scales were the same for all variables. PCA was performed using the PROC FACTOR procedure (Paudel et al. 2019) in principal components mode with VARIMAX rotation for axis rotation.

3.2.3.2 Analysis of Variance (ANOVA)

A two-way ANOVA was performed to analyze variations in the inorganic and organic nutrients, and hydroclimatic and SGD indicators (i.e., salinity, Rn, and Ra) between different regions within the bay. Samples were collected from stations within each region as defined earlier; thus, stations are nested within the regions. The experimental design is partial-hierarchical two-way ANOVA that can be described by the following statistical model: $Y_{ijkl} = \mu + \alpha_j + \beta_k + \alpha\beta_{jk} + \gamma_{k(l)} + \varepsilon_{(i)jkl}$, where Y_{ijkl} is the dependent response variable; μ is the overall

sample mean; α_j is the main fixed effect for sampling date where j = 1 to 8; β_k is the main fixed effect for region where k = 1 to 6 for either NR, RM, WB, MB, NB, or CCB; $\alpha\beta_{jk}$ is the main fixed effect for the interaction between dates and regions; $\gamma_{k(l)}$ is the main effect for stations that are nested (or unique) to the regions and are thus a random effect as denoted by the parentheses around the subscript l that represents the 15 stations; $\varepsilon_{(i)jkl}$ and in the random error term for each of the i measurements within cells. This model was computed using PROC GLM. The expected mean squares (EMS), variance components, and correct F-tests were also computed because this is a mixed model. The F-test for date, date*region interaction, and station(region) is formed by dividing the EMS for the main effects by the mean square error. The F-test for the regions is formed by dividing the EMS for the main effect by the sum of EMS of the station effect and the mean square error.

A one-way model was applied to the porewater samples from each station and between each sampling event, where sampling data was the main effect and stations were the replicates. A Tukey post hoc multiple comparisons test was performed to identify the difference among group means. Pearson's correlation was performed between nutrients and hydroclimatic and SGD indicators to assess the link between these variables.

3.3 Results

3.3.1 Surface Water Salinity, Nutrients, and Chlorophyll-α

Salinities were different seasonally and spatially (ANOVA, $p < 0.0001$). The results of the Tukey test confirmed the major hydroclimatic events as defined, i.e., the prior drought (September 2014 and December 2014), flood (June 2015), and normal designations (April 2015, September 2015, December 2015, March 2016). Though June 2016 is different from the other seasons in the normal designation (Tukey Test), this is due to the considerably lower salinities in

the river (0.91 – 7.41; **Figure 3.2E**) following some moderate precipitation events. However, the bay salinities are in the same range as the other seasons in the normal designation. Across all seasons, Nueces River salinities were substantially lower than any bay regions by 1.5 to 21 times.

The first three principal components, PC1, PC2, and PC3, explained 28.8%, 15.6%, and 11.2%, respectively, of the variation in surface water in all seasons for a total of 55.5% of the variability (**Figure 3.2**). PC1 had temperature, chl-α, PO_4^{3-}, SiO_4^{4-}, and DOC that were inversely correlated with salinity (**Figure 3.2A, 3.2D**). Thus, PC1 represents freshwater inflow such that when river discharge rates are high, salinity is low, and nutrient concentrations are high. PC2 revealed that AR, DON and NH_4^+ are inversely correlated to pH (**Figure 3.2A**). Thus, PC2 represents recycled or "old" N as AR represents the saline/recirculated component of SGD and DON and NH_4^+ are the reduced species of N. PC3 revealed that Rn and $NO_{2\text{-}3}^-$ are positively correlated to each other (**Figure 3.2D**). Thus, PC3 represents the "new" N as Rn represents total SGD (i.e., terrestrial+recirculated or fresh+saline) which brings $NO_{2\text{-}3}^-$ directly into the system or converts NH_4^+ to $NO_{2\text{-}3}^-$ through nitrification in the more oxic top few mm of the sediment layer when the bottom water column is oxic (Jäntti and Hietanen 2012) or through ammonium oxidation coupled to Mn reduction (i.e., anoxic nitrification) (Mortimer et al. 2004). The June 2015 flood event and NR samples have the highest PC1 scores and are followed in magnitude by September 2015 flooding recession, whereas the NB, MB, and CCB regions exhibit the lowest PC1 scores, which indicates that freshwater inflow had the greatest effect in the tidal river and during flooding (**Figure 3.2B, 3.2C**). Samples from before the flood event (i.e., September 2014, December 2014, and April 2015) had higher PC2 scores compared to samples following the flood event (i.e., September 2015, December 2015, and March 2016), which indicates greater

contributions of "old" N and saline/recirculated SGD before flooding than following flooding. December 2014, June 2015, December 2015, and June 2016 had the higher PC3 scores, particularly in NR and NB, compared to scores for April 2015, September 2015, and March 2016, particularly in CCB, NB, and MB, indicating that the total SGD and "new" N are greater in the river and nearer shore than further offshore in the bay (**Figure 3.2E, 3.2F**).

There were temporal differences for all variables (**Table 3.1A and Figure 3.3**). For all variables except, pH, NH_4^+, ^{224}Ra, ^{226}Ra, and radium activity ratios, there were spatial differences. Within regions, there were differences by station for temperature, salinity, chl-α, TDN, DON, NH_4^+, PO_4^{3-}, SiO_4^{4-}, Rn, ^{224}Ra, and ARs, but not for secchi, DOC, NO_{2-3}^-, and ^{226}Ra (**Table 3.1A**). Temperature, which varies seasonally, had 99% of its variation explained by season (**Table 3.1B**). All other variables had at least 49% of their variability explained by sampling date except for NO_{2-3}^- (21%). Overall, the average variance explained by date was 67%, by region was 14%, and by station was 8%. Thus, spatial variance is responsible for approximately 22% of all variability on average, which is one-third of the variability accounted for by temporal variance. Therefore, temporal variance exhibits greater control on discharge and geochemical perturbations in semi-arid estuaries.

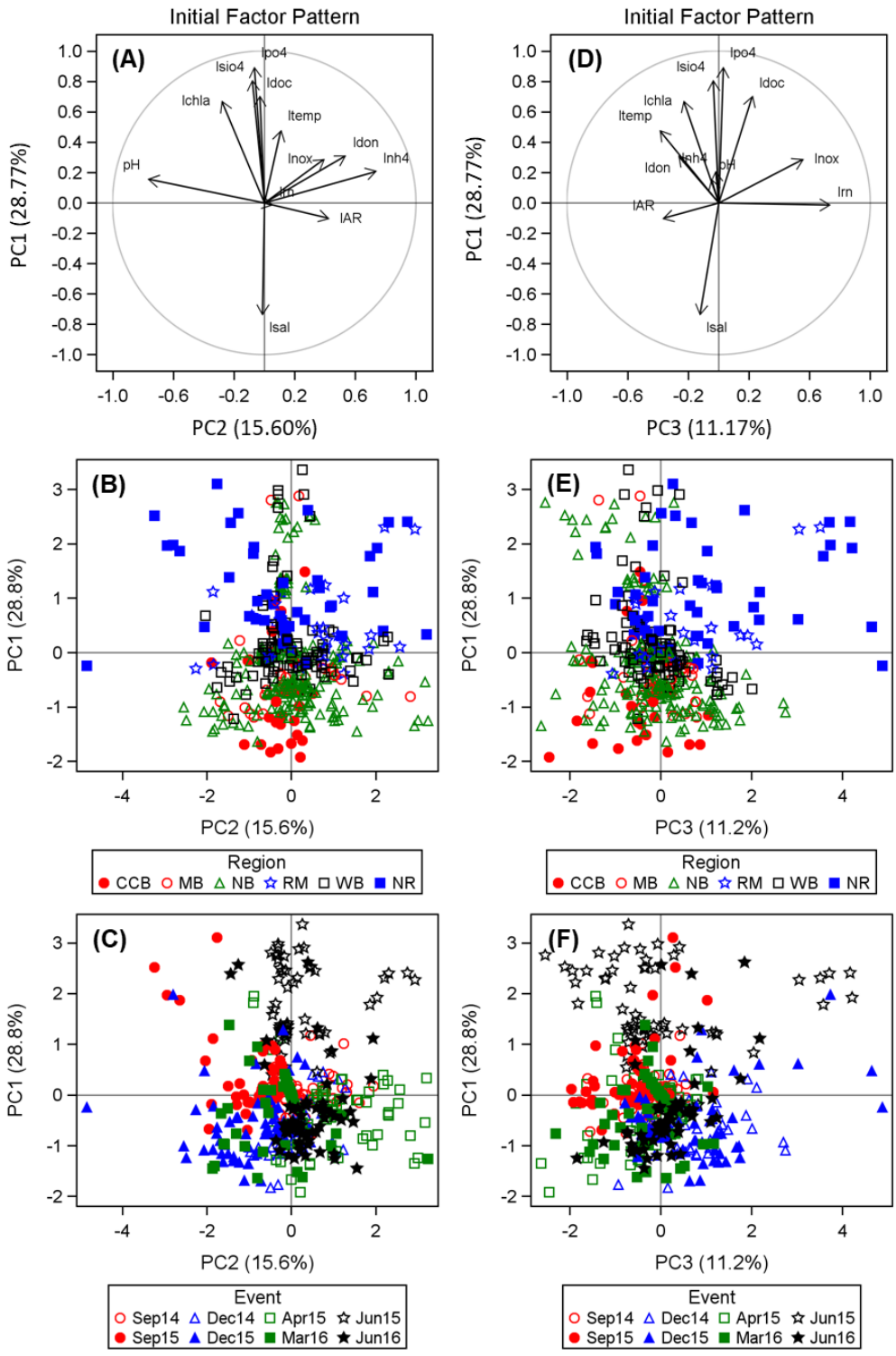

Figure 3.2: Principal components (PC) analysis of water quality and SGD tracers. A) Variable loads for PC1 and PC2. B) Sample scores by region for PC1 and PC2. C) Sample scores by

sampling event for PC1 and PC2. D) Variable loads for PC1 and PC3. E) Sample scores by region for PC1 and PC3. F) Sample scores by sampling event for PC1 and PC3. Abbreviations: temp, temperature; sal, salinity; chl-a, chlorophyll-α; doc, dissolved organic carbon; don, dissolved organic nitrogen; NH4, ammonium; NOx, nitrate+nitrite; PO4, phosphate; SiO4, silicate; Rn, radon-222; AR, radium 224:226 activity ratio; CCB, Corpus Christi Bay; MB, mid-bay; NB, north-bay; WB, west-bay; RM, river mouth; NR, Nueces River.

Table 3.1: Results of ANOVA for each variable. (A) Probability (p) values for null hypothesis in the mixed ANOVA. (B) Variance components analysis.

(A)	**p-values for mixed ANOVA**			
Variable	**Date**	**Region**	**Date *Region**	**Station (Region)**
Temperature	<0.01	0.05	<0.01	0.00
Salinity	<0.01	<0.01	<0.01	<0.01
pH	<0.01	**0.08**	<0.01	<0.01
Secchi	<0.01	0.00	<0.01	**0.18**
Chl-a	<0.01	<0.01	<0.01	<0.01
DOC	<0.01	<0.01	0.03	**0.20**
TDN	<0.01	0.01	**0.06**	0.00
DON	<0.01	0.01	<0.01	0.00
$NO_{2\text{-}3}^-$	<0.01	<0.01	<0.01	**0.06**
NH_4^+	<0.01	**0.27**	<0.01	<0.01
PO_4^-	<0.01	<0.01	<0.01	<0.01
SiO_4^-	<0.01	0.00	<0.01	0.03
Rn	<0.01	0.02	0.00	<0.01
Ra-224	<0.01	**0.71**	0.02	0.00
Ra-226	<0.01	**0.17**	0.00	**0.10**
AR	<0.01	**0.43**	**0.75**	0.05
(B)	**Variance components (percent)**			
Variable	**Date**	**Region**	**Date *Region**	**Station (Region)**
Temperature	99	0.3	0.3	0.2
Salinity	92	5	2	1
pH	49	4	37	10
Secchi	60	29	9	2
Chl-a	52	17	26	4
DOC	50	45	2	2
TDN	74	14	4	9
DON	82	9	5	4
$NO_{2\text{-}3}^-$	21	50	24	5
NH_4^+	78	2	11	9
PO_4^-	88	7	3	2
SiO_4^-	74	14	9	3
Rn	49	19	9	24
Ra-224	60	2	7	31
Ra-226	84	5	7	3
AR	65	9	5	21
Average	67	14	10	8

Surface water NH_4^+ concentrations ranged from below detection limit (0.25 µmol·L^{-1}) to 10.7 µmol·L^{-1} ($\bar{x}$ = 2.02 µmol·L^{-1}; n=222; **Figure 3.3A**) and there was no relationship with salinity. Generally, CCB had the lowest NH_4^+ concentrations, though concentrations increased in December 2015 and March 2016. All other regions followed similar trends with the greatest NH_4^+ concentrations occurring in April 2015 and June 2016 following moderate precipitation. The RM also experienced elevated NH_4^+ concentrations in December 2014.

Nitrite plus nitrate ($NO_{2\text{-}3}^-$) concentrations ranged from below detection limit (0.25 µmol·L^{-1}) to 45.2 µmol·L^{-1} ($\bar{x}$ = 1.97 µmol·L^{-1}; n=230; **Figure 3.3B**) and were generally < 2 µmol·L^{-1}. $NO_{2\text{-}3}^-$ concentrations show no relationship to salinity (**Figure 3.4B**). The highest $NO_{2\text{-}3}^-$ concentrations were measured in NR over three consecutive events: June 2015 (10.1 µmol·L^{-1}), September 2015 (12.3 µmol·L^{-1}), and December 2015 (27.6 µmol·L^{-1}). The RM and NB also had slightly elevated $NO_{2\text{-}3}^-$ concentrations in December 2014 (3.6 µmol·L^{-1} and 3.9 µmol·L^{-1}, respectively) and NR again in June 2015 (6.0 µmol·L^{-1}). Stable isotopes of NO_3^- show large enrichment in $\delta^{18}O$ during drought, which is an indication of wet/dry deposition (**Figure 3.5A**), compared to the relatively lower $\delta^{18}O$ during flooding and normal conditions. Furthermore, a plot of $\delta^{15}N$ vs. 1/[$NO_{2\text{-}3}^-$] (**Figure 3.5B**) shows that most drought samples plot near the mixing trend indicating that atmospheric deposition may be influential on $NO_{2\text{-}3}^-$ concentrations. However, there were large deviations from mixing in the north bay during drought that may indicate groundwater input may originate from anoxic sediments where nitrification/denitrification, with some anammox, is occurring (Granger and Wankel 2016), or reflect a greater influence of NO_2^- fractionation in these low $NO_{2\text{-}3}^-$ concentration samples. The strong positive correlations during flood (r = 0.95, p = 0.0003) and normal conditions (r = 0.64, p

= 0.003) with positive slopes (0.65 and 0.48, respectively) indicate denitrification conditions or that these processes are actively occurring (Granger and Wankel 2016; Kendall et al. 2007).

Surface water PO_4^{3-} concentrations ranged from 0.14 µmol·L^{-1} to 18.2 µmol·L^{-1} ($\overline{x}$ = 2.40 µmol·L^{-1}; n=229; **Figure 3.3C**). NR had significantly higher PO_4^{3-} concentrations than the other regions. PO_4^{3-} decreased along increasing salinity gradient (**Figure 3.4C**) and peaked in all regions during June 2015 flooding. While all other regions' concentrations decreased in September 2015 following flooding, NR's concentration continued to increase until the subsequent December 2015 sampling.

Concentrations of SiO_4^{4-} ranged from 25.7 µmol·L^{-1} to 284.4 µmol·L^{-1} ($\overline{x}$ = 98.9 µmol·L^{-1}; n=230; **Figure 3.3D**) and like PO_4^{3-}, NR had significantly higher SiO_4^{4-} than the other regions and generally decreased along increasing salinity gradient (**Figure 3.4D**). However, unlike PO_4^{3-}, there appears to be production of SiO_4^{4-} under drought conditions. SiO_4^{4-} concentrations peaked during flooding in all regions and remained high in NR and RM in September 2015. NR SiO_4^{4-} concentrations were high in June 2016 while concentrations in all other regions remained low.

Surface water DOC concentrations ranged from 254 µmol·L^{-1} to 756.3 µmol·L^{-1} ($\overline{x}$ = 442.2 µmol·L^{-1}; n=212; **Figure 3.3F**) and were highest in NR and RM and lowest in CCB. Under drought and normal conditions, DOC decreased along an increasing salinity gradient (**Figure 3.4E**). However, under drought conditions there appears to be production of DOC in the RM, WB, MB, and NB.

Concentrations of DON ranged from 3.88 µmol·L^{-1} to 233.8 µmol·L^{-1} ($\overline{x}$ = 24.3 µmol·L^{-1}; n=202; **Figure 3.3G**) and were highest in September 2014 and December 2014 under drought conditions and lowest in September 2015 and December 2015 following flooding. DON concentrations generally decrease along an increasing salinity gradient; however, flood

conditions show some dilution in NR and NB (4.79 – 30.3 μmol·L^{-1}) whereas drought conditions show some input in CCB, NB, WB, and RM (**Figure 3.4F**).

Chl-α concentrations ranged from 0.6 μg·L^{-1} to 103.7 μg·L^{-1} ($\overline{x}$ = 12.4 μg·L^{-1}; n=231; **Figure 3.3H**) with the highest in NR in September 2015 and under flood recession conditions (**Figure 3.4G**). Chl-α peaked in all regions of the bay except NR and RM during flooding. Concentrations peaked at RM in September 2014 and 2015 and at WB in March 2016. NB and CCB generally had the lowest chl-α concentrations across all seasons. Chl-α was negatively correlated with salinity and positively correlated with DOC, $NO_{2\text{-}3}^{-}$, PO_4^{3-}, and SiO_4^{4-}.

Across the sampling dates, PO_4^{3-}, SiO_4^{4-}, and DOC generally decrease linearly with increasing salinity until a salinity of ~33 above which higher nutrient concentrations were observed. These higher concentrations indicate an additional source or lower uptake at the high salinity end (under higher salinity ranges) (**Figure 3.4**). In contrast, NH_4^{+}, $NO_{2\text{-}3}^{-}$, and DON exhibit no pattern with salinity.

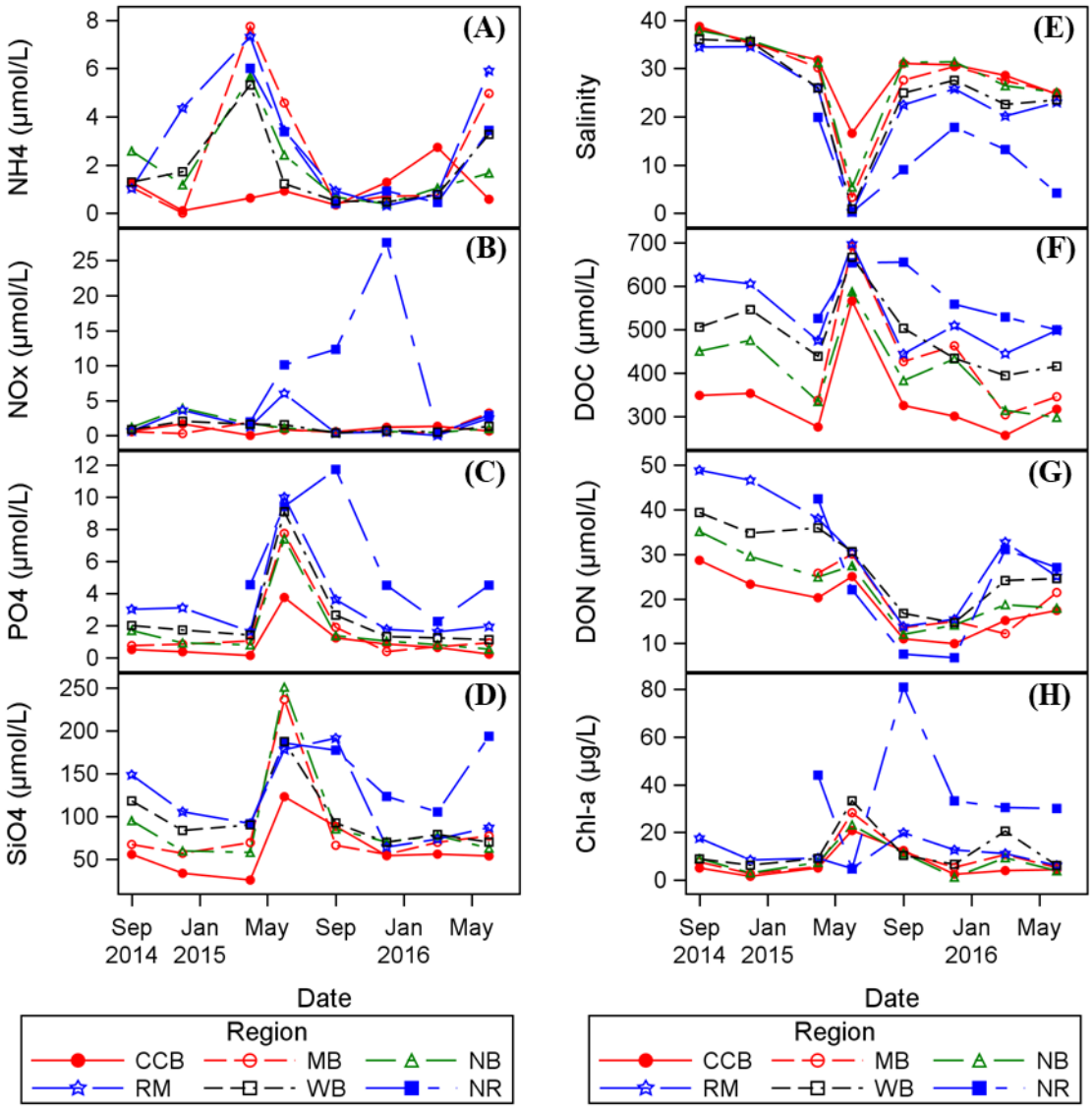

Figure 3.3: Average concentrations of nutrients and chlorophyll-α by bay region over time compared to salinity. A) Ammonium (NH_4^+). B) Nitrate+nitrite ($NO_{2\text{-}3}^-$). C) Phosphate (PO_4^{3-}). D) Silicate (SiO_4^{4-}). E) Salinity. F) Dissolved organic carbon (DOC). G) Dissolved organic nitrogen (DON). H) Chlorophyll-α (Chl-a). Bay region abbreviations: Nueces River (NR), Nueces River mouth (RM), west bay (WB), middle bay (MB), north bay (NB), and Corpus Christi Bay (CCB).

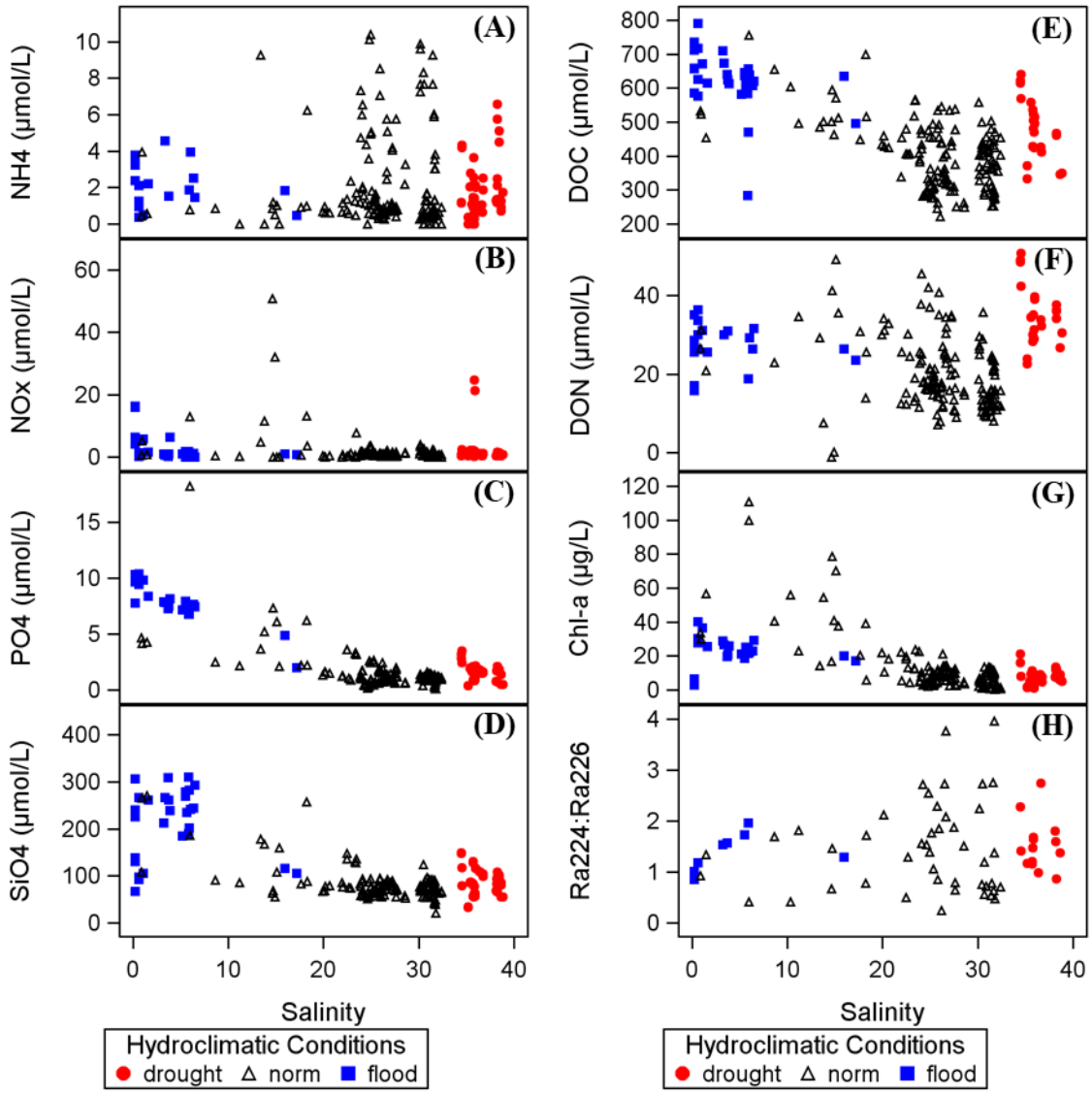

Figure 3.4: Concentrations of nutrients and chlorophyll-α by salinity compared to hydroclimatic conditions. A) Ammonium (NH_4^+). B) Nitrate+nitrite ($NO_{2\text{-}3}^-$). C) Phosphate (PO_4^{3-}). D) Silicate (SiO_4^{4-}). E) Dissolved organic carbon (DOC). F) Dissolved organic nitrogen (DON). G) Chlorophyll-α (Chl-a). H) ^{224}Ra:^{226}Ra activity ratio.

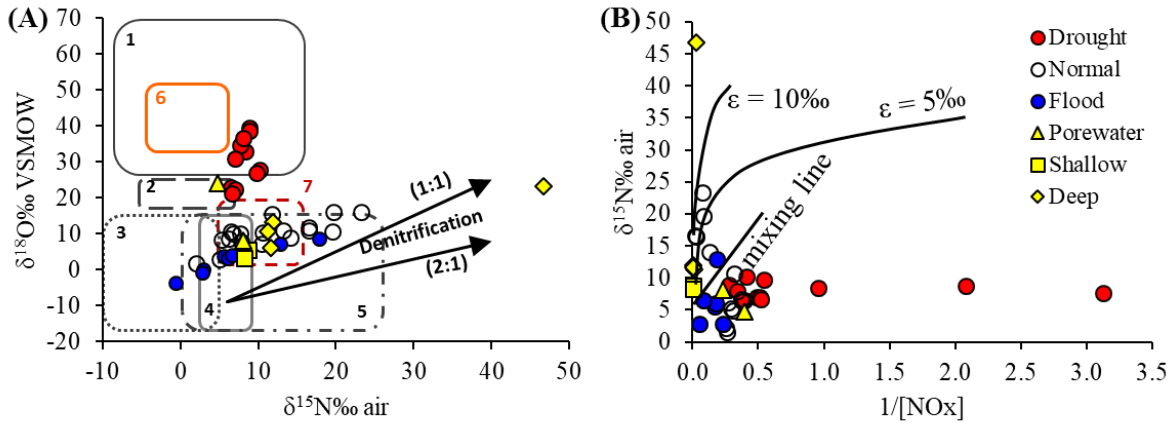

Figure 3.5: Stable isotope values in surface and pore waters and sources. A) Average values of $\delta^{15}N$ and $\delta^{18}O$ of nitrate from various N sources. Regions for N sources are modified from Kendall (1998) and Kendall et al. (2007). 1) Atmospheric NO_3^-. 2) NO_3^- fertilizer. 3) NH_4^+ fertilizer and rain. 4) Soil N. 5) Manure and septic waste. 6) Desert NO_3^- deposits. 7) Marine NO_3^-. The two arrows indicate typical expected slopes for data resulting from denitrification of nitrate with initial $\delta^{15}N$ = +6‰ and $\delta^{18}O_{NO3-}$ = -9‰ (Kendall et al. 2007). Typical ranges of $\delta^{18}O$ values produced by nitrification of ammonium and organic matter are -15‰ to 15‰. B) Plot of $\delta^{15}N_{NO3-}$ vs. 1/[NO_{2-3}^-] for surface water, porewater, and groundwater. Theoretical curves from Kendall et al. (2007) resulting from mixing of two sources of nitrate with different concentrations and from denitrification with two with two different fractionations, where mixing yields a straight line whereas denitrification yields curved lines.

3.3.2 Porewater Salinity and Nutrients

Porewater salinities ranged from 23.6 – 40.8 and distributions were not different ($p = 0.52$) across sampling events. The lowest porewater salinities occurred in the river at the station further downstream (station 14) in September 2015 and near the river mouth (stations 8 and 9) in December 2014 and June 2015. The RM porewater salinity (25.4) in December 2014 was lower

than the surface water (34.5), supporting the increased fresher groundwater input shown in the PCA. While the low porewater salinities in June (25.1) and September 2015 (23.6) are much higher than the corresponding surface water (1.1 – 1.6 and 10.4 – 13.8, respectively), these low salinity porewaters correspond to high PC3 scores indicating greater influence from fresh groundwater than from recirculated fresh surface water. The highest porewater salinities occurred at the river station furthest upstream (station 15), in the north bay (stations 1 and 3), and in the west-bay (station 11). Within the bay, average porewater salinities were lowest in June 2015 ($\overline{x}$ = 29.2), March 2016 ($\overline{x}$ = 30.1), and December 2014 ($\overline{x}$ = 30.2) and highest in September 2014 ($\overline{x}$ = 38.7), December 2015 ($\overline{x}$ = 36.8), June 2016 ($\overline{x}$ = 35.5), and April 2015 ($\overline{x}$ = 34.9).

Distributions of NH_4^+ (32.0 – 896.0 μmol·L^{-1}, $\overline{x}$ = 198.5 μmol·L^{-1}), PO_4^{3-} (0.72 – 31.8 μmol·L^{-1}, $\overline{x}$ = 13.9 μmol·L^{-1}), and SiO_4^{4-} (95.6 – 443.3 μmol·L^{-1}, $\overline{x}$ = 207.4 μmol·L^{-1}) were similar across events. Temperature (17.4 – 31.4°C, $\overline{x}$ = 24.7°C, $p < 0.0001$), DOC (69.3 – 15,243.5 μmol·L^{-1}, $\overline{x}$ = 909.2 μmol·L^{-1}, $p < 0.0001$), and $NO_{2\text{-}3}^-$ (BDL – 167.0 μmol·L^{-1}, $\overline{x}$ = 12.5 μmol·L^{-1}, $p < 0.0002$) distributions were different across events . December 2014 DOC concentrations were two orders of magnitude greater than all other events and 20 times greater than the next highest measurement. The $NO_{2\text{-}3}^-$ concentrations for June 2015 were greater than all events. $NH_4^+/NO_{2\text{-}3}^-$ was lowest in June 2015 (1.6), September 2014 (45.1), and September 2015 (95.8) and highest in March 2016 (1,201.3) and April 2015 (482.3). The ratio of $NH_4^+/NO_{2\text{-}3}^-$ in porewater provides an indication of flushing as higher relative concentrations of $NO_{2\text{-}3}^-$. For instance, lower ratio values reflect shorter residence times and greater inputs from groundwater. On the other hand, lower relative concentrations of $NO_{2\text{-}3}^-$, i.e., higher ratio values, indicate more stagnant, anoxic conditions where DOC and reduced inorganic species (e.g. NH_4^+, Mn^{2+}, Fe^{2+}) may accumulate (Abdulla et al. 2018; Komada et al. 2016; Slomp and Van Cappellen 2004).

3.3.3 SGD-derived Nutrient Fluxes

Douglas et al. (2020b) and Murgulet et al. (2018) found a large range of SGD rates depending on the method used to quantify SGD and due to large variations in the groundwater endmember. This study presents the range of nutrient fluxes calculated from saline SGD (Ra-based) and total SGD (average Rn groundwater endmember), as determined in these companion studies, for average porewater nutrient concentrations and average groundwater concentrations (**Table 3.2**). Due to the unbalanced spatial spread of porewater nutrient measurements, the event-averaged porewater nutrient concentrations were used. No SGD rates were calculated from ^{222}Rn for September 2014 or for Ra for June 2015; thus, no solute fluxes are provided for these events with the corresponding parameters.

As total SGD was 1-2 orders of magnitude greater than the saline SGD rates, the resulting total nutrient fluxes were also up to several orders of magnitude greater than the saline nutrient fluxes (**Table 3.2 and Figure 3.6**). Total fluxes for DOC, NH_4^+, PO_4^{3-}, and SiO_4^{4-} were highest in December 2014 and lowest in June 2015 (**Figure 3.6A, C-E**). In contrast, the highest total flux for NO_{2-3}^- occurred in June 2015 when SGD rates were lowest but porewater NO_{2-3}^- concentrations were highest. NO_{2-3}^- fluxes were also relatively elevated in December 2014. The high NO_{2-3}^- fluxes in June 2015 and December 2014 correspond with NR samples that load positively on PC3 (**Figure 3.2B**), indicative of a significant groundwater flux of new N to the river. Following wet conditions, groundwater recharge within the watershed to the surficial aquifer increases leading to enhanced groundwater discharge to the river as the hydraulic gradients are steeper along riverbanks. December 2014 inputs are higher in general due to large SGD rates in the river (Douglas et al. 2020). The lowest NO_{2-3}^- fluxes occurred in March 2016 which loads negatively on PC3.

For saline fluxes, the highest fluxes for DOC were in December 2014, while PO_4^{3-} and SiO_4^{4-} were highest in April 2015 and elevated in December 2014 and December 2015. The lowest DOC fluxes occurred in March and June 2016. The lowest PO_4^{3-} and SiO_4^{4-} fluxes occurred in September 2014 and 2015 and June 2015, respectively. Saline NH_4^+ fluxes were highest in December 2015 and April 2015 and lowest in September 2014. The lowest NO_{2-3}^- fluxes were in March 2016, whereas the highest NO_{2-3}^- fluxes occurred in December 2015.

Porewater fluxes were greater than groundwater fluxes across all seasons for DOC, NH_4^+, and PO_4^{3-} while SiO_4^{4-} porewater fluxes were less than groundwater fluxes across all seasons. June 2015 was the only time NO_{2-3}^- fluxes from porewater exceeded fluxes from groundwater, indicative of either NO_{2-3}^- accumulation or production in the porewater or a groundwater source not accounted for, such as from the agricultural area to the north.

Table 3.2: Average bay-wide total (Rn) and saline (Ra) nutrient fluxes as $x10^3$ $mol \cdot d^{-1}$ for average porewater nutrient concentrations.

		Sept 14	Dec 14	Apr 15	Jun 15	Sept 15	Dec 15	Mar 16	Jun 16
DOC	Rn		$2.61x10^6$	$1.97x10^4$	$6.79x10^3$	$2.38x10^4$	$1.90x10^4$	$1.63x10^4$	$1.57x10^4$
	Ra	483.5	$1.73x10^4$	705.2		602.2	718.4	267.9	199.5
NH_4^+	Rn		$4.89x10^4$	$1.43x10^4$	$2.12x10^3$	$4.29x10^3$	$1.67x10^4$	$1.82x10^4$	$1.55x10^4$
	Ra	38.6	323.6	512.3		108.3	630.8	299.5	196.3
NO_{2-3}^-	Rn		174.0	29.7	$1.32x10^3$	44.7	94.0	15.2	49.8
	Ra	0.9	1.2	1.1		1.1	3.6	0.2	0.6
PO_4^-	Rn		$3.63x10^3$	$1.16x10^3$	221.0	279.4	917.2	912.7	891.9
	Ra	6.8	24.0	41.3		7.1	34.7	15.0	11.3
SiO_4^-	Rn		$5.10x10^4$	$1.76x10^4$	$4.05x10^3$	$8.46x10^3$	$8.44x10^3$	$1.52x10^4$	$8.70x10^3$
	Ra	179.8	337.4	627.8		213.7	319.6	249.4	110.5

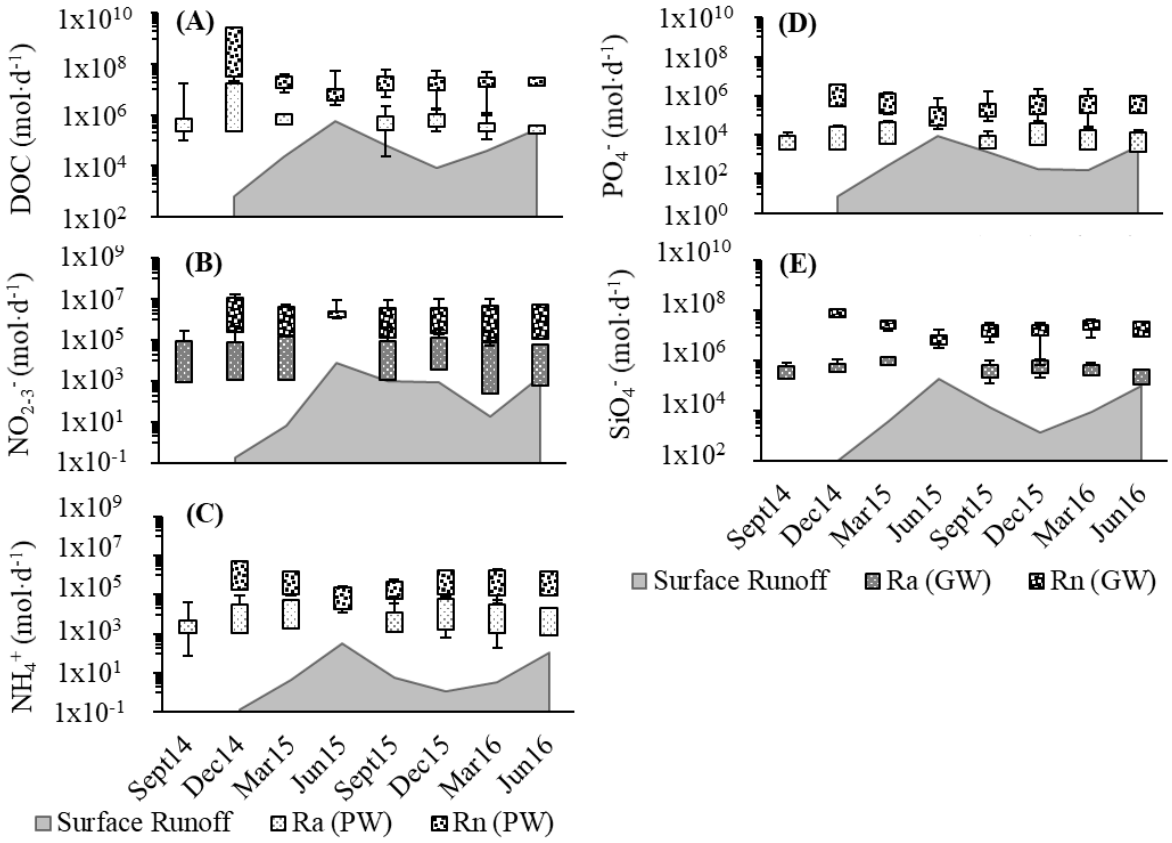

Figure 3.6: Nutrient fluxes for surface runoff (grey area), total SGD (black/white bars), and saline SGD (grey/white bars) over time. Color patterns reflect the greater fluxes are from average porewater endmember (PW, white with black/grey dots) or average groundwater endmember (GW, grey/black with white dots) A) Dissolved organic carbon fluxes. B) Nitrate+nitrite fluxes. C) Ammonium fluxes. D) Phosphate fluxes. E) Silicate fluxes.

3.4 Discussion

3.4.1 Relationship Between Nutrients, Chlorophyll-α, and SGD Tracers

As a result of extreme changes in hydroclimatic conditions, temporal fluctuations in freshwater inflows were important drivers of differences in hydrologic and salinity regimes and nutrient sources and fate over the study period. As observed in other estuaries across the northwest Gulf of Mexico coast (Montagna et al. 2018), Nueces Bay experienced a significant drop in salinity due to higher precipitation and subsequent freshwater inflow following the spring-summer 2015 flood event. These lower salinities during flooding were associated with higher concentrations of major inorganic nutrient species ($NO_{2\text{-}3}^{-}$, PO_4^{3-}, SiO_4^{4-}) and DOC (**Figure 3.3**). A smaller drop in salinity was observed in spring-summer 2016 with a smaller increase in inorganic N nutrients in the bay. This is consistent with findings in nearby Copano Bay (Mooney and McClelland 2012), a secondary bay in the Mission-Aransas estuary, and other bays along the Texas coast (Montagna et al. 2018), which exhibited ephemeral high inorganic nutrient concentrations following episodic rain events.

Though temporal changes in hydroclimatic conditions and salinity changes accounted for most of the variance observed, spatial variability further explains these temporal processes. For example, bay concentrations of $NO_{2\text{-}3}^{-}$, PO_4^{3-}, SiO_4^{4-}, and DOC returned to pre-flood levels relatively quickly following flood recession. On the other hand, river PO_4^{3-}, SiO_4^{4-}, and DOC concentrations remained high 3 months post flooding before returning to baseflow concentrations. However, $NO_{2\text{-}3}^{-}$ concentrations continued to increase and did not return to baseflow concentrations until December 2015, nine months post flooding. This significant increase in $NO_{2\text{-}3}^{-}$ concentrations over several months in the river was accompanied by a peak in Rn activity indicating substantial groundwater contributions of “new” N within the river either

directly as NO_{2-3}^- or as NH_4^+ which was converted to NO_{2-3}^- through nitrification once in the more oxic water column. However, while Rn activities were still elevated downstream at RM where SGD rates increased each sampling event after flooding, higher concentrations of NO_{2-3}^- were not observed post flooding, thus, removal of NO_{2-3}^- from the surface water and dilution with lower concentration bay water as riverine discharge decreased was likely. Possible NO_{2-3}^- removal pathways include high denitrification or dissimilatory nitrate reduction to ammonium (DNRA) rates in the river, or microbial uptake or biotic assimilation (Burgin and Hamilton 2007).

In September 2015, NO_{2-3}^- was likely consumed by high primary production as chl-α in the river was the highest observed in this study. Indeed, Murgulet et al. (2018) found aerobic respiration to be the dominant biogeochemical process controlling alkalinity and dissolved inorganic carbon in Nueces Bay in September 2015. However, cooler temperatures and reduced daylight in December 2015 would have reduced primary production allowing for NO_{2-3}^- concentrations to increase in surface water. Furthermore, as the river system returned to baseflow conditions following flooding, riverine discharge became negligible downstream of the saltwater barrier dam (**Figure 3.1**) and the lower river became tidally dominated. Thus, mixing with lower concentration bay waters also dilutes the high NO_{2-3}^- concentrations near the RM. However, conservative mixing lines between upstream NR (station 15) and RM show slight addition of NO_{2-3}^- in September 2015 and consumption/removal in December 2015 (**Figure 3.7**). Thus, dilution alone does not account for the loss of NO_{2-3}^-.

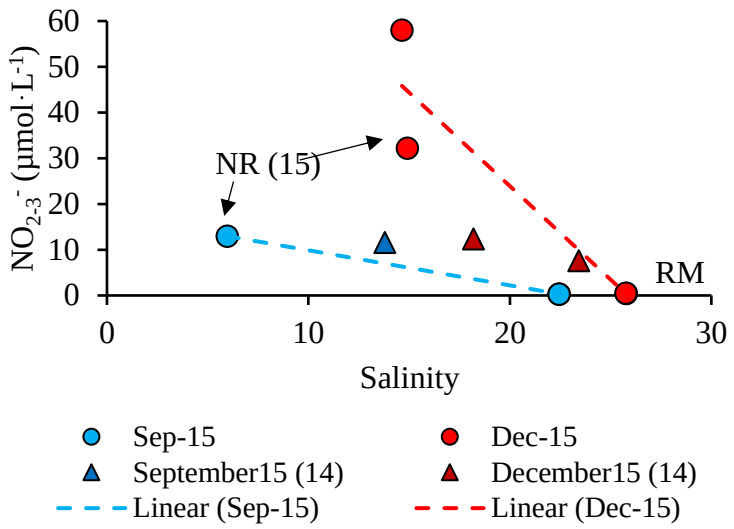

Figure 3.7: Conservative mixing trends between Nueces River (NR) station 15 and river mouth (RM) for September 2015 and December 2015.

Denitrification takes place under anoxic conditions when organic carbon and NO_3^- are available (Jäntti and Hietanen 2012). Anoxic conditions were not observed in surface water; thus, denitrification may be considered an insignificant N sink within these shallow surface waters. Nevertheless, denitrification may be a significant N sink in estuarine porewaters. Rapid denitrification may occur in heterogeneous sediments with a high silt content (25%-80% silt) and low permeability where inefficient mixing allows anoxic zones to form and in the presence of high organic matter content or microbial activity (Sawyer 2015), conditions observed in NR. Thus, NO_3^- may be removed from surface water as it circulates through aquatic sediments (the hyporheic zone) in response to currents, waves, and tides (Cardenas et al. 2008; Sawyer 2015; Triska et al. 1989; Zarnetske et al. 2011). Furthermore, the deviation below the conservative mixing line in December 2015 (**Figure 3.7**) indicates consumption/removal of NO_{2-3}^-, which is likely due to high denitrification rates accompanied by reduced microbial uptake in December 2015. This is further supported by the $\delta^{15}N$ and $\delta^{18}O$ values that follow denitrification trends

from soil N during flood and normal conditions (**Figure 3.5A**) and the $\delta^{15}N$ vs. $1/[NO_{2\text{-}3}^{-}]$ deviating toward denitrification for river stations during normal conditions (**Figure 3.5B**).

DNRA has similar requirements as denitrification (i.e., anoxic conditions, available nitrate, and organic substrates); however, DNRA is thought to be favored in high-carbon low-nitrate systems while denitrification is favored under high-nitrate low-carbon conditions (Burgin and Hamilton 2007). In estuarine sediments, DNRA competes with denitrification and conserves N as NH_4^+ rather than removing it from aquatic systems as N_2 (Giblin et al. 2013). In December 2014 and April 2015, NH_4^+ increased first in the river mouth and then throughout the bay as well while CCB remained low, thus little to no ammonium was exported out of the bay (**Figure 3.2A**). DNRA can be influenced by anthropogenic NO_3^- input as it can affect N cycling in marsh sediments by stimulating ammonia mineralization in anaerobic conditions (Ma and Aelion 2005). As the bay is bordered by the city of Corpus Christi to the south and agricultural croplands to the north, significant anthropogenic $NO_{2\text{-}3}^-$ and NH_4^+ additions through dry/wet deposition are expected (Kendall et al. 2007; Paerl 1997). Thus, the persistent strong southerly winds throughout most of the year (Ockerman 2001) would favor more urban/industrial deposition, while winter cold fronts would bring more agricultural deposition. Stable isotopes of nitrate indicate dry deposition of NO_3^- may have been a significant source in the bay during drought conditions in Winter 2014 (**Figure 3.5A**). Thus, shallow estuaries and tidal flats that occur under reducing conditions and are abundant in organic matter, such as in this study, may favor DNRA, which has been found to have rates as high as denitrification rates in some places, such as nearby Baffin Bay (An and Gardner 2002). In addition to DNRA, ammonification of organic matter within the sediments or photooxidation of organic matter from SGD may also produce NH_4^+

(Sipler and Bronk 2015). However, the rates of NH_4^+ production from these processes are still not well constrained.

In June 2015, high $NO_{2\text{-}3}^-$ concentrations were observed in porewater across the bay along with lower dissolved oxygen but no significant change in NH_4^+ concentrations, i.e., conditions favorable to denitrification. Production of total alkalinity in summer, fall, and winter was shown to be driven by SGD and denitrification in the companion study by Murgulet et al. (2018). Denitrification has been shown to be favored over anammox in marine sediments at temperatures above 25°C (Dalsgaard and Thamdrup 2002), as seen in the porewater in June and September. Although this indicates that anammox may have not played a large role in the conversion of NH_4^+ and $NO_{2\text{-}3}^-$ to N_2 during summer flooding in this subtropical estuary, NO_2^- concentrations would be needed to further confirm such processes. In the absence of internal sources, shallow groundwater transport from the agricultural fields north of the bay is deemed to be an important source of $NO_{2\text{-}3}^-$ following reoccurring precipitation events in the months prior.

The minor precipitation events that occurred between November 2014 and April 2015 are believed to have transported the $NO_{2\text{-}3}^-$ accumulated through deposition into the sediments thus stimulating DNRA. The accumulated NH_4^+ was then flushed from the sediments into the bay as the unconfined aquifers rising water table increased hydraulic gradients following spring precipitation events. Interestingly, a similar minor increase in $NO_{2\text{-}3}^-$ concentrations accompanied high NH_4^+ concentrations in June 2016, also following minor precipitation events after a dry winter, which indicates the transition from dry to wet conditions may help stimulate DNRA. The following flood event continued to flush the remaining accumulated NH_4^+ and DON from the shallow anoxic sediments while also increasing the terrestrial $NO_{2\text{-}3}^-$ and DOC through surface runoff. Concentrations of $NO_{2\text{-}3}^-$ continued to increase following flooding due to enhanced SGD

rates that sustained flushing of the sediments as well as increased input of "new" N from deeper groundwater (Douglas et al. 2020b). Nutrients returned to pre-flood levels along with SGD rates by 9 months post-flooding.

3.4.2 Nutrient Fluxes

One of the main challenges in estimating benthic nutrient fluxes is defining the nutrient concentrations that represent the groundwater source as production or consumption along flow paths and/or that are occurring within the bottom sediments (Murgulet et al. 2018; Spalt et al. 2020; Urquidi-Gaume et al. 2016). To account for the different SGD types and variable groundwater endmember solute concentrations, this study used both the total and saline SGD rates derived using the average groundwater endmember (Douglas et al. 2020b; Murgulet et al. 2018) and the nutrient concentrations from average porewater and average groundwater (> 3m and < 100m below ground surface). Douglas et al. (2020b) found average porewater Ra activity ratios (AR 6.5) were very similar to the average of all groundwater, including deep (ARs<1) and shallow (ARs>1), activity ratios (AR 6.6) due to source mixing within the sediment. Thus, the average SGD rates derived from the average groundwater endmember and the average porewater nutrient concentrations provide the best representation of the groundwater source. Nevertheless, as porewater was extracted from >20 cm below the sediment-water interface, this study assumes no change in the porewater chemistry throughout the sediment profile. However, looking to the $NO_{2\text{-}3}^{-}$ and NH_4^{+} fluxes from the groundwater informs about terrestrial solute contributions to the system. Groundwater is generally a source of oxidized forms of N (i.e., $NO_{2\text{-}3}^{-}$) (Majumdar and Gupta 2000), which, when transported to the anoxic and organic matter rich subterranean estuaries is likely to be converted to more reduced N species, such as increased NH_4^{+} and decreased $NO_{2\text{-}3}^{-}$ concentrations in porewater (Slomp and Van Cappellen 2004).

Nutrient fluxes attributed to both total and saline SGD exceeded inputs derived from surface water runoff alone for all seasons (**Figure 3.6**). Riverine nutrient fluxes into the coastal ocean have long been regarded as the primary source for coastal ecosystems (Jickells 1998; Wang et al. 2018) though SGD nutrient fluxes greater than surface runoff/riverine inputs have been observed in subtropical bays (Lee et al. 2012; Wang et al. 2017) and oceanic islands (Stewart et al. 2018). However, the total SGD nutrient fluxes in this study are one to three orders of magnitude greater than in the literature while the saline fluxes are of similar magnitudes (**Table 3.3**). The June 2015 flood and June 2016 moderately wet periods are the only times nutrient fluxes from surface runoff approach fluxes from SGD due to the orders of magnitude greater volume of river discharge. There is generally large separation between total SGD and saline nutrient fluxes. Saline solute fluxes account for less than 4% of the total solute fluxes using the average groundwater endmember SGD rates, and less than 14% using the most conservative total SGD estimates. Furthermore, similar flux ranges of $NO_{2\text{-}3}^{-}$ and NH_4^{+} with different dominant groundwater endmember fluxes reflects the conversion of the considerable supply of $NO_{2\text{-}3}^{-}$ in groundwater to NH_4^{+} within the subterranean estuary. The only nutrients with consistently higher concentrations in groundwater than porewater are $NO_{2\text{-}3}^{-}$ and SiO_4^{4-}, resulting in greater fluxes from groundwater than in porewater (**Figure 3.6B, 3.6C**). However, considering the large scale of nutrient fluxes, SiO_4^{4-} is the only solute exhibiting little difference between the groundwater and porewater concentrations due to its conservative nature. Thus, there is significant terrestrial input to the system, which is likely due to enhanced groundwater flow from short circuiting around oil/gas wells and pipelines, growth faults, and steep topography along the north shore (Douglas et al. 2020b). In comparison, DOC and PO_4^{3-} have greater fluxes from porewater than groundwater likely due to burial of organic matter, P desorption from sediments under anoxic

conditions, mineralization of P from organic matter within the sediments in porewater, and P precipitation under oxic conditions within the aquifer (Slomp and Van Cappellen 2004).

The high NH_4^+ concentrations in surface water in December 2014 and April 2015 correspond with the highest SGD fluxes of NH_4^+ and DOC. The NO_{2-3}^- fluxes in December 2014 and 2015, while elevated compared to NO_{2-3}^- fluxes for other seasons, were an order of magnitude lower compared to the maximum fluxes during the June 2015 flood event but an order of magnitude greater than the lowest fluxes in April 2015 and March 2016. In contrast, while the NO_{2-3}^- flux was highest during flood conditions the NH_4^+ flux was the lowest. Thus, the SGD-derived N, and DOC, is more reduced and recycled during drought conditions when nutrient additions from recharge to groundwater are limited and more oxidized or "new" during flooding. Furthermore, the higher porewater NO_{2-3}^- during flooding could indicate more flushing of the sediment as the water table rises and the hydraulic gradient increases. In particular, as discussed above, porewater NO_{2-3}^- was highest in June 2015 in the NB (18 – 179 $\mu mol \cdot L^{-1}$) and are believed to be the result of increased hydraulic gradients following the preceding months' wet conditions, facilitating leaching of N from the surrounding agricultural soils into the unconfined aquifer and transport to the bay. Thus, while the salinity difference between surface water and porewater kept offshore SGD rates low, due to density-difference effects (Santos et al. 2012a), increased hydraulic gradients and the orders of magnitude higher concentration in porewater are responsible for these high NO_{2-3}^- fluxes. By 3 to 6 months post flooding, deep groundwater signatures were apparent in the porewater (Douglas et al. 2020b) and NO_{2-3}^- concentrations had decreased as contamination of deeper groundwater is unlikely and, therefore, this source was likely responsible for diluting shallow groundwater and corresponding NO_{2-3}^- concentrations.

Table 3.3: Comparison of SGD and solute fluxes in similar coastal and estuarine settings (expressed as $m^3 \cdot m^{-2} d^{-1}$ and $mmol \cdot m^{-2} d^{-1}$, respectively). DIN is NO_2^-, NO_3^-, and NH_4^+ combined.

Site	Method	SGD	DOC	DIN	PO_4^{3-}	SiO_4^{4-}	References
Gulf of Aqaba, Israel	^{223,224}Ra mass balance	0.06 - 0.26		2.9 - 10	0.02 - 0.2		Shellenbarger et. al. 2006
Gamak Bay, Korea		0.08 - 0.11		8.8 - 12.1	0.10 - 0.23		Hwang et. al. 2010
Geoje Bay, Korea	^{222}Rn mass balance	0.05		2	0.03	5.9	Hwang et al. 2016
Hampyeong Bay, South Korea	^{226}Ra mass balance	0.14 - 0.35		6.7 - 7.5	0.09 - 0.38	5.5 - 12.9	Waska and Kim 2011
Obama Bay, Japan	^{222}Rn mass balance Salinity mass balance	0.001 - 0.01		0.54	0.02	0.55	Sugimoto et al. 2016
Tolo Harbor, Hong Kong	^{226}Ra mass balance	0.17		21	0.28	27.8	Lee et al. 2014
Tolo Harbor, Hong Kong	^{222}Rn mass balance Ra mass balance Silica mass balance	0.02 - 0.05		2.9 - 6.7	0.02 - 0.12		Luo and Jiao 2016
Tauranga Harbour, New Zealand	^{226}Ra mass balance	0.005 - 0.03		1.07	0.05		Stewart et al. 2018
La Paz Bay, Mexico	^{222}Rn mass balance	0.02 - 0.18		1.5 - 28.2	0.02 - 0.93	6.7 - 95.3	Urquidi-Gaume et. al. 2016
Yucatan Peninsula, Quintana Roo, Mexico	^{223}Ra mass balance Salinity mass balance	48 - 568 2.7 - 8.5		0.002 - 0.01			Null et al. 2014
Hawaii, USA	^{222}Rn mass balance Ra mass balance Silica mass balance	0.02 - 0.65		0.04 - 40	0.01 - 1.6		Street et al. 2008
Huntington Beach, California, USA	Ra mass balance	0.06 - 0.92		0.7 - 12	0.04 - 0.54	-	Boehm et. al. 2004
Turkey Point, Florida, USA	^{222}Rn mass balance	0.11	34.3	5.94	0.35	5.1	Santos et al. 2008
Copano Bay, Texas, USA	^{222}Rn mass balance				0.3 - 3.4	56 - 220	Spalt et al. 2020
Nueces Bay, Texas, USA	^{222}Rn mass balance ^{226}Ra mass balance	0.13 - 3.85 0.01 - 0.39	95.9 - 36,838.5 2.8 - 243.9	30.1 - 709.0 0.54 - 9.0	3.1 - 51.3 0.01 - 0.58	57.1 - 719.7 1.6 - 8.9	This study

3.4.3 Implications for Estuarine Nitrogen Budget

Previous nitrogen budgets for Nueces Bay and Nueces Estuary generated net negative balances (Anchor QEA 2017; Brock 2001) indicating more N was leaving the system through diversions, tidal exchange, denitrification, and nitrogen burial than entering from known sources (i.e., gauged streams, ungauged watersheds, wastewater treatment plants, other return flows, wet/dry deposition, nitrogen fixation, and SGD). However, these budgets either did not account for SGD-derived N (Brock 2001) or estimated SGD-derived N from NO_3^-, and thus likely underestimated the contribution of total N from groundwater (Anchor QEA 2017). This study applied the bay-wide TDN porewater fluxes for June 2015, September 2015, December 2015, and March 2016 from Douglas et al (in prep), which removed ammonium prior to measurement, to the most recent N budget from Anchor QEA (2017) for years 1986-2015. Anchor QEA (2017) had a N budget of -611 10^6 g $N \cdot yr^{-1}$ (million g $N \cdot yr^{-1}$, after removing the estimated 75 10^6 g $N \cdot yr^{-1}$ from regional groundwater NO_3^- concentrations). This study found total Rn-derived N fluxes ranged from 16.2 – 82.6 10^9 g $N \cdot d^{-1}$ and averaged 45.8 10^9 g $N \cdot yr^{-1}$. In contrast, the saline Ra-derived N fluxes ranged from 591 – 2313 10^6 g $N \cdot d^{-1}$ and averaged 1.4 10^9 g $N \cdot yr^{-1}$. These Ra-derived annual average TDN fluxes are up to an order of magnitude greater than those used by Anchor QEA (2017); however, the Rn-derived annual average TDN fluxes are two orders of magnitude greater than the N fluxes Anchor QEA (2017) used.

Total N fluxes for the current study are calculated from applying the average SGD flux to the previous N budget. On average, SGD supplies more N to the system than accounted for by all estimated inputs and sinks creating an excess of 45.2 10^9 g $N \cdot yr^{-1}$. Nitrogen fluxes could be over 3 times greater by applying the SGD rate using the average porewater endmember (i.e., least conservative SGD rates) or 3.5 times less with the SGD rate using the highest groundwater

endmember (i.e., most conservative SGD rates) than the average groundwater endmember SGD rates provide. However, even these most conservative total fluxes and the significantly smaller saline/recirculated fluxes generate a substantial surplus of N (4.6 – 23.6 10^9 g N·yr^{-1} and 0.8 10^9 g N·yr^{-1}, respectively) to the system which may have considerable impacts on microbial and planktonic communities within the larger Nueces Estuary.

This study provides critical information for the development of appropriate and necessary mitigation strategies required to maintain the estuarine health. With the groundwater input the most significant in this estuary, efforts should be directed at mitigating groundwater pollution. For integrated management measures, further investigations of N levels and sources in groundwater within the watershed, as well as a deeper understanding of the hydrologic system combined with local farmers and stakeholders participation is necessary (Kazakis et al. 2020). To aid development of rational N management strategies, future studies should incorporate mathematical prediction of nutrient concentrations with assessments of the hydrogeochemical processes to better understand how water quality parameters within an aquifer interact (Bui et al. 2020).

3.5 Conclusions

Assuming the results in Nueces Bay are typical of semi-arid bays, then the temporal change in hydroclimatic conditions and freshwater inflows have significant impacts on the delivery of nutrients to semi-arid estuaries and relatively small, shallow bays. Observations of spatial variability of SGD rates and nutrient levels throughout the system over time further elucidate the processes occurring (e.g., nitrification, dentrification, and DNRA) and the relative control that system heterogeneity has on these processes. While overall SGD is inhibited during flooding, N enrichment in porewater occurs particularly near the agricultural fields as a result of soil N

flushing and percolation to groundwater, which facilitates N-rich groundwater fluxes. Evidence points to substantial "new" N inputs from terrestrial groundwater to the porewater and then to the bay, while saline/recirculated SGD accounts for a much smaller fraction of total SGD inputs, thereby contributing to the recycled N portion in the system. This study adds to the body of work that has found SGD-derived nutrient fluxes equivalent to or greater than the riverine-derived nutrient fluxes to a system. However, the present study also demonstrates that nutrient fluxes from SGD in semi-arid and anthropogenically disturbed, estuaries may be significant. Thus, increased N and P contamination of groundwater from industrial and agricultural practices may increase occurrences of eutrophication and harmful algal blooms in semi-arid estuaries. Although N inputs from atmospheric deposition or remineralization are important, because groundwater is the highest contributor to the nutrient budget, management strategies should focus on land-use practices to reduce N contamination of shallow groundwater and subsequent contamination of estuaries.

Acknowledgements

Texas Sea Grant (award number NA14OAR4170102) and the Center for Water Supply Studies at Texas A&M University-Corpus Christi financially supported this research and ARD's dissertation from which this paper has been derived. Partial support to PAM for this publication was made possible by the National Oceanic and Atmospheric Administration, Office of Education Educational Partnership Program (award number NA16SEC4810009).The authors thank all those who assisted in the lab and/or in the field. Finally, the authors thank the reviewers for their comments. All views, opinions, findings, conclusions, and recommendations expressed in this material are those of the authors and do not necessarily reflect the opinions of the Texas

Sea Grant College Program or the U.S. Department of Commerce, National Oceanic and Atmospheric Administration.

CHAPTER IV: HYDROCLIMATIC VARIABILITY IMPACTS ON SURFACE AND POREWATER DISSOLVED ORGANIC MATTER IN A SEMI-ARID ESTUARY

To be submitted to JGR Biogeochemistry as: Douglas, A. R., D. Murgulet, H.A.N. Abdulla. "Impacts of hydroclimatic variability on surface water and porewater dissolved organic matter in a semi-arid estuary."

Abstract

Seasonal molecular DOM changes were evaluated in a semi-arid estuary across different hydroclimatic conditions: from flood peak, to flood recession, to typical dry to semi-wet conditions. The PPL-SPE and UPLC-Orbitrap Fusion mass spectrometry, in positive mode, was utilized to molecularly characterize surface- and porewater DOM. During summer and fall, >57% of the identified compounds are CHO which decreases to 43.3% by winter as sulfur and phosphorous containing compounds decrease and CHON compounds increase from 25% to 47%. Volcano plots generated from predefined ratios were used to evaluate statistically significant (p-values ≤ 0.05) differences between seasons and surface- and porewater. Fall DOM, during flood recession, is significantly different from all other seasons with over 1800 compounds significantly specific to this season. This difference is likely due to enhanced benthic fluxes as the volcano plot for fall surface- to porewater shows very few compounds significant to either group and the DOC and DON mixing plots deviate toward the porewater. Post-flooding winter and spring samples are highly similar and show a diminution of flooding impacts within six months from summer.

4.1 Introduction

Estuarine dissolved organic matter (DOM) consists of a diverse array of allochthonous (i.e., terrestrial runoff, river discharge, and benthic fluxes) and autochthonous (i.e., phytoplankton

metabolism and excretion, viral lysis, and slopping feeding) sources (Carlson and Hansell 2015; Repeta 2015; Sipler and Bronk 2015). Annually, an estimated $0.25x10^{15}$ g C are transported from land to the sea in the form of dissolved organic carbon (DOC) (Hedges et al. 1997) while the DOM sediment benthic fluxes are equivalent to riverine fluxes in coastal regions (Burdige et al. 1999). These estimated fluxes are likely an underestimate of allochthonous DOC fluxes to regions where groundwater discharge, diffuse sediment fluxes, and effects of extreme wet events (e.g., flooding) are still not well constrained.

Generally, bulk DOC concentrations decrease along salinity gradients from the river to the open ocean while the DOM composition is simultaneously changing. With increasing salinity, it is expected the molecular weight, carbohydrate content (Abdulla et al. 2010), heteroelement content (Sleighter and Hatcher 2008), photoammonification (Aarnos et al. 2012), and lability (D'Andrilli et al. 2015) will increase while the aromaticity (Abdulla et al. 2010), photoproduction of dissolved inorganic carbon (DIC) (Aarnos et al. 2012), and carbon:nitrogen (C:N) ratio (Sipler and Bronk 2015) of the DOM decreases. In tropical and temperate marine basins, the riverine DOM pool is rapidly transformed through a multitude of biotic (microbial) and abiotic (photochemical) processes (Spencer et al. 2009), such that terrigenous DOC constitutes approximately 1-2% of total DOC in the oceans (Hernes and Benner 2006). Furthermore, the photochemical reactions that occur when DOM is exposed to sunlight may result in the production of DIC (Aarnos et al. 2018), ammonium (NH_4^+) and other dissolved inorganic nitrogen (DIN) compounds (Bushaw et al. 1996; Felix and Campbell 2019), and labile organic compounds (Aarnos et al. 2012). Reviews have found photoproduction rates in estuaries and marine environments range from 0 to 15.92 µmol L^{-1} h^{-1}, which can result in photoammonification rates comparable to or in excess of atmospheric deposition of reactive

inorganic nitrogen (Bronk et al. 2014; Kitidis and Uher 2008; Sipler and Bronk 2015; Stedmon et al. 2007; Vähätalo and Zepp 2005). Thus, photochemical degradation may be a significant source of new bioavailable nutrients to primary producers (Kitidis and Uher 2008).

The quantity and composition of riverine DOM was shown to affect biogeochemical cycling in estuaries with magnitudes that vary with changes in hydroclimatic conditions (Letourneau and Medeiros 2019; Liu and Lu 2019; Majidzadeh et al. 2017; Raymond and Saiers 2010; Spencer et al. 2009). Additionally, changes in riverine DOM composition have been shown to lag behind changes in DOM fluxes during storm events (Yang et al. 2013). Extreme flooding events result in large "pulse" releases of terrestrial DOM (tDOM) into fluvial systems, thus, increasing DOM concentrations that are "shunted" rapidly downstream due to increased discharge and flushing (Raymond et al. 2016). A survey of 31 forested watersheds in the eastern United States, demonstrated that 86% of annual DOC export occurs following major precipitation events and that 60% of this export occurs during large flow events that account for 5% of the year (Raymond and Saiers 2010). For example, during a storm event three small watersheds in Oregon were shown to experience approximately 3-fold increases in DOC concentrations with an increase in the proportion of humic DOM (Hood et al. 2006). Thus, low-frequency large flow events, anticipated to increase with climate change (Stocker 2014), are responsible for a significant portion of annual tDOM input to estuaries and coastal oceans. Further, the export of DOM during extreme wet events approaches the mean annual DOM export during non-extreme flow event years (Caverly et al. 2013; Jung et al. 2014; Raymond and Saiers 2010; Sánchez-Murillo et al. 2019; Yoon and Raymond 2012). Therefore, in the face of a rapidly changing climate, there is an immediate need to understand the mechanisms that control the fate and

transport pathways of DOM for successful management of aquatic food webs and sustainable ecosystem health.

To date, studies that focused on the DOM composition that accompany temporal hydroclimatic changes have largely focused on riverine surface water (Liu and Lu 2019; Raymond and Saiers 2010; Yang et al. 2013), temperate systems with perennial stream flow (Dixon et al. 2014; Osterholz et al. 2016; Powers et al. 2018), and the arctic (Rossel et al. 2020). Most estuarine and coastal DOM characterization studies have not considered inter- and intra-seasonal changes in both surface- and porewater DOM molecular composition (Mori et al. 2019; Rossel et al. 2020) in response to extreme hydroclimatic events, such as flooding. To our knowledge, no such studies exist for semi-arid estuaries where precipitation is infrequent and riverine discharge is flashy. Further high-resolution studies of the DOM molecular composition along terrestrial to marine gradients under different hydroclimatic conditions is still necessary.

Fourier transform ion cyclotron MS (FTICR-MS) has been used widely to characterize DOM at molecular level (Abdulla et al. 2018; Longnecker and Kujawinski 2011; Mori et al. 2019; Osterholz et al. 2016; Simon et al. 2019; Sleighter et al. 2010). Recent studies conducted a direct comparison of Orbitrap and FT-ICR-MS analyses of DOM introduced by direct-injection (Hawkes et al. 2016; Simon et al. 2018). In these studies, the main trends among samples and most of the information content within the mass spectra were preserved in the lower-resolution Orbitrap instrument; however, there was less identification of heteroatom species, due most likely to limits in resolving power (Hawkes et al. 2016; Simon et al. 2018). However, these comparison studies were conducted using Orbitrap Velos and Orbitrap Elite instruments, which have a maximum mass resolution of 100,000 and 240,000 respectively, i.e., less than half of the resolution of the Orbitrap Fusion Tribrid Mass Spectrometer (OT-FTMS) that was used in this

study. OT-FTMS offers one of the highest resolving power of its kind (500,000 FWHM at m/z 200), with ability to measure sub-ppm mass accuracy, making it comparable to FT-ICR-MS (Zubarev and Makarov 2013). The high resolution and mass accuracy of Orbitrap Fusion Tribrid MS (OT-FTMS), 500,000 FWHM at m/z 200, can resolve complex DOM mixtures, which allows for the assignment of molecular formulas to individual mass spectral peaks . The OT-FTMS is the only mass spectrometer system commercially available today that combines three state-of-the-art mass analyzers: 1) Quadrupole mass filter that provides high ion transmission at isolation widths down to 0.4 amu to improve sensitivity and selectivity; 2) A High-Field Orbitrap analyzer (HF-Orbitrap) operating at 5 kV; and 3) High performance linear ion trap, with dual-pressure configuration. This design allows for new experiments that were not previously possible, especially in *de novo* structure elucidation of compounds within complex mixtures like DOM. Thus, one of the major advantages of the OT-FTMS is its ability to do simultaneous identification and quantification by using three mass analyzers working in parallel at high speed, selectivity, accuracy, and sensitivity with high reproducibility. A high degree of structural diversity can be contained within the molecular formulas assigned to mass spectral peaks and each assigned formula represents many possible structural isomers. However, the fast scan speed of OT-FTMS, up to 30 Hz, relative to FTICR-MS, 1 Hz, allows it to couple with different chromatography techniques, like ultrahigh performance liquid chromatography (UPLC). Thus, reducing the complexity of DOM mixtures (separation in additional dimension) before mass spectrometer analyses therefore improving Orbitrap identification of heteroatom species and separating molecular isomer compounds (that have the same molecular formulas but different chemical structure) that could not be identified using direct injection. Hence, coupled OT-FTMS

and chromatography allows us to move from just identifying molecular formulas (as in FTICR-MS) towards actual structural elucidation of individual molecules within the DOM pool.

The current study used UPLC-OT-FTMS to investigate the DOM molecular composition in a semi-arid estuary across four seasons with different hydroclimatic conditions to better understand the impact of changing hydroclimatic conditions on DOM composition. To better constrain DOM inputs to the estuary, both river and benthic endmembers are evaluated. Furthermore, characterization of bottom sediment porewater within the estuary was conducted to evaluate benthic flux influences on DOM inputs into and composition in the system in response to hydroclimatic changes.

4.2 Materials and Methods

4.2.1 Study Area

This study was performed in semi-arid Nueces Bay, Texas. Nueces Bay, located on the south Texas Gulf Coast, is contiguous to Corpus Christi Bay in the Nueces Estuary system (**Figure 4.1**). The area is characterized by dry to sub-humid climates with annual precipitation averages around 76.2 cm and an average evaporation rate of 145 cm (Ockerman 2001; Shafer 1968). Due to low precipitation in the watershed as well as dams and diversions on the river, Nueces River discharge into the bay is typically minimal, resulting in high average salinities and often low nutrient levels (Longley et al. 1994). Prior to the start of this study, the region was experiencing one of the most severe multi-year (4-5 years) droughts on record, which ended in spring 2015 (TWDB 2017; TWDB (Texas Water Development Board) 2017). Sampling began after multiple precipitation events over a short period, mainly in the upstream watershed, triggered major flooding. The sampling seasons encompass a progression from immediately post peak flooding (June-July 2015), to the falling flooding limb or recession (September 2015), to

typical dry (December 2015) and semi-wet (March-April 2016) conditions. More information on freshwater inflows to the estuary, including impacts of hydrologic alterations and hydroclimatic variability, and aquifer characteristics (i.e., porosity, hydraulic conductivity, and more) are presented elsewhere (Douglas et al. 2020b; Longley et al. 1994; Murgulet et al. 2016; Murgulet et al. 2018; Ockerman 2001; Shafer 1968).

Nueces bay has a long history of anthropogenic disturbances, including oil/gas development, pipelines transecting the bay, dredging, and agricultural land-use. Dry land crop agriculture (i.e., grain sorghum, corn, and cotton) and ranching activities dominate the area's land use (TDWR 1981). Nueces Bay and the areas of Nueces and San Patricio counties immediately surrounding the bay have been heavily developed for oil and gas extraction (D'Unger et al. 1996; Douglas et al. 2020b). The long-term discharge of oil-brine to surface water and other disturbances associated with oil/gas industry into coastal estuaries was a longstanding practice in Texas until a new rule, 40 CFR Part 435, passed in 1996 effectively banned such practices (D'Unger et al. 1996).

Companion studies found that the bay receives significant submarine groundwater discharge (SGD) due to steeper hydrologic gradients closer to shore and at transitions among bottom sediments of different permeabilities (i.e., sand to clay) (Douglas et al. 2020b; Murgulet et al. 2018). Additionally, the SGD rates in the bay were lowest in summer ($\overline{x}$ = 0.27 $m \cdot d^{-1}$) and increased steadily from fall ($\overline{x}$ = 0.41 $m \cdot d^{-1}$) to winter ($\overline{x}$ = 0.69 $m \cdot d^{-1}$) to spring ($\overline{x}$ = 0.92 $m \cdot d^{-1}$) to summer ($\overline{x}$ = 1.00 $m \cdot d^{-1}$) while the rates measured in the river were greatest in fall (1.61 $m \cdot d^{-1}$) and decreased in spring (1.14 $m \cdot d^{-1}$) and summer (1.08 $m \cdot d^{-1}$) (Murgulet et al. 2018). The magnitude of SGD rates lagged changes in climatic conditions by weeks (surficial aquifers) and months (deeper aquifers) (Douglas et al. 2020b). Moreover, the lowest reported SGD rates were

during the summer flood when increased surface water levels likely reduced the hydraulic gradient toward the bay.

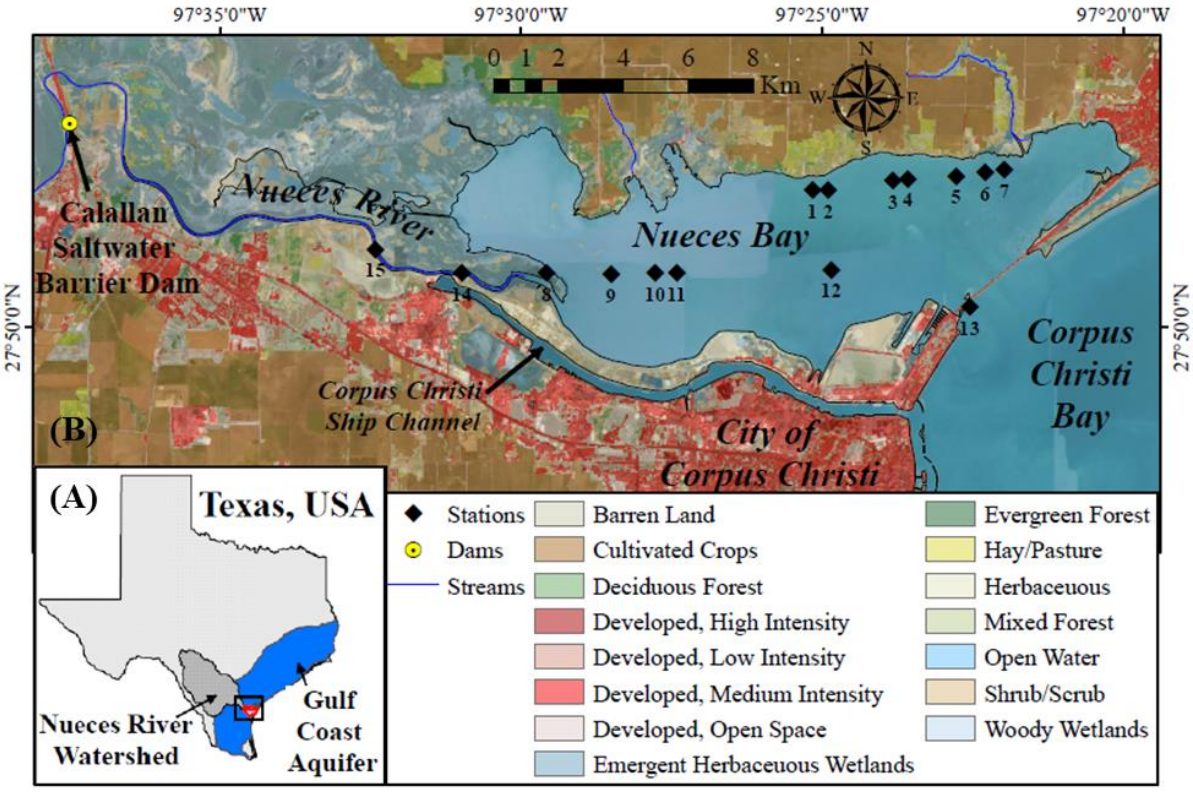

Figure 4.1: Study area. A) Inset of Texas, USA, with location of the Gulf Coast Aquifer and Nueces River watershed. B) Location of sample stations in Nueces Bay, Texas.

4.2.2 Samples and Preparation

Seasonal surface water samples (n=60) were collected along a riverine to estuarine gradient (from the lower Nueces River and Nueces Bay) at 8 locations and along a shore-parallel transect at 7 stations (**Figure 4.1**) in June-July (summer), September (fall), and December 2015 (winter) and March-April 2016 (spring). Porewater samples (n=15) were collected from a subset of stations in each season via push-point piezometer from 0.5 – 2 m depths as described in detail in our companion studies (Douglas et al. 2020b; Murgulet et al. 2018).

Field parameters (i.e., temperature, dissolved oxygen, salinity, and pH) were measured at the time of sample collection with a multi-probe YSI series 6 sonde. Chlorophyll-α (chl-α) samples were filtered (0.7 µm GF/F filter paper) on site and then stored frozen until analysis. Chl-α was measured within 12-16 hours of methanol addition by a Turner Design Trilogy fluorometer using a methanol extraction method (Krauk et al. 2006; Montagna et al. 2018; Paudel et al. 2019).

All DOM water samples were collected in 1 L polycarbonate bottles. The bottles were cleaned with alconox and HCl solution and pre-conditioned with sample. In the field all samples bottles were stored on ice in a dark cooler until return to laboratory where processing of samples occurred. All samples were sterile filtered through 0.2 µm polyestersulfone filters conditioned with 5-10 mL of sample and kept frozen until analysis (Abdulla et al. 2010; Sipler and Bronk 2015). Sub-samples were analyzed for dissolved organic carbon (DOC) and total dissolved nitrogen (TDN) using a Shimadzu TOC-V analyzer with nitrogen module. Other studies show that porewater samples are high in ammonium (Burdige and Zheng 1998; Murgulet et al. 2019), which may create interference during the TDN analysis and lead to increased error propagation for DON by including one more error term (Burdige and Zheng 1998). Ammonium was, thus, removed from the porewater samples prior to DOC/TDN analysis by: 1) raising the pH of each sample to ~12 with a 10 M NaOH solution, 2) sparging the sample with N_2 gas, and 3) lowering the pH to ~2 with 10 M phosphoric acid for analysis (Burdige and Zheng 1998). Inorganic nutrients (i.e., NO_3^-, NO_2^-, NH_4^+) were analyzed by Seal QuAAtro nutrients autoanalyzer (EPA 2011). Samples with concentrations exceeding the linear range (i.e., porewaters) were diluted and reanalyzed. The MDL (in $\mu mol \cdot L^{-1}$) for the inorganic nutrients are: 0.11 for NO_3^-, 0.012 for NO_2^-, and 0.057 for NH_4^+. Dissolved organic nitrogen (DON) was determined as the difference between TDN and dissolved inorganic nitrogen (i.e. $DIN=NO_3^-+NO_2^-+NH_4^+$) for surface water

and the difference between measured TDN and nitrate+nitrite (i.e., DON=TDN–NO_3^-–NO_2^-) for porewater. A conservative mixing model was developed using the river (NR) and seawater (offshore Corpus Christi: CCB) endmembers (stations 15 and 13, respectively) to understand the influence of these inputs on the DOC and DON characteristics of the bay.

4.2.3 UPLC and Orbitrap Fusion Tribrid MS

Samples were prepared for mass spectrometric analysis using 100 mg, 3 mL Bond Elut-PPL solid phase extraction (SPE) cartridges according to the procedure recommended by Dittmar et al. (2008). Prior to extraction, 100 ml of the samples were acidified to pH of 2 with hydrochloric acid. The samples were eluted with 6 mL Optima LC/MS grade methanol. Milli-q was processed through the same PPL-SPE method and used as a blank for UPLC-OT-FTMS analysis. All methanol eluents were dried down in a Centrivap benchtop concentrator and reconstituted in 1 mL of 95:5 water:acetonitrile. Aliquots of sample were analyzed on Vanquish UPLC - Orbitrap Fusion Tribrid Mass Spectrometer (UPLC-OT-FTMS). The analysis was performed on a 1.7 µm ACQUITY UPLC BEH C18 reversed phase column (Waters, 30Å, 1.7 µm, 2.1 mm X 100 mm) via a heated ESI (H-ESI) source to Orbitrap Fusion Tribrid Mass Spectrometer (Thermo Scientific) operated under positive mode. Eluent A was Milli-Q water with 0.1% (v/v) formic acid and eluent B was acetonitrile with 0.1% (v/v) formic acid. The following gradient was used: hold at 5% B for 2 min; ramp to 65% B for 16 min; ramp to 100% B for 7 min and hold for 8 min. An 8 min column re-equilibration with the starting ratio of eluents was carried out between sample analyses. The flow rate was 0.2 $ml \cdot min^{-1}$ with injection volume of 20 µL. The H-ESI setting was 3200 volts, 30 Sheath gas, 10 Aux gas, 325°C ion transfer tube temp, and 200°C vaporizer temp. The Orbitrap full scan was run at 500,000 (FWHM at m/z 200) resolutions with a scan range 100-1000 m/z and RF Lens at 40%. For MS^2, the isolation window was set at 0.7

m/z with preforming both collision-induced dissociation (CID) and higher-energy collisional dissociation (HCD) using ion trap mass spectrometer as the detector. The AGC was set at 1.0e4.

Compound Discoverer software 3.0 (Thermo Fisher) was used to identify the DOM compounds. The retention times (RT) of all chromatography spectra were aligned using adaptive curve with maximum shift of 0.2 min and 5 ppm mass tolerance. In order to identify a compound, we required it meet the following conservative criteria: 1) a signal-to-noise (S/N) above 3, 2) a minimum of 5 mass scans per chromatographic peak, 3) a minimum peak intensity of 50,000, and 4) at least one isotope peak (M+1) was detected.

The workflow considered the possibility of the presence of multiple positive adducts ($(2M+ACN+H)^{+1}$; $[2M+ACN+Na]^{+1}$; $[2M+H]^{+1}$; $[2M+K]^{+1}$; $[2M+Na]^{+1}$; $[2M+NH_4]^{+1}$; $[M+2H]^{+2}$; $[M+3H]^{+3}$; $[M+ACN+2H]^{+2}$; $[M+ACN+H]^{+1}$; $[M+ACN+Na]^{+1}$; $[M+H]^{+1}$; $[M+H+K]^{+2}$; $[M+H+MeOH]^{+1}$; $[M+H+Na]^{+2}$; $[M+H+NH_4]^{+2}$; $[M+H-H_2O]^{+1}$; $[M+H-NH_3]^{+1}$; $[M+K]^{+1}$; $[M+Na]^{+1}$; $[M+NH_4]^{+1}$). In case multiple adducts were detected, all adducts of the same compound were grouped together with a tolerance of 0.2 min (in retention time). Based on our observed analysis there were limited cases where multiple adducts were detected for the same compounds. A total of 2751 out of 3432 compounds detected had a single adduct and the maximum number of adducts detected for a single compound was 5.

The molecular formula for each peak was calculated using a molecular formula calculator (Molecular Formula Calc version 1.0 NHMFL, 1998) with the following parameters: $C_{4-100}H_{4-200}O_{0-50}N_{0-10}S_{0-3}P_{0-3}$. Molecular formulas that are unlikely to occur in nature (or that are not chemically possible) were removed, as described in detail in (Abdulla et al. 2013). In summary, we applied a modified version of the rules set in Kind and Fiehn (2007), which requires that formulas satisfy the following inequalities: $H/C < 2.50$, $O/C \leq 1.20$,$O/P \geq 3.00$, and

N/C < 0.50. All assigned formulas were further tested for the physical existence of chemical structures using LEWIS and SENIOR chemical rules, again according to Kind and Fiehn (2007). The molecular ^{13}C isotope and ^{34}S isotope peaks (when they were detected above the S/N threshold) were also validated with the chemical building block approach (e.g., CH_2 homologies series) described by Koch et al. (2007). As we did not use internal standards when analyzing these samples, the calculated masses of the assigned formulas are all within 2.0 ppm of the masses detected by OT-FTMS.

4.2.4 Statistical Analysis

Data were exported from Compound Discoverer and a suite of multivariate tools was used for statistical analyses. Compound absence in each sample was determined if it does not meet the above four criteria. For these absent compounds, a gap filling approach that integrates the area where the peak is expected but not detected, was performed so that the statistical analysis will not be skewed toward missing values (i.e., zero value). These gap-filled areas usually correspond to spectra noise so no bias is introduced by integrating them. . Peak magnitude-weighted O/C, H/C, and double bond equivalent (O/C_w, H/C_w, and DBE_w) were calculated to describe each sample and facilitate discussion of DOM composition (Schmidt et al. 2017; Sleighter et al. 2010). DBE were calculated as: ½*(2*#C + #N + 3*#P – #H + 2), where # represents the number of the specified atoms in the formula.

Principal component analysis (PCA) was used to visualize the correlation between multivariate data in the samples. Briefly, PCA transforms possibly correlated variables into an artificial set of independent linear combinations of the original variables known as principal components (PC). The data was gap filled and normalized to constant sum. A sample score plot and a variable loading plot, which shows the distribution of the samples and variables,

respectively, were generated. The more distal the variable loading is from the origin, the more impact that variable has on the variance of the samples.

Volcano plots were used to identify the chemical compounds that are significantly different between consecutive seasons (e.g., summer to fall, fall to winter, and winter to spring) and individual season's surface water to porewater (e.g., summer surface to summer pore, fall surface to fall pore). A spring-summer comparison was not conducted because the summer samples were collected during an extreme wet El Niño event. Thus, the transition between the two seasons is not "typical" leading to a lack of technical coupling between the two datasets. The volcano plots evaluate these differences by plotting significance ($-\log_{10}$ of p-value from an ANOVA or t-test) on the y-axis versus $\log_2$ of fold-change (FC) on the x-axis (Hur et al. 2018). The compounds with p-values below the chosen significance level and $\log_2 <$ FC threshold are considered significantly down-regulated or significantly specific to the denominator whereas the compounds meeting the same p-value threshold and $\log_2 >$ FC threshold are considered significantly up-regulated or significantly specific to the numerator. Compounds with significant p-values and FC meeting the upper or lower FC threshold are specific to that group of samples or can be said to be characteristic of that sample group. For all plots, p-value was set to 0.05 and FC was set to 1. The larger the $\log_2$ FC, the higher intensity that compound has in that sample compared to the others. The likelihood that a compound is present is higher with increasingly larger $-\log_{10}$ p-value. Thus, compounds in the upper left and upper right portions of the volcano plot are statistically more characteristic of that group and different from the other groups. It follows that these statistically distinct compounds can be isolated to explore how sample groups differ based on compound class and structure.

4.3 Results

4.3.1 Environmental Characterization

This study began at the end of one of the strongest multi-year (4-5 years) droughts on record for the state of Texas (Murgulet et al. 2017; TWDB 2017). During the drought preceding this study, Nueces Bay had become a reverse estuary with salinities as high as 38 in the bay compared to 35 of typical seawater. Further, the salinities in the lower Nueces River had steadily climbed to ~16 in low-flow fall and winter 2014 (**Figure 4.2A, Table 4.1**), indicating negligible fresh riverine influence on the bay under drought conditions. River and bay salinities dropped to 0.2 and <6.5, respectively, during peak flooding, high-flow conditions in summer 2015 (**Figure 4.2C, Table 4.1**) before rising to 22-32 in the bay and >6 in the river in fall 2015 during moderate-flow conditions (**Figure 4.2D, Table 4.1**). Salinities remained above 20 in the bay and 15 in the river through low-flow winter 2015 and spring 2016 (**Figure 4.2E-F, Table 4.1**). The increase in salinity throughout the bay, and in the lower Nueces River, demonstrates the minimal river and freshwater inflows due to upstream dams and diversions, under typical conditions (Murgulet et al. 2016).

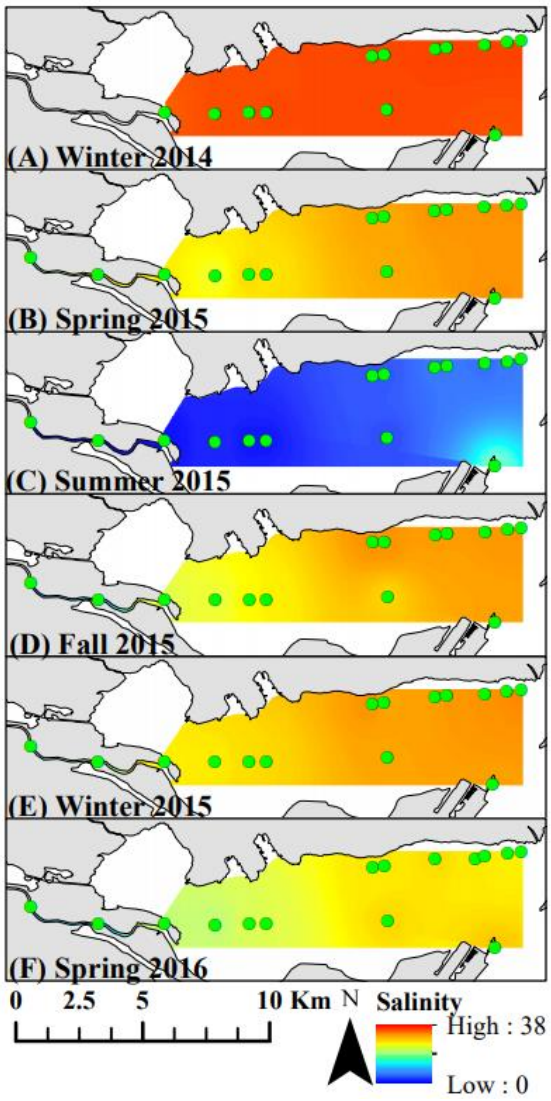

Figure 4.2: Inverse distance weighted interpolations of seasonal salinity from winter 2014 drought conditions through spring 2016 typical semi-wet conditions.

Table 4.1: Summary are surface- and porewater quality parameters.

	Station	Secchi (m)	Temp (°C)	DO (mg/L)	Sal	pH	Chl-α (µg/L)	DOC (µmol/L)	DON (µmol/L)	NO_2^-+NO_3^- (µmol/L)	NH_4^+ (µmol/L)
Summer	1	0.2	29.5	3.2	3.7	8.5	18.88	687.09	20.57	0.11	1.52
2015	2	0.2	29.2	2.9	6.0	8.3	21.61	682.51	16.53	1.55	3.94
	3	0.2	30	2.4	5.9	8.4	25.04	669.98	17.63	0.75	3.68
	4	0.2	29	1.5	5.5	8.3	19.36	609.65	17.64	0.17	1.84
	5	0.15	29.3	1.5	5.9	8.2	20.81	614.74	19.14	0.24	1.88
	6	0.2	29.4	1.4	6.3	8.2	22.17	681.17	20.12	0.15	2.53
	7	0.2	29.1	1.6	6.5	8.3	27.53	597.31	18.31	0.17	1.46
	8	0.35	30.3	1.7	0.2	7.3	5.77	1135.56	26.57	7.17	8.05
	9	0.2	28.7	1.7	1.6	8.5	27.60	743.54	25.37	1.30	1.79
	10	0.25	28.8	2.2	0.6	8.2	35.10	691.17	25.36	1.21	12.58
	11	0.35	28.2	2.1	0.6	8.2	32.65	941.89	25.87	0.08	1.69
	12	0.35	28.4	2.9	3.3	8.5	27.49	812.89	21.26	0.58	4.57
	13	0.3	29.2	3.2	17.2	8.2	19.68	662.83	20.98	0.12	2.30
	14	0.4	30	1.8	0.2	7.2	3.66	917.94	26.29	8.35	9.30
	15	0.65	29.7	1.2	0.2	7.4	4.57	704.88	37.52	5.05	3.50
	1P	-	28.8	0.4	30.5	7.4	-	242.06	22.97	0.03	32.33
	3P	-	29.9	0.5	31.9	7.3	-	434.21	111.93	0.03	209.25
	9P	-	31.4	0.7	25.1	7.1	-	415.06	364.00	0.01	466.54
	15P	-	27.2	1.2	39.7	6.7	-	131.10	33.69	0.14	83.61
	Surface Avg.	0.3	29.3	2.1	4.3	8.1	20.79	743.54	22.61	1.80	4.04
	Porewater Avg.	-	29.3	0.7	31.8	7.1	-	305.61	133.15	0.05	197.93
Fall	1	0.5	29.5	4.6	31.7	8.2	10.12	833.87	150.96	1.02	3.30
2015	2	0.4	29.7	4.7	31.7	8.2	12.01	392.50	16.87	1.18	2.79
	3	0.5	30.1	4.7	31.0	8.2	11.64	332.62	15.66	0.56	2.49
	4	0.5	30.4	4.6	30.9	8.2	8.12	427.42	19.10	1.51	3.25
	5	0.4	30.8	5.1	31.1	8.2	13.21	423.32	20.39	0.32	1.84
	6	0.5	30.8	5.5	31.3	8.2	13.03	545.18	19.31	0.15	1.86
	7	0.4	31.4	6.1	31.5	8.3	10.43	386.18	15.60	0.07	1.55
	8	0.2	29.9	5.7	22.4	8.2	18.58	697.98	20.62	0.01	1.96
	9	0.4	29.4	5.5	23.4	8.3	12.32	708.67	24.90	0.29	2.25
	10	0.5	29.2	5.0	25.2	8.3	8.94	528.61	37.69	0.03	2.27
	11	0.7	29.0	4.5	26.2	8.2	9.42	478.11	19.36	0.27	2.32
	12	0.5	29.3	4.4	27.6	8.2	12.97	573.16	19.45	0.29	2.16
	13	0.7	29.8	4.4	31.4	8.3	11.93	456.70	11.48	0.18	4.70
	14	0.2	29.4	4.6	13.8	8.7	57.53	895.88	27.23	11.62	2.00
	15	0.2	30.1	7.4	6.0	8.9	114.69	941.43	26.05	12.98	2.52
	7P	-	29.1	1.1	32.1	7.7	-	400.10	77.30	0.59	47.02
	14P	-	30.4	2.7	23.6	7.7	-	500.82	61.68	1.37	82.76
	15P	-	-	-	-	-	-	275.61	63.23	0.52	65.75
	Surface Avg.	0.4	29.9	5.1	26.3	8.3	21.66	574.77	29.65	2.03	2.48
	Porewater Avg.	-	29.8	1.9	27.8	7.7	-	392.18	67.41	0.82	65.18
Winter	1	1.6	17.8	-	31.8	8.3	1.24	715.62	19.50	0.04	0.96
2015	2	1.6	16.3	-	30.4	8.4	1.16	614.28	19.57	0.11	1.50
	3	1.6	16.3	-	30.4	8.4	1.23	454.14	27.38	0.16	1.42
	4	1.2	16.8	-	31.4	8.1	1.13	535.65	19.31	0.04	0.84
	5	1.3	16.7	-	31.3	8.2	0.60	418.32	11.73	0.21	1.69
	6	0.6	17.3	-	32.0	8.3	1.74	741.98	23.07	0.02	1.81
	7	1.2	17.8	-	32.4	8.3	1.34	1326.08	25.41	0.02	1.14
	8	0.5	16.0	-	25.8	8.4	11.84	1152.80	24.36	0.04	1.75
	9	0.6	16.0	-	26.3	8.3	14.76	776.83	22.41	0.04	1.80
	10	1.1	-	-	27.7	8.3	3.77	842.14	19.80	0.03	1.87
	11	1.7	16.9	-	30.5	8.1	6.56	619.12	18.73	1.48	0.97
	12	0.7	15.7	-	30.4	8.3	5.45	878.28	23.44	0.00	1.13
	13	1.2	15.6	-	30.8	8.1	2.01	728.62	20.88	0.80	2.02
	14	0.5	16.9	-	23.4	8.2	25.04	836.79	29.02	0.03	3.31
	15	0.4	15.8	-	14.9	8.6	40.92	824.93	3.88	40.56	1.94
	3P	-	20.2	-	37.7	7.4	-	332.19	114.07	0.03	212.73
	11P	-		-	35.8		-	404.00	415.13	2.79	576.47
	14P	-	21.9	-	28.9	7.6	-	485.60	98.18	0.18	81.23

	Surface Avg.	1.1	16.6	-	28.6	8.3	7.92	764.37	20.57	2.91	1.61
	Porewater Avg.	-	21.1	-	34.1	7.5	-	407.26	209.13	1.00	290.15
Spring 2016	1	0.4	18.9	8.3	26.5	8.1	13.92	452.60	13.93	0.06	2.14
	2	0.4	19.2	8.7	26.7	8.1	14.43	443.47	14.75	0.09	2.13
	3	0.4	18.7	8.0	27.2	8.1	8.58	413.57	14.32	0.10	1.71
	4	0.4	18.8	7.7	26.6	7.8	5.57	439.84	8.77	4.52	3.87
	5	0.9	18.4	9.2	26.3	8.3	7.98	449.06	15.37	0.08	2.00
	6	0.8	18.0	9.2	26.0	8.3	9.45	455.09	16.50	0.62	2.31
	7	0.9	18.0	8.2	25.8	8.3	5.99	425.23	14.31	0.44	2.07
	8	0.3	19.0	8.1	20.1	8.0	10.97	578.05	19.98	0.18	2.44
	9	0.5	19.2	10.4	20.6	8.3	19.06	693.22	21.85	0.32	3.15
	10	0.6	17.7	11.2	23.8	8.3	22.77	588.99	19.42	0.29	2.46
	11	0.6	17.8	9.8	26.3	8.3	20.81	547.49	18.87	0.70	2.36
	12	0.7	18.1	7.9	27.5	8.2	9.93	305.61	14.58	0.13	2.66
	13	0.6	18.0	7.7	28.6	8.1	3.58	351.08	10.49	1.29	4.38
	14	0.3	19.1	7.3	17.6	8.1	21.86	538.30	32.94	0.13	2.78
	15	0.2	20.0	6.7	15.4	8.2	35.31	607.63	23.68	0.25	1.85
	3P	-	21.0	2.7	31.4	7.5	-	246.72	47.96	0.02	82.80
	4P	-	17.4	2.4	31.6	7.1	-	341.70	595.43	0.06	714.69
	8P	-	21.7	2.6	27.3	7.0	-	395.88	235.15	0.00	334.65
	14P	-	22.6	2.2	27.2	7.2	-	470.38	70.14	0.01	140.49
	15P	-	23.9	2.3	38.7	6.6	-	101.59	23.14	0.08	50.92
	Surface Avg.	0.5	18.6	8.5	24.3	8.2	14.01	485.95	17.32	0.61	2.55
	Porewater Avg.	-	21.3	2.5	31.3	7.1	-	311.25	194.36	0.04	264.71

4.3.2 DOC, DON, C:N ratios, and Chlorophyll-α

The highest average surface water DOC concentrations (n=15) were measured in summer and winter (744 ± 149 and 764 ± 241 µM-C, respectively) followed by fall (575 ± 196 µM-C) while the lowest was in spring (486 ± 104 µM-C) (**Table 4.1, Figure 4.3A**). The highest surface water DON concentrations were measured in fall (30 ± 34 µM-N) while the lowest concentrations occurred in spring (17 ± 6 µM-N) (**Figure 4.3B**). The average C:N ratio (C:N = [DOC]/[DON]; **Figure 4.4**) ranged from 26 to 47 indicating a predominantly terrestrial source of DOM (Bianchi 2006). The fall season had a significantly lower C:N ratio ($\bar{x}$ = 26) relative to the other three seasons ($\bar{x}$ = 30 - 47).

Surface water DOC concentrations were 1.5 – 2.4 times greater than porewater concentrations across all seasons. The greatest difference in DOC concentration between surface

water and porewater occurred in summer during flooding. In contrast, porewater DON concentrations were 2.3 – 11.2 times greater than surface water concentrations with the greatest difference occurring in winter and spring. Fall exhibited the least difference between surface- and porewater DOC and DON concentrations. Additionally, the porewater show significantly higher NH_4^+ relative to $NO_{2\text{-}3}^-$ in summer, winter, and spring; however, in fall, there was relatively high $NO_{2\text{-}3}^-$ and low NH_4^+ in porewater (**Figure 4.5**).

In the bay, the lowest chl-α concentrations were observed in winter ($\overline{x}$ = 4.23 $\mu g \cdot L^{-1}$), the highest concentrations were observed in summer ($\overline{x}$ = 23.67 $\mu g \cdot L^{-1}$), while fall and spring were similar ($\overline{x}$ = 11.73 $\mu g \cdot L^{-1}$ and 12.45 $\mu g \cdot L^{-1}$, respectively) (**Table 4.1**). These chl-α concentrations follow expected seasonal trends with decreased primary productivity in colder winter months and increased primary productivity in warmer summer months. Overall, the highest chl-α concentrations were observed in the river in fall (57.53 – 114.69 $\mu g \cdot L^{-1}$) while the lowest chl-α concentrations were observed along the northern shore in winter (0.60 – 1.74 $\mu g \cdot L^{-1}$).

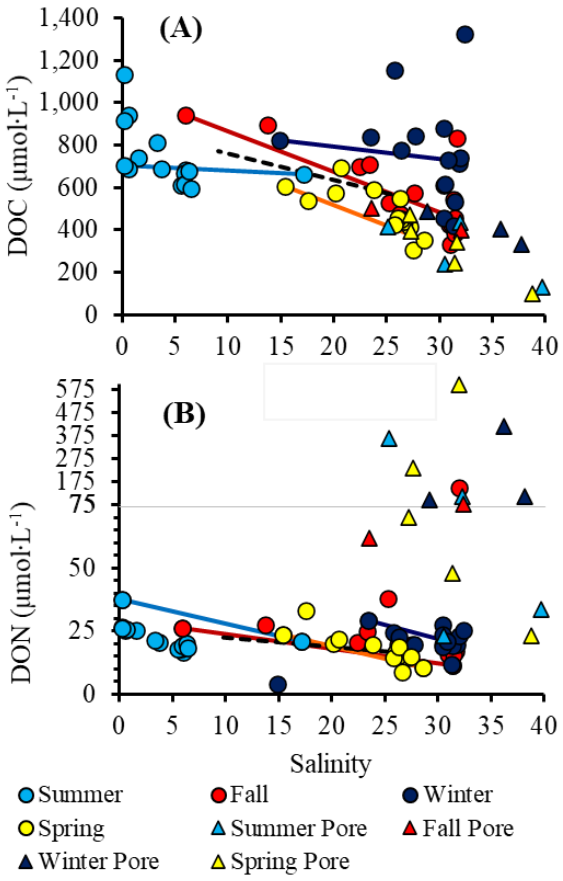

Figure 4.3: DOC and DON concentrations for surface-water (filled circles) and porewater (filled triangles) for each season. Seasonal conservative mixing lines (solid lines) and the average mixing line (black dashed line) between Nueces River and Corpus Christi Bay are provided. (A) DOC. (B) DON (Note the change in axis units above 75 µmol·L^{-1}).

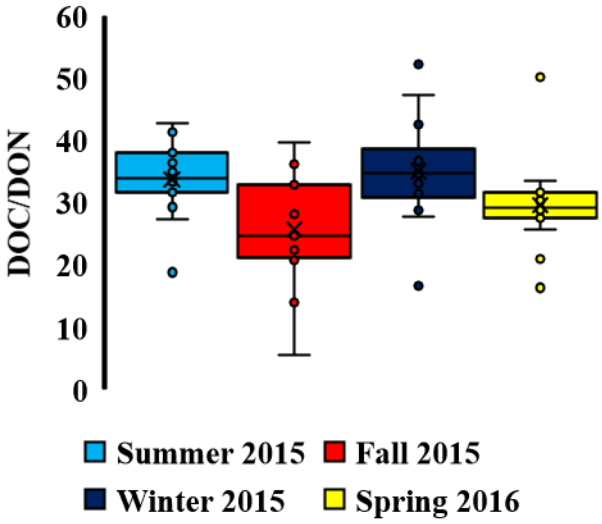

Figure 4.4: Box plots of DOC/DON ratios for each season showing the mean, median, interquartile ranges, and outliers.

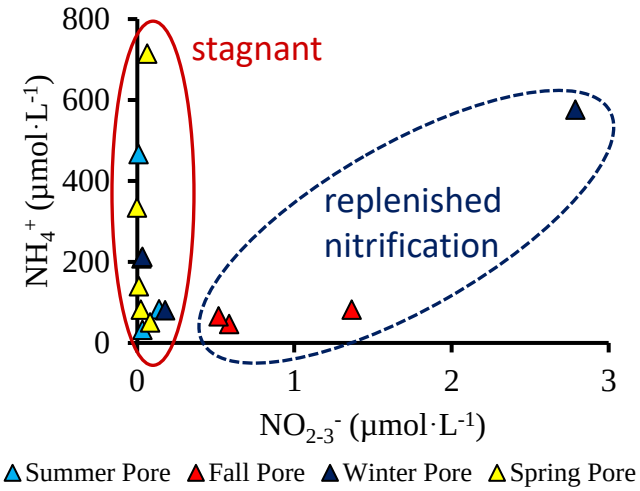

Figure 4.5: Biplot of NO_{2-3}^- (nitrate+nitrite) and NH_4^+ (ammonium) in Nueces Bay porewater.

4.3.3 Dissolved Organic Matter Molecular Composition

A total of 2977 unique compounds were detected in surface- and porewater samples by UPLC-OT-FTMS. Of these compounds, molecular formulas were assigned to 2283 compounds (~77%). Over half of the assigned compounds occur as CHO (55%) with the remaining compounds falling predominantly into nitrogen and sulfur containing compounds: CHON (25.2%), CHONS (7%), and CHOS (6.5%) (**Figure 4.6A**). Phosphorus containing compounds (i.e., CHOP, CHONP, and CHOPS) make up the residual 7%. The much lower percentages of P containing compounds are expected with ESI+ mode due to the preferential ionization of N containing compounds (Liu and Lu 2019; Ohno et al. 2016). Looking to each season, fall has more compounds present (2150) than summer (1514) and both have similar overall compound distributions (**Figure 4.6B-C**) when compared to the entire dataset (**Figure 4.6A**), though with 2-4% more CHO compounds present in summer and fall. Winter and spring have a marked decrease in total compounds present (443 and 421, respectively; **Figure 4.6D-E**) and a shift in

compound class distribution. These later seasons have a decreased percentage of CHO compounds (43.3 – 48.4%), increased percentage of CHON (42.3 – 46.9%), and decreased percentages of sulfur (CHOS, CHONS 5.5 – 7.2%) and phosphorous containing compounds (0.3 – 0.6%) compared to previous seasons (**Figure 4.6D-E**). However, while organic phosphorus compounds are not commonly observed in DOM using MS, it is possible their presence in this bay may be a legacy of the historic oil-brine discharges directly to the bay and past agricultural use of organophosphorus pesticides and fertilizers (Gunnars and Blomqvist 1997; Gunnars et al. 2002; Hupfer and Lewandowski 2008).

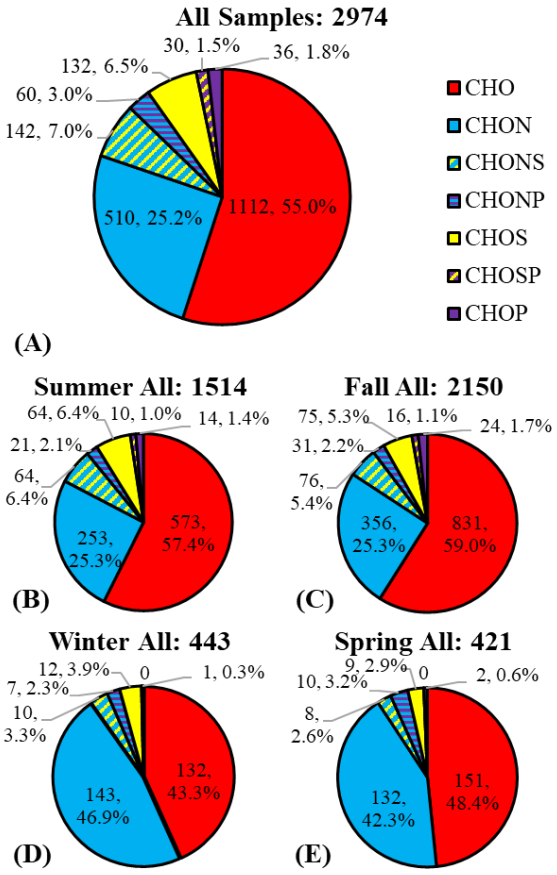

Figure 4.6: Pie charts of the compound class distribution as total compounds present for each class and percentage of the total compounds present for all surface- and porewater samples. (A)

All surface- and porewater samples. (B) All summer/flooding surface- and porewater samples. (C) All fall/flooding recession surface- and porewater samples. (D) All winter surface- and porewater samples. (E) All spring surface- and porewater samples.

4.3.4 PCA, Volcano Plots, and van Krevelen Diagrams

The PCA analysis shows most of the variance among samples is due to the characteristic differences among fall surface- (n = 13) and porewater (n = 3) and a few summer surface- (n = 3) and porewater (n = 2) signatures/characteristics which are separated from all other seasons samples on the PC1 axis (**Figure 4.7**). While PC1 explains ~33% of the variance in the samples, PC2 explains ~9% of the variance. There is less substantial separation of samples along the PC2 axis, with a handful of surface water samples from summer (n=3), fall (n=2), and spring (n=1) with larger positive scores. Thus, only PC1 is used for further discussion.

Samples with positive PC1 scores have lower O/C_w ($\overline{x}$ = 0.10), H/C_w ($\overline{x}$ = 0.87), and a greater number of compounds present ($\overline{x}$ = 462.7) than compounds with negative scores (O/C_w $\overline{x}$ = 0.14, H/C_w $\overline{x}$ = 0.91, presence $\overline{x}$ = 116.5). Thus, the positive PC1 scores are associated with greater DOM diversity that is comprised of slightly less oxygenated and unsaturated compounds while negative PC1 scores are associated with less DOM diversity that is slightly more oxygenated and saturated. Further, the DOM in the bay was less oxygenated in fall (O/C_w $\overline{x}$ = 0.09), less saturated (H/C_w $\overline{x}$ = 0.80), and contained more N compounds (C:N $\overline{x}$ = 23.05) than any other season (O/C_w $\overline{x}$ >0.12, C:N $\overline{x}$ >30.8) (**Table 4.2**). However, the average DBE_w for compounds loading positively and negatively on PC1 were similar ($\overline{x}$ = 2.70 and 2.71, respectively), indicating little change in overall aromaticity.

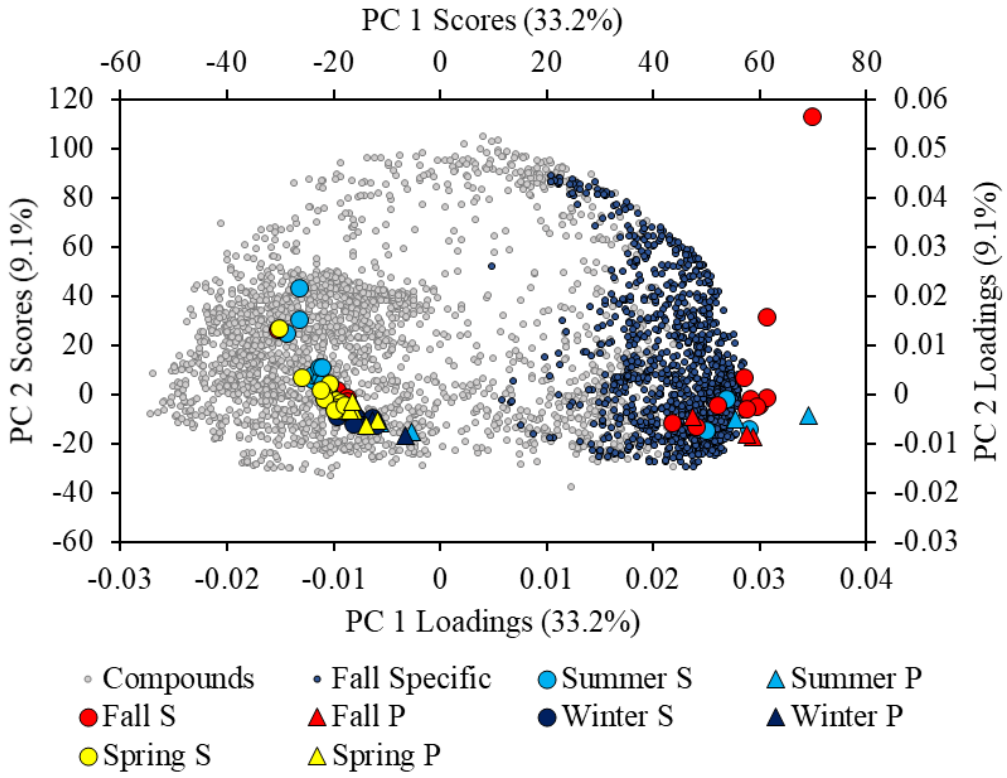

Figure 4.7: Principal components analysis plot of scores for surface- (circles) and porewater (triangles) in summer (light blue), fall (red), winter (dark blue), and summer (yellow) and loadings for all compounds (small grey circles). Compounds specific to fall surface- and porewater only, as determined from volcano plot seasonal comparisons (see **Figure 4.8**), are shown (small dark blue circles). To determine which compounds are significant to the samples and how the samples group, a PCA is performed with the centered and scaled and mean normalized intensities for each compound across all samples.

Table 4.2: Average (± 1 standard deviation) of all bay stations (1-12). Texas Water Development Board freshwater inflow estimates (FWI) are $x10^5$ $m \cdot d^{-1}$ (Douglas et al. 2020b; TWDB 2018).

	SU	F	W	SP
FWI	170	1.50	0.06	0.70
Chl-α	**23.67**±7.6	**11.73**±2.75	**4.23**±4.68	**12.45**±5.78
C:N	**34.98**±4.58	**23.05**±7.49	**35.62**±9.17	**30.76**±6.74
Temp	**29.16**±0.61	**29.96**±0.75	**16.69**±0.72	**18.48**±0.55
Present	**1642**±630	**2514**±552	**1201**±88.1	**1330**±95.2
O/C_w	**0.15**±0.02	**0.09**±0.01	**0.12**±0.03	**0.14**±0.02
H/C_w	**1.09**±0.12	**0.80**±0.09	**0.78**±0.19	**0.93**±0.17
DBE_w	**2.84**±0.22	**2.57**±0.33	**2.40**±0.51	**2.84**±0.20

The volcano plots show that the fall DOM composition was significantly different from all other seasons both in terms of presence of more compounds ($p<0.05$) and in terms of greater concentrations of the compounds (FC) (**Figure 4.8-A1, B1; Table 4.3**). These volcano plot observations agree with the PCA analysis as the compounds significantly specific only to fall load positively on PC1 and correspond to most of the fall surface- and porewater samples (**Figure 4.7**). A closer look at the DOM compounds that are significantly different in fall relative to summer (or winter) shows around 2000 compounds are specific to fall relative to the other two seasons. These fall specific DOM compounds are characterized by high abundances of N and S containing compounds and are predominantly low O/C (< 0.4) and high H/C (> 1) (**Figure 4.8-A2, B3**) whereas summer and winter specific DOM are higher O/C (> 0.2) and lower H/C (< 1.75) (**Figure 4.8-A3, B3**).

There is very little difference in DOM composition in both presence and concentration between winter and spring samples (**Figure 4.8-C1**). Winter and spring have similar compound

distributions in van Krevelen space (**Figure 4.8-C2, C3**), though winter CHO compounds appear to be more degraded ($\overline{x}$ O/C = 0.29, H/C = 1.3) than spring samples ($\overline{x}$ O/C = 0.21, H/C = 1.4).

Overall, the compounds specific to porewater are predominantly CHO compounds with a wide range of H/C (0.5 – 2.25) and N containing compounds with low O/C (<0.2). Porewater also contains several condensed aromatics, a compound class indicative of incomplete combustion of organic matter, that are also represented in fall DOM surface water samples (**Figure 4.9-B1**) but not summer, winter, or spring (**Figure 4.9-A1, C1, D1**). In contrast, the compounds representative of surface water contain more S and P compounds with high H/C (i.e., more aliphatic), CHO compounds with a more restricted range of H/C (1 – 1.75), and N containing compounds that have predominantly shifted to higher O/C (>0.2) and lower H/C (0.5 – 1.75) (**Figure 4.9-A2, A3, B2, B3, C2, C3**). This shift in N containing compounds reflects more degraded DOM, which indicates the presence of deaminated peptides in surface water from the degradation of porewater DOM (Abdulla et al. 2018).

Table 4.3: Summary of seasonal volcano plot comparison including total number of compounds specific to each season, total number of compounds non-specific (Nonsig) to either season, and the molecular composition of the compounds with an assigned formula. SU = summer 2015. F = fall 2015. W=winter 2015. SP = spring 2016.

		Total Compounds	Assigned Formulas	CHO	N	S	P	NS	NP	SP
SU vs. F	SU	117	78	30	37	2	0	0	9	0
	F	**1,882**	**1,118**	**532**	**264**	**100**	**27**	**129**	**38**	**28**
	Nonsig	978	822	546	209	30	9	13	13	2
F vs. W	F	**2,094**	**1,320**	**708**	**273**	**107**	**31**	**130**	**41**	**30**
	W	106	77	16	50	5	0	1	5	0
	Nonsig	777	623	385	188	20	5	11	14	0
W vs. SP	W	67	64	27	31	3	0	1	2	0
	SP	89	80	44	33	1	0	1	1	0
	Nonsig	**2,821**	**1,874**	**1,037**	**446**	**128**	**36**	**140**	**57**	**30**

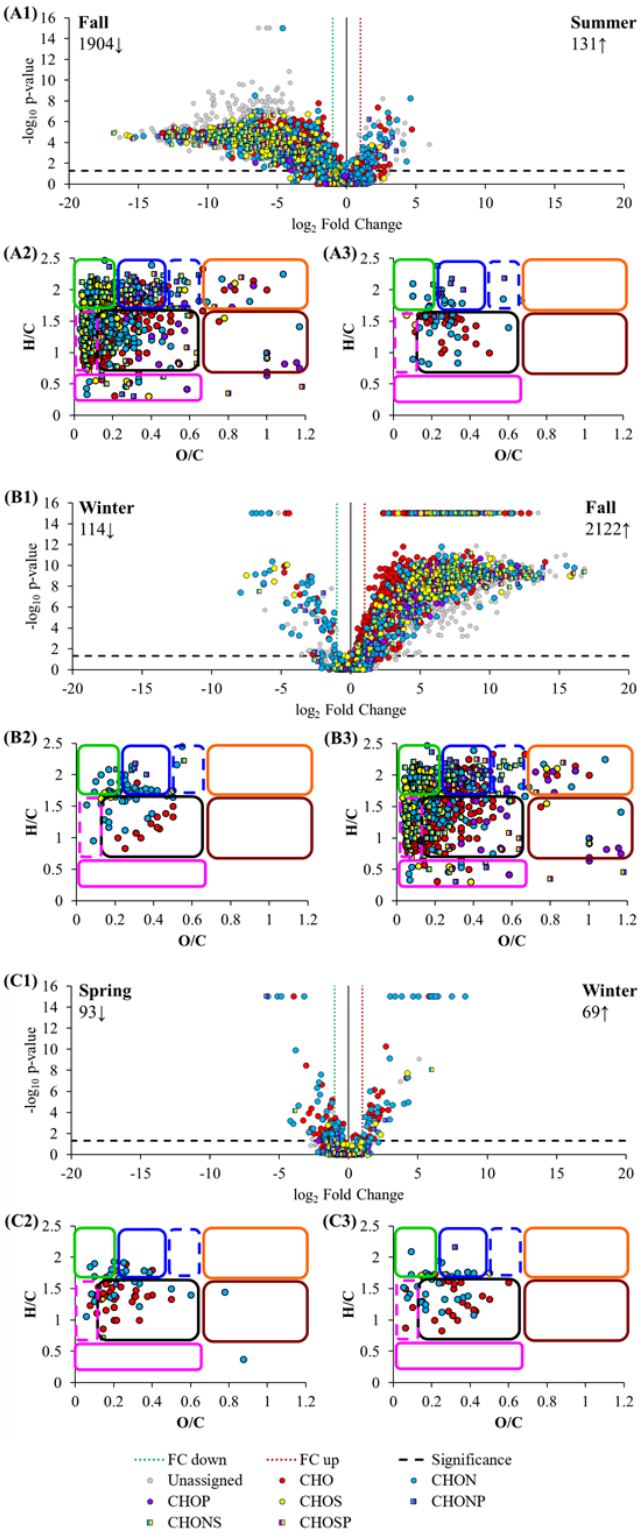

Figure 4.8: Volcano plot and van Krevelen diagrams for Summer vs. Fall (A), Fall vs. Winter (B), and Winter vs. Spring (C) seasonal comparisons. Significant compounds (p-values ≤ 0.05)

plot above the horizontal black dashed line. Compounds exceeding the upper FC threshold (log_2 FC ≥ 1) plot to the right of the red vertical dotted line and compounds meeting the lower FC threshold (log_2 FC ≤ -1) plot to the left of the green vertical dotted line. Generalized compound class regions are defined by the boxes within the van Krevelen diagrams as follows: lignin/CRAM (black), lipids (green), peptides (solid blue), amino-sugars (dashed blue), condensed hydrocarbons (solid pink), unsaturated hydrocarbons (dashed pink), carbohydrate (orange), and tannins (dark red).

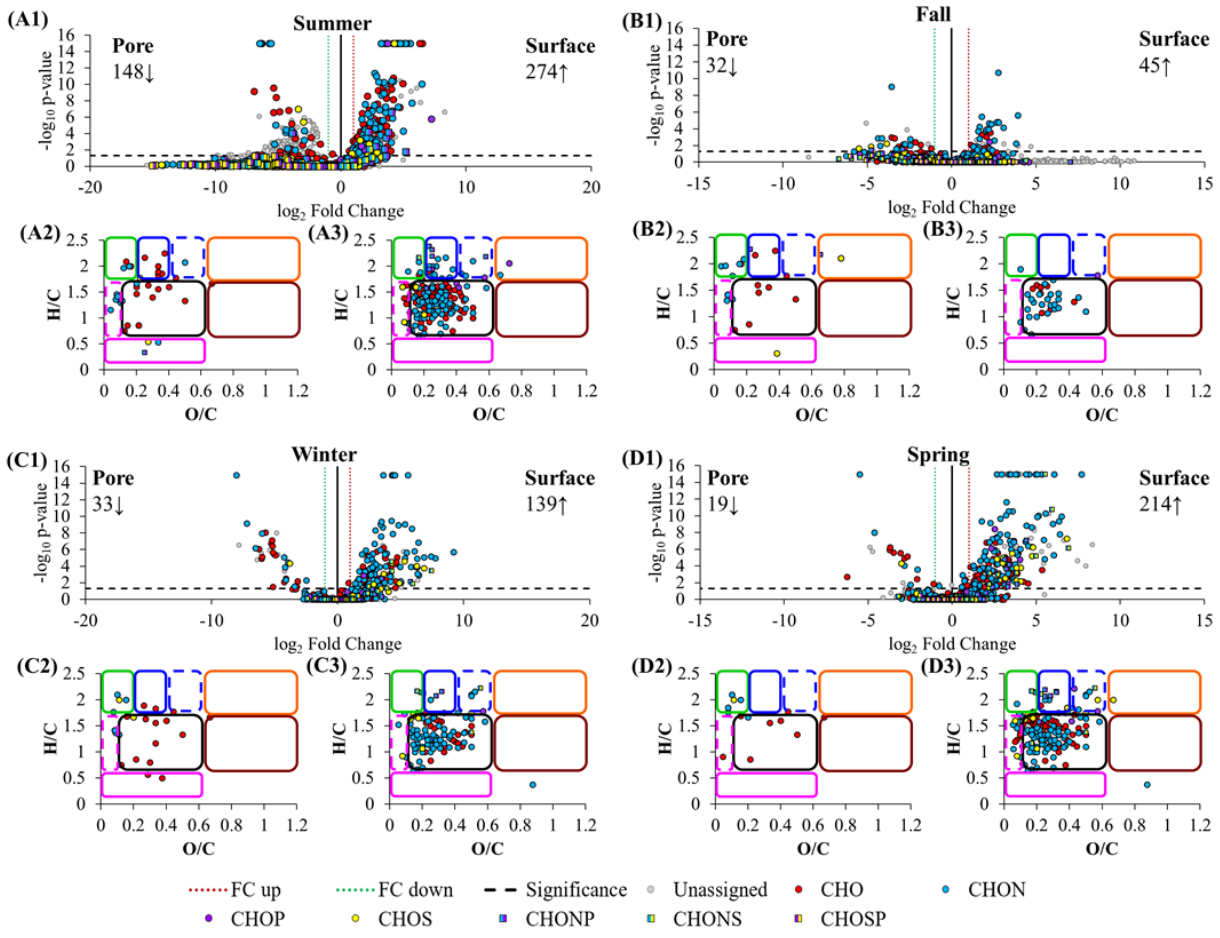

Figure 4.9: Volcano plot and van Krevelen diagrams for Summer Surface vs. Pore (A), Fall Surface vs. Pore (B), and Winter Surface vs. Pore (C) seasonal comparisons. Significant compounds (p-values ≤ 0.05) plot above the horizontal black dashed line. Compounds exceeding the upper FC threshold ($\log_2$ FC ≥ 1) plot to the right of the red vertical dotted line and compounds meeting the lower FC threshold ($\log_2$ FC ≤ -1) plot to the left of the green vertical dotted line. Generalized compound class regions are defined by the boxes within the van Krevelen diagrams as follows: lignin/CRAM (black), lipids (green), peptides (solid blue), amino-sugars (dashed blue), condensed hydrocarbons (solid pink), unsaturated hydrocarbons (dashed pink), carbohydrate (orange), and tannins (dark red).

4.4 Discussion

4.4.1 C:N Ratios

The substantially lower C:N ratio in fall relative to the other seasons indicates a significant change in the DOM sources from fall to the other seasons possibly due to changes in the riverine DOM input, in-situ production, or an input of DOM from another source, such as groundwater. Riverine C:N ratios increase under episodic high-flow conditions, i.e., pulse-shunt concept (Raymond et al. 2016), as there is insufficient time for primary production and degradation processes to occur in order for autochthonous DOM to overcome the allochthonous DOM signal (Dixon et al. 2014). Thus, higher flow and runoff conditions could explain the high C:N ratio in summer and spring but not low-flow winter. Instead, high C:N ratios in the bay in winter and spring may be attributed in part to decreased in-situ production of autochthonous DOM. The highest C:N ratios and lowest chl-α were observed during winter, following several weeks after substantial precipitation events (65-82 mm) and experiencing low-flow, with low winds, low turbidity, and seasonally low water levels. While the low-flow and low turbidity would generally facilitate more photooxidation and degradation of DOM, the simultaneously low chl-α concentrations, low temperatures ($\overline{x}$ = 16.6°C), and short daylight hours would reduce these degradation processes and autochthonous DOM production. Discharge of deeper groundwater into the bay in winter 2015 was shown to occur with radium 224:226 signature (Douglas et al. 2020b). While groundwater is typically low in DOC concentrations (Beck et al. 2007; Longnecker and Kujawinski 2011; Sañudo-Wilhelmy et al. 2002), high C:N ratios have been observed during high recharge events (Montluçon and Sañudo-Wilhelmy 2001). Thus, potentially elevated C:N ratios following substantial precipitation events in combination with the

enhanced deeper groundwater discharge and reduced DOM degradation processes would favor a dominant groundwater source of DOM in the winter season.

In contrast to the other seasons, in fall the bay shows enrichment in DON. Further, the low average C:N ratio could not be attributed merely to higher contribution of in-situ production of autochthonous DOM during the fall season relative to the other seasons as the average chl-α concentrations in the bay were low in fall. Moreover, the low bay chl-α concentrations in fall were similar to bay chl-α concentrations in spring but still had lower average C:N ratios with moderate discharge rates. Mixing of surface water with a lower C:N ratio DOM from a diffuse source, such as the porewater (C:N $\bar{x}$ = 3 – 6; **Table 4.1**), is perhaps a more likely process explaining the lower C:N ratios. Further, nearshore surface water DOC concentrations plot closely with the porewater DOC in fall (**Figure 4.3A**). Additionally, the porewater show significantly higher NH_4^+ relative to $NO_{2\text{-}3}^-$ which indicates stagnant anoxic conditions in summer, winter, and spring. However, in fall, relatively high $NO_{2\text{-}3}^-$ and low NH_4^+ in porewater indicate groundwater replenishment, porewater flushing, or nitrification (**Figure 4.5**). Hydrologic conditions (Douglas et al. 2020b; Murgulet et al. 2018) support these trends.

Flood events can represent a large pulse of terrigenous DOM derived from river catchments, which, because of the rapid transport to the coastal ocean, remains relatively unaltered by the estuarine filter (Mori et al. 2019; Raymond et al. 2016). The catchment area of Nueces River estuary is largely deforested and subject to urban, industrial, and agricultural influences, which leads to increased runoff following heavy precipitation events. In relation to hydrologic changes in the estuary, surface water DOC and DON concentrations generally decreased as salinity increased offshore into the primary bay (**Figure 4.3**). During summer and winter, DOC concentrations show large enrichments compared to seasonal conservative mixing. These

enrichments indicate more input of DOM further downstream from the river endmember. Saltmarshes, which are present at the head of the bay, are expected to contribute DOM enriched waters following flood events (Medeiros et al. 2015). On the other hand, during dry, low wind winter conditions following a precipitation event, a combination of reduced wind-driven mixing (i.e., seawater recirculation and sediment resuspension) (Dixon et al. 2014), SGD (Murgulet et al. 2018), and less biogeochemical transformations in the bay (Mori et al. 2019) combined could account for the DOC enrichment.

4.4.2 Dissolved Organic Matter Molecular Composition

The greater DOM molecular diversity in summer and fall than winter and spring, exhibited by the greater number of compounds present and increased percentages of heteroatom compounds in summer and fall, is not explained by the seasonal DOC and salinity characteristics. Instead the inter-seasonal changes in DOM sources and degradation processes could account for these changes in DOM molecular diversity. To take a closer look at the molecular diversity between the different seasons, we applied different multivariate analysis techniques to the detected compounds.

4.2.1 Seasonal Trends

The fall specific DOM compounds are characterized by high abundances of N and S containing compounds and are predominantly low O/C (< 0.4) and high H/C (> 1) with many compounds in the unsaturated hydrocarbon (i.e., low O/C and lower H/C), lipid (i.e., high H/C and low O/C), and peptide (i.e., high H/C, O/C <0.7) regions (**Figure 4.8-A2, B3**). Previous studies have shown that DOM become more aliphatic (i.e., increase H/C), increase heteroatom content, and decrease oxygenation (i.e., decrease O/C) along gradients of increasing salinity in

temperate and tropical estuaries as marine DOM influences increase (Osterholz et al. 2016; Sleighter et al. 2010). In fall, as riverine discharge decreased, marine influences increased which could account for the consistently high DOM diversity from summer to fall.

In contrast, DOM compounds specific to summer (**Figure 4.8-A3**) and winter (**Figure 4.8-B2**) plot predominantly in the peptide and lignin/carboxylic-rich alicyclic molecules (CRAM) regions with some low H/C nitrogen compounds that could be deaminated peptides (Abdulla et al. 2018). On average, CHO compounds are less oxygenated and more saturated in fall ($\overline{x}$ O/C = 0.2, H/C = 1.2-1.4) than in summer ($\overline{x}$ O/C = 0.27, H/C = 1.5) or winter ($\overline{x}$ O/C = 0.36, H/C = 1.4), which could indicate higher alteration (oxidation) of DOM in summer and winter compared to fall season. The elevated presence of N and S containing heteroatoms combined with the more saturated aliphatic characteristics (i.e., higher H/C and lower O/C) in fall indicate biotransformation of terrestrial DOM and input of autochthonous microbial DOM (Medeiros et al. 2015; Mori et al. 2019; Osterholz et al. 2016; Sleighter and Hatcher 2008) as well as possible porewater input of S-containing DOM from sulfidic porewaters (Mori et al. 2019; Schmidt et al. 2009; Schmidt et al. 2017; Sleighter et al. 2014). A distinct hydrogen sulfide smell and low dissolved oxygen was observed while sampling porewater but not in surface water. Sulfur-enriched DOM is generally observed in sulfidic environments and can be the result of abiotic chemical reactions of sulfide with DOM (Abdulla et al. 2020; Gomez-Saez et al. 2016; Mori et al. 2019; Pohlabeln et al. 2017; Schmidt et al. 2009; Schmidt et al. 2017), which also result in lower C:N ratios (Abdulla et al. 2018; Beck et al. 2008; Hansen et al. 1993; Jørgensen 1982). As the fall surface water specific compounds are also related to a lower average C:N ratio and group with the summer and fall porewater in the PCA, we suggest that the fall DOM composition is strongly influenced by the input of microbially transformed porewater DOM.

Interestingly, fall specific DOM compounds also include condensed hydrocarbons (i.e., low H/C), carbohydrate-like (i.e., high H/C and high O/C), and tannin-like (i.e., high O/C and low H/C) which are not present in summer or winter. Condensed aromatic compounds (dissolved black carbon) usually result from the incomplete combustion of organic compounds and may include direct input from local combustion sources or atmospheric deposition from distant combustion sources such as industrial, automobile, agricultural, domestic wildfire, or biomass burning (Dittmar 2008; Maria et al. 2019; Stubbins et al. 2012a). Several studies have detected condensed aromatic compounds in both terrestrial and aquatic DOM pools (Dittmar 2008; Stubbins et al. 2015; Wagner et al. 2015a; Ziolkowski and Druffel 2010) as well as a significant fraction of soil DOM as condensed aromatics (Maria et al. 2019). Although dissolved black carbon is traditionally considered refractory based on its old apparent radio carbon age (Ziolkowski and Druffel 2010), dissolved black carbon may photo-degrade more rapidly and more extensively than bulk DOC and colored DOM (Stubbins et al. 2012b). Thus, while local combustion sources (e.g., refineries, automobiles) may not vary greatly between seasons, the groundwater inputs do. Therefore, the presence of these easily photo-degradable condensed aromatic compounds supports the possibility of benthic DOM source from both porewater and groundwater. Tannins, ubiquitous in vascular plant tissues (e.g., leaves, roots, wood, fruit), represent a significant portion of terrestrial biomass (Kraus et al. 2003). Tannins enter soils and groundwater by leaching and litter inputs above and below ground where they can remain in solution, precipitate, adsorb to sediment particles or complex metals, or be transformed biotically or abiotically (Maria et al. 2019). In contrast, carbohydrates are highly bioavailable and are taken up quickly by microbial activity. Thus, the presence of highly labile carbohydrate-like

compounds indicates an autochthonous source which could be from benthic flux or in-situ production.

The similarities between winter and spring samples (as indicated from volcano plots and PCA) are further confirmed through the very little difference in DOM composition in both presence and concentration between these seasons (**Figure 4.8-C1**). While winter and spring have similar compound distributions in van Krevelen space (**Figure 4.8-C2, C3**), winter CHO compounds appear to be more degraded ($\overline{x}$ O/C = 0.29, H/C = 1.3) than spring samples ($\overline{x}$ O/C = 0.21, H/C = 1.4). Winter samples were collected during a period of relatively low winds and calm waters with little to no turbidity (secchi depths = water column depth). As such, the bay water was clear potentially allowing for more photooxidative degradation of DOM, limited seawater recirculation, and less input from sediment resuspension (Dixon et al. 2014) in winter than in spring.

4.2.2. Surface water vs. Porewater

Within the same season there are clear differences between surface- and porewater for summer, winter, and spring (**Figure 4.9-A, C-D**) while fall signatures are more similar (**Figure 4.9B**). Summer surface water specific compounds are predominantly CHO and CHON that plot within the lignin/CRAM region (**Figure 4.9-A3**), whereas compounds specific to summer porewater are of largely unassigned molecular composition (**Figure 4.9-A1**). Those porewater compounds that are assigned have a slightly higher average H/C ($\overline{x}$ = 1.49) compared to surface water ($\overline{x}$ = 1.43) (**Figure 4.9-A2**). Very few heteroatom compounds are significantly specific to either surface- or porewater in summer; however, the majority of heteroatom compounds have higher abundances in porewater than surface water (i.e., exceed the lower FC>2 threshold). Winter (**Figure 4.9-C1, C3**) and spring (**Figure 4.9-D1, D3**) surface water specific DOM

compounds follow similar trends to summer but with fewer specific compounds and proportionally more CHON in winter. Fewer porewater DOM compounds are specific to winter (**Figure 4.9-C1, C2**) and spring (**Figure 4.9-D1, D2**) and, unlike summer heteroatom compounds, have similar concentrations to surface water. The increased concentration of heteroatom compounds in porewater in summer is likely a result of inhibited benthic fluxes due to the significantly lower surface water salinity (0.2 – 17.2, $\overline{x}$ = 4.3) preventing convective exchange with the higher salinity porewater (25.1 – 39.7, $\overline{x}$ = 31.8) and the decreased hydraulic gradient toward the bay. During this period of inhibited benthic fluxes, DOM would accumulate in the porewater.

The largest similarities between surface- and porewater DOM composition observed in fall (**Figure 4.9-B1**) showed more degraded characteristics with more oxygenated CHON compounds in surface water than those in porewater plotting almost entirely within the lignin/CRAM region (lower H/C) (**Figure 4.9-B3**). The similarity between fall porewater and surface water confirms the earlier hypothesis of a significant flux between porewater and surface water in this season. Recall that SGD rates were the lowest in summer but increased in subsequent sampling trips (Murgulet et al. 2018). Increases in SGD have been shown to lag precipitation by weeks (shallow groundwater) to months (deep groundwater) (Douglas et al. 2020b; Urquidi-Gaume et al. 2016), so enhanced SGD to the river and the bay in fall accompanied by moderate riverine discharge could result in the increased uniformity in DOM composition between surface- and porewater (Murgulet et al. 2018).

4.4.3 Implications of Seasonal Hydroclimatic Conditions on Estuarine DOM

Following significant wet conditions and flooding, slow recharge to the water table and an increase in groundwater level are associated with flood recession and return to baseflow

conditions. Consequently, increasing hydraulic gradients facilitate greater lateral groundwater, hence porewater, contribution to the bay in the nearshore. Thus, during flooding recession, i.e., moderate-flow fall, the estuary has transitioned from river dominant to porewater and marine dominant. As a result, the DOM composition reflects the more complex mixture of the anoxic porewater and marine DOM with the higher percentage of N- and S-heteroatoms (Abdulla et al. 2018; Rossel et al. 2016; Schmidt et al. 2017; Sleighter and Hatcher 2008; Sleighter et al. 2010). However, the dominant groundwater source appears to shift over time as shallow aquifers will respond to hydroclimatic conditions within the watershed more quickly than deeper aquifers (Douglas et al. 2020b). So, by winter, which follows six months after the large late spring/early summer precipitation and 4-6 weeks after two substantial precipitation events, the initial runoff and nearshore SGD response has diminished and the offshore SGD response, which includes a deeper groundwater source (Douglas et al. 2020b), becomes apparent (i.e., expected high C:N ratios, high DOC concentrations with low-flow) .

While Abdulla et al. (2020) has shown that abiotic sulfurization is a major pathway forming dissolved organic sulfur in anoxic sediments, the shift in overall DOM composition from flooding to flood recession reflects changes in DOM sources and transformations that are associated with hydrologic changes. Under these conditions, the DOM composition may be enriched in anthropogenic DOM (e.g., detergents and surfactants) with a greater abundance of N- and S-containing molecular formulas (Gonsior et al. 2011; Wagner et al. 2015b). Thus, the DOM composition may retain the anthropogenic N- and S-containing compounds brought into the system with the first flush of flood water or porewater following a large wet event as it reaches the bay. As the bay is bordered by agricultural croplands to the north and the city of Corpus Christi to the south (**Figure 4.1**), substantial anthropogenic DOM additions through atmospheric

deposition or percolation to shallow groundwater are expected (Douglas et al. 2020a). Thus, while the salinity difference between surface water and porewater in summer kept offshore SGD rates low, due to density-difference effects (Santos et al. 2012a), accumulated DOM from dry deposition during the drought preceding this study that was not immediately transported to the bay with runoff had time to infiltrate to the water table and flow to the bay with the shallow groundwater. Consequently, while SGD rates are relatively low in fall compared to the following winter and spring, these compounds are more concentrated in the porewater after percolation of dry and wet deposition DOM and anthropogenic DOM to the water table and subsequent flow toward to the bay.

4.5 Conclusions

Hydroclimatic disturbances, like flood events, greatly influence DOM composition in semi-arid estuaries by changing hydraulic gradients, groundwater residence times, and seafloor recirculation in the system. In this study, DOM molecular characterization of surface water and porewater showed significant responses to these hydrologic changes, which are shown to affect the source and processing of OM within the estuary. The results of this study indicate that: 1) changing hydroclimatic conditions impact seasonal DOM composition, 2) the first flush following a large wet event brings more anthropogenic N- and S-containing DOM compounds and greater DOM diversity to coastal systems, and 3) porewater and marine DOM sources become more dominant as flooding recedes though maintain a higher percentage of N- and S-containing DOM compounds. The persistence of heteroatom compounds generated within anoxic sediments and/or anthropogenically-derived may have major implications for the cycling of nutrients such as N, S, and P and their fate in estuarine and coastal systems. SGD-derived DOM requires further investigation in coastal systems as many DOM compounds are known to be

photodegradable and breakdown into more labile components which may potentially contribute to eutrophication and subsequent harmful algal blooms. Future studies need to evaluate how DOM compositions in both surface water and porewater are impacted both spatially and temporally by hydrology, climatic disturbances, and changing land use. As human populations continue to grow and agriculture and urban development replace natural landscapes, the composition and reactivity of DOM is expected to continue to change. Combined with an increasing number of upstream water impoundments and a changing climate, the long-term effects of these changes on DOM composition might be significant and its potential consequences remain largely unknown.

Acknowledgements

Texas Sea Grant (award number: NA14OAR4170102), Texas Sea Grant GIAR, and the Center for Water Supply Studies at Texas A&M University-Corpus Christi financially supported this research and ARD's dissertation from which this paper has been derived. The authors thank all those who assisted in the lab and/or in the field. All views, opinions, findings, conclusions, and recommendations expressed in this material are those of the authors and do not necessarily reflect the opinions of the Texas Sea Grant College Program or the National Oceanic and Atmospheric Administration

CHAPTER V: SUMMARY AND CONCLUSIONS

Submarine groundwater discharge (SGD) comprises any flow of water across the sediment/water interface, regardless of their origin, composition, or driving forces, and may be both volumetrically and biogeochemically important to coastal zones. Within coastal zones nutrient and contaminant inputs via SGD and geochemical cycling may be strongly influenced by seawater recirculation or direct discharge of groundwater into the sea. Quantification of SGD remains a challenge due to its large spatial and temporal variability that may be exacerbated by natural heterogeneity (e.g., climatic conditions and hydrogeologic settings) and anthropogenic disturbances (e.g., dredging, oil/gas extraction, and oil/field brine discharges). Therefore, understanding the spatial and temporal variability of SGD and SGD-derived nutrients is paramount in coastal and estuarine research. In this dissertation, spatial and temporal variability of SGD, nutrient concentrations and fluxes, and molecular composition of dissolved organic matter (DOM) were assessed in a semi-arid, highly disturbed estuary across hydroclimatic conditions ranging from drought to normal, to flood.

The first study investigated the spatial and temporal variability of SGD during different hydroclimatic conditions spanning from extreme drought to flood (September 2014 – June 2016) in a semi-arid estuary highly disturbed by anthropogenic activities and with predominantly fine bottom sediments (Chapter II, Douglas et al. 2020b). SGD was assessed using electrical resistivity imaging, Darcy's law (i.e., fresh/terrestrial SGD) and radon (^{222}Rn, total SGD) and radium (^{226}Ra, saline/recirculated SGD) isotope mass balances. The highest SGD rates occurred in areas with sandier substrates and near transitions from low hydraulic conductivity to higher hydraulic conductivity bottom sediments. Radium-226 derived SGD rates ($1.3x10^{-2}$ – $2.7x10^{-2}$ $m \cdot d^{-1}$ using the average groundwater endmember) fall short of ^{222}Rn-derived SGD due to

inability to account for radium tracer reactivity within the sediment. Local Darcy estimates (wet: 0.09 – 8.28 $m \cdot d^{-1}$, dry: -0.02 – 7.84 $m \cdot d^{-1}$) agree well with the range of ^{222}Rn (this study: 0.79 – 1.81 $m \cdot d^{-1}$, previous study: 0.13 – 3.85 $m \cdot d^{-1}$), likely due to the steeper gradients near shore. Radium activity ratios and SGD rates reflect mixing of shallow and deep groundwater beneath the bay, likely due to anthropogenic disturbances with a greater influence from deep groundwater 3 – 6 months following major precipitation events.

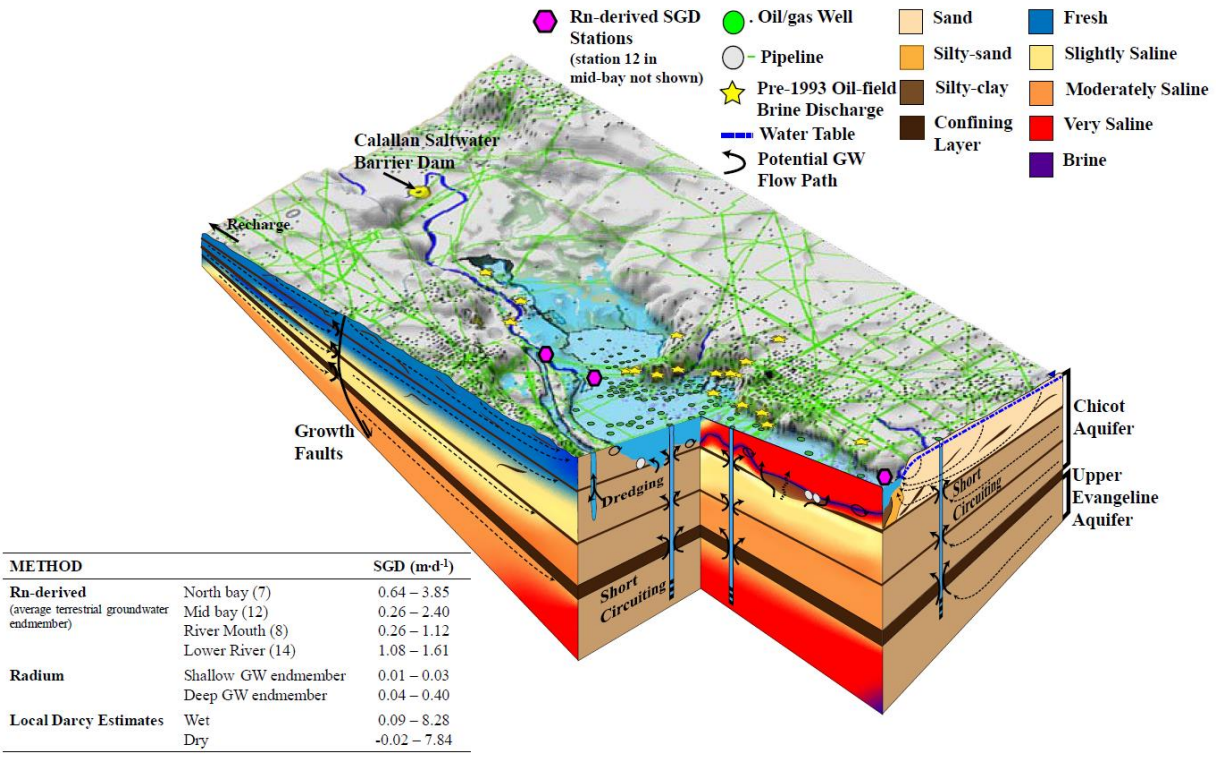

METHOD		SGD ($m \cdot d^{-1}$)
Rn-derived (average terrestrial groundwater endmember)	North bay (7)	0.64 – 3.85
	Mid bay (12)	0.26 – 2.40
	River Mouth (8)	0.26 – 1.12
	Lower River (14)	1.08 – 1.61
Radium	Shallow GW endmember	0.01 – 0.03
	Deep GW endmember	0.04 – 0.40
Local Darcy Estimates	Wet	0.09 – 8.28
	Dry	-0.02 – 7.84

Figure 5.1: Conceptual model illustrating the influences of anthropogenic disturbances (i.e., oil/gas wells, pipelines, and dredging) and natural subsurface heterogeneities (i.e., changes in sediment lithology and growth faults) on groundwater flow paths and submarine groundwater discharge in Nueces Bay.

The second study analyzed the inorganic and organic nutrient concentrations and water quality parameters by principal components analysis (PCA) and analysis of variance to assess the spatiotemporal variability across variable hydroclimatic conditions. Further, the SGD rates from the first study are used to calculate groundwater nutrient fluxes to the system and assess the contribution of SGD-derived N to the system's N budget (Chapter III, Douglas et al. 2020a). The variance in water quality is primarily due to temporal differences not spatial. Three principal components explain a total of 55.5% of the variability: freshwater inflow (PC1 28.8%), saline/recirculated SGD and recycled nitrogen (PC2 15.6%), and total SGD and "new" nitrogen (PC3 11.2%). Total SGD porewater fluxes ranged from 29.9-690.3 $mmol \cdot m^{-2}d^{-1}$ for ammonium, 0.21-18.7 $mmol \cdot m^{-2}d^{-1}$ for nitrite+nitrate, 3.1-51.3 $mmol \cdot m^{-2}d^{-1}$ for phosphate, 57.1-719.7 $mmol \cdot m^{-2}d^{-1}$ for silicate, and 95.9-36,838.5 $mmol \cdot m^{-2}d^{-1}$ for dissolved organic carbon. Total and saline/recirculated SGD fluxes were on average 150 - 26,000-fold and 5.8 - 466-fold, respectively, greater than surface runoff fluxes across all seasons. There were substantial "new" N inputs from terrestrial groundwater following precipitation and soil nitrogen flushing and percolation to groundwater form agricultural fields while saline/recirculated SGD of recycled N accounts for only <4% of total SGD inputs. The "new" N inputs occur in the river and closer to the river mouth during flooding, and near the north shore where topography and hydraulic gradients are in general steeper.

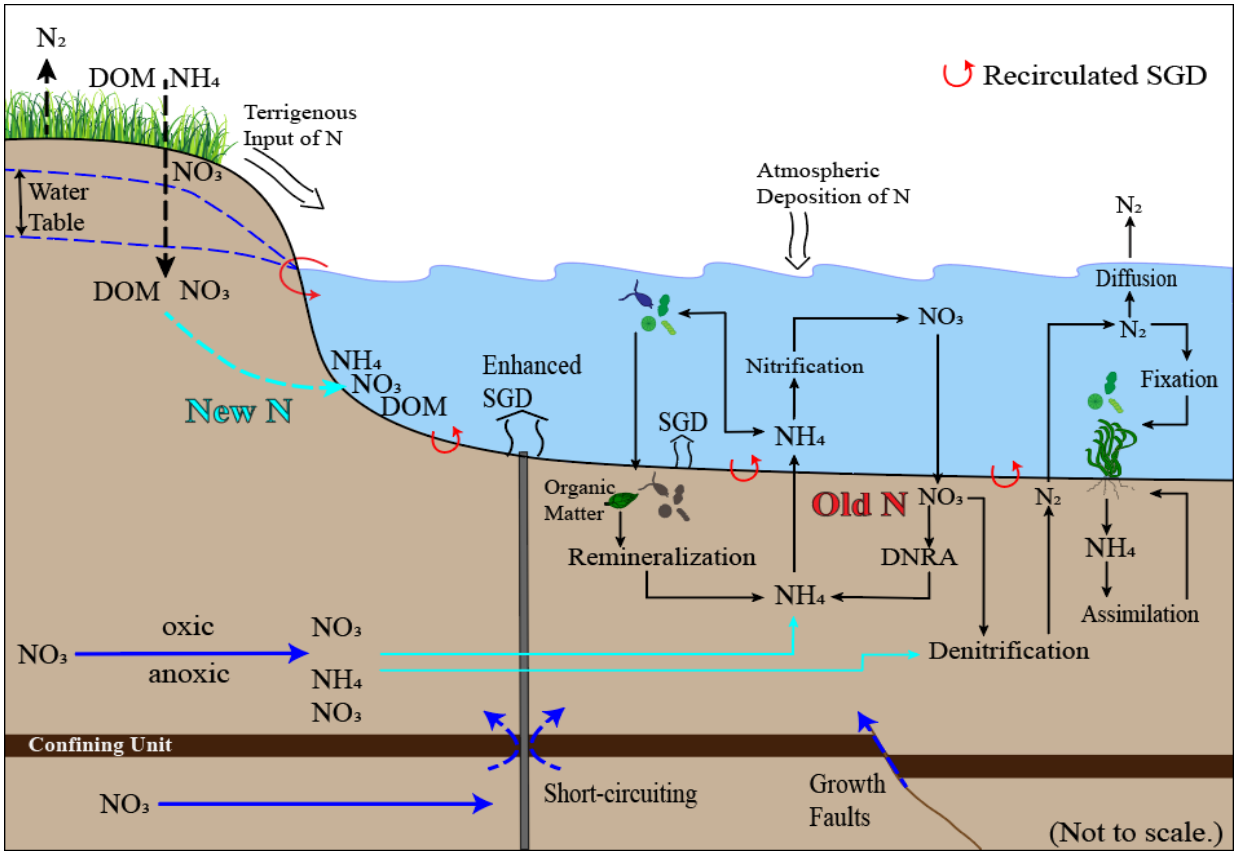

Figure 5.2: Conceptual model illustrating nitrogen sources and cycling.

The third study evaluated the seasonal changes in surface water and groundwater DOM molecular composition in a semi-arid estuary across different hydroclimatic conditions: from flood peak, to flood recession, to typical dry to semi-wet conditions (June 2015 – March 2016; Chapter IV). The PPL-SPE and UPLC-Orbitrap Fusion Tribrid mass spectrometry, in positive mode, was utilized to molecularly characterize surface and porewater DOM. During summer and fall, 55% of the identified compounds are CHO, which increases to over 62% by winter as sulfur and phosphorous containing compounds decrease. However, CHON compounds comprise 25% of all identified compounds across all seasons indicating the organic nitrogen pool is more consistent than the organic sulfur and phosphorous pools. Volcano plots generated from

predefined ratios were used to evaluate statistically significant (p-values ≤ 0.05) differences between seasons and surface- and porewater. Fall DOM is significantly different from all other seasons with over 1800 compounds significantly specific to this season. This difference is likely due to enhanced benthic fluxes as the volcano plot for fall post flooding surface- to porewater shows very few compounds significant to either group and the DOC and DON mixing plots deviate toward the porewater. Winter and spring samples are highly similar indicating the influence of heavy precipitation had dissipated by 6 months post flooding.

While other studies have suggested that semi-arid systems receive significant SGD, this dissertation further suggests that SGD in highly anthropogenically disturbed systems is derived from both shallower/shorter and deeper/longer groundwater flowpaths and lag the climatic conditions by weeks (shallow inputs) and months or longer (deeper inputs) (Figure 5.1). Furthermore, this dissertation demonstrates the importance of characterizing natural heterogeneities (i.e., sediment type, depositional environment, growth faults, hydroclimatic conditions) and anthropogenic disturbances (i.e., oil/gas drilling, dredging, oil-field brine discharges, industrial and agricultural practices) within a system to improve understanding of spatial and temporal variations in SGD rates and nutrient fluxes. This dissertation adds to the body of work that has found SGD-derived nutrient fluxes equivalent to or greater than the riverine-derived nutrient fluxes to a system. Assuming the results in Nueces Bay are typical of semi-arid bays, the present study shows that nutrient fluxes in semi-arid, highly disturbed estuaries may be significant. Thus, increased groundwater contamination (e.g., nitrogen, phosphorus, and organic matter) from industrial and agricultural practices may increase occurrences of eutrophication and harmful algal blooms in semi-arid coastal zones and this study provides essential information for mitigation strategies required to maintain the health of the

estuary. Future studies need to evaluate the spatial and temporal variability of SGD rates, surface and groundwater nutrient concentrations, SGD-derived nutrient fluxes, and DOM composition to better constrain influences of hydrology, climatic and structural disturbances, and changing land use and land cover on estuarine health and nutrient management strategies.

REFERENCES

Aarnos, H., Y. Gélinas, V. Kasurinen, Y. Gu, V. M. Puupponen & A. V. Vähätalo, 2018. Photochemical mineralization of terrigenous DOC to dissolved inorganic carbon in ocean. Global Biogeochemical Cycles 32(2):250-266.

Aarnos, H., P. Ylöstalo & A. V. Vähätalo, 2012. Seasonal phototransformation of dissolved organic matter to ammonium, dissolved inorganic carbon, and labile substrates supporting bacterial biomass across the Baltic Sea. Journal of Geophysical Research: Biogeosciences 117(G1).

Abdulla, H. A., D. J. Burdige & T. Komada, 2018. Accumulation of deaminated peptides in anoxic sediments of Santa Barbara Basin. Geochimica et Cosmochimica Acta 223:245-258.

Abdulla, H. A., D. J. Burdige & T. Komada, 2020. Abiotic formation of dissolved organic sulfur in anoxic sediments of Santa Barbara Basin. Organic Geochemistry 139:103879.

Abdulla, H. A. N., E. C. Minor, R. F. Dias & P. G. Hatcher, 2010. Changes in the compound classes of dissolved organic matter along an estuarine transect: A study using FTIR and C-13 NMR. Geochimica Et Cosmochimica Acta 74(13):3815-3838.

Abdulla, H. A. N., R. L. Sleighter & P. G. Hatcher, 2013. Two Dimensional Correlation Analysis of Fourier Transform Ion Cyclotron Resonance Mass Spectra of Dissolved Organic Matter: A New Graphical Analysis of Trends. Analytical Chemistry 85(8):3895-3902 doi:10.1021/ac303221j.

Advanced Geosciences, I. A., 2016. SuperSting Marine Resistivity. In. https://www.agiusa.com/supersting-marine-resistivity Accessed March 2016.

An, S. & W. S. Gardner, 2002. Dissimilatory nitrate reduction to ammonium (DNRA) as a nitrogen link, versus denitrification as a sink in a shallow estuary (Laguna Madre/Baffin Bay, Texas). Marine Ecology Progress Series 237:41-50.

Anchor QEA, 2017. Nutrient Budget for Nueces Bay. vol TWDB Contract# 1600012015. TWDB, Austin, TX.

Ashworth, J. & J. Hopkins, 1995. Aquifers of Texas: Texas Water Development Board Report 345. Austin.

Barbour, S. & D. Fredlund, 1989. Mechanisms of osmotic flow and volume change in clay soils. Canadian Geotechnical Journal 26(4):551-562.

Baudron, P., S. Cockenpot, F. Lopez-Castejon, O. Radakovitch, J. Gilabert, A. Mayer, J. L. Garcia-Arostegui, D. Martinez-Vicente, C. Leduc & C. Claude, 2015. Combining radon, short-lived radium isotopes and hydrodynamic modeling to assess submarine groundwater discharge from an anthropized semiarid watershed to a Mediterranean lagoon (Mar Menor, SE Spain). J Hydrol 525:55-71 doi:https://doi.org/10.1016/j.jhydrol.2015.03.015.

Beck, A. J., Y. Tsukamoto, A. Tovar-Sanchez, M. Huerta-Diaz, H. J. Bokuniewicz & S. A. Sañudo-Wilhelmy, 2007. Importance of geochemical transformations in determining submarine groundwater discharge-derived trace metal and nutrient fluxes. Applied Geochemistry 22(2):477-490.

Beck, M., O. Dellwig, G. Liebezeit, B. Schnetger & H.-J. Brumsack, 2008. Spatial and seasonal variations of sulphate, dissolved organic carbon, and nutrients in deep pore waters of intertidal flat sediments. Estuarine, Coastal and Shelf Science 79(2):307-316.

Bianchi, T. S., 2006. Biogeochemistry of estuaries. Oxford University Press.

Bighash, P. & D. Murgulet, 2015. Application of factor analysis and electrical resistivity to understand groundwater contributions to coastal embayments in semi-arid and hypersaline coastal settings. Science of the Total Environment 532:688-701.

Bishop, J. K., 1988. The barite-opal-organic carbon association in oceanic particulate matter. Nature 332(6162):341.

Boehm, A. B., A. Paytan, G. G. Shellenbarger & K. A. Davis, 2006. Composition and flux of groundwater from a California beach aquifer: Implications for nutrient supply to the surf zone. Continental Shelf Research 26(2):269-282 doi:https://doi.org/10.1016/j.csr.2005.11.008.

Breier, J. A., C. F. Breier & H. N. Edmonds, 2005. Detecting submarine groundwater discharge with synoptic surveys of sediment resistivity, radium, and salinity. Geophysical Research Letters 32(23) doi:Artn L23612 10.1029/2005gl024639.

Breier, J. A., C. F. Breier & H. N. Edmonds, 2010. Seasonal dynamics of dissolved Ra isotopes in the semi-arid bays of south Texas. Marine Chemistry 122(1-4):39-50.

Breier, J. A. & H. N. Edmonds, 2007. High 226Ra and 228Ra activities in Nueces Bay, Texas indicate large submarine saline discharges. Marine Chemistry:131-145.

Brock, D. A., 2001. Nitrogen budget for low and high freshwater inflows, Nueces Estuary, Texas. Estuaries 24(4):509-521.

Bronk, D. A., L. Killberg-Thoreson, R. E. Sipler, M. R. Mulholland, Q. N. Roberts, P. W. Bernhardt, M. Garrett, J. M. O'Neil & C. A. Heil, 2014. Nitrogen uptake and regeneration (ammonium regeneration, nitrification and photoproduction) in waters of the West Florida Shelf prone to blooms of Karenia brevis. Harmful Algae 38:50-62.

Brown Jr, L. F., R. G. Loucks & R. H. Trevio, 2005. Site-specific sequence-stratigraphic section benchmark charts are key to regional chronostratigraphic systems tract analysis in growth-faulted basins. AAPG bulletin 89(6):715-724.

Brown Jr, L. F., R. G. Loucks, R. H. Trevio & U. Hammes, 2004. Understanding growth-faulted, intraslope subbasins by applying sequence-stratigraphic principles: Examples from the south Texas Oligocene Frio Formation. AAPG bulletin 88(11):1501-1522.

Bruesewitz, D. A., W. S. Gardner, R. F. Mooney & E. J. Buskey, 2015. Seasonal water column NH 4+ cycling along a semi-arid sub-tropical river–estuary continuum: responses to episodic events and drought conditions. Ecosystems 18(5):792-812.

Bui, D. T., K. Khosravi, M. Karimi, G. Busico, Z. S. Khozani, H. Nguyen, M. Mastrocicco, D. Tedesco, E. Cuoco & N. Kazakis, 2020. Enhancing nitrate and strontium concentration prediction in groundwater by using new data mining algorithm. Science of The Total Environment 715:136836 doi:https://doi.org/10.1016/j.scitotenv.2020.136836.

Burdige, D. J., W. M. Berelson, K. H. Coale, J. McManus & K. S. Johnson, 1999. Fluxes of dissolved organic carbon from California continental margin sediments. Geochimica et Cosmochimica Acta 63(10):1507-1515.

Burdige, D. J. & S. Zheng, 1998. The biogeochemical cycling of dissolved organic nitrogen in estuarine sediments. Limnology and Oceanography 43(8):1796-1813.

Bureau of Reclamation, 2000. Ricon Bayou Demonstration Project: Concluding Report Findings. vol 2. Bureau of Reclamation, Austin, Texas.

Burgin, A. J. & S. K. Hamilton, 2007. Have we overemphasized the role of denitrification in aquatic ecosystems? A review of nitrate removal pathways. Frontiers in Ecology and the Environment 5(2):89-96.

Burnett, W. C., 2003. Radon and radium isotopes as tracers in the coastal ocean. Abstracts of Papers of the American Chemical Society 226:U81-U81.

Burnett, W. C., P. K. Aggarwal, A. Aureli, H. Bokuniewicz, J. E. Cable, M. A. Charette, E. Kontar, S. Krupa, K. M. Kulkarni, A. Loveless, W. S. Moore, J. A. Oberdorfer, J. Oliveira, N. Ozyurt, P. Povinec, A. M. G. Privitera, R. Rajar, R. T. Ramassur, J. Scholten, T. Stieglitz, M. Taniguchi & J. V. Turner, 2006. Quantifying submarine groundwater discharge in the coastal zone via multiple methods. Science of the Total Environment 367(2-3):498-543.

Burnett, W. C., H. Bokuniewicz, M. Huettel, W. S. Moore & M. Taniguchi, 2003. Groundwater and pore water inputs to the coastal zone. Biogeochemistry 66(1-2):3-33.

Burnett, W. C. & H. Dulaiova, 2003. Estimating the dynamics of groundwater input into the coastal zone via continuous radon-222 measurements. Journal of Environmental Radioactivity 69(1-2):21-35.

Burnett, W. C., R. Peterson, W. S. Moore & J. de Oliveira, 2008. Radon and radium isotopes as tracers of submarine groundwater discharge - Results from the Ubatuba Brazil SGD assessment intercomparison. Estuarine Coastal and Shelf Science 76(3):501-511.

Burnett, W. C., M. Taniguchi & J. Oberdorfer, 2001. Measurement and significance of the direct discharge of groundwater into the coastal zone. Journal of Sea Research 46(2):109-116.

Bushaw, K. L., R. G. Zepp, M. A. Tarr, D. Schulz-Jander, R. A. Bourbonniere, R. E. Hodson, W. L. Miller, D. A. Bronk & M. A. Moran, 1996. Photochemical release of biologically available nitrogen from aquatic dissolved organic matter. Nature 381(6581):404-407 doi:10.1038/381404a0.

Capuano, R. & R. Jan, 1996. In Situ Hydraulic Conductivity of Clay and Silty-Clay Fluvial-Deltaic Sediments, Texas Gulf Coast. Groundwater 34(3):545-551.

Cardenas, M. B., P. L. Cook, H. Jiang & P. Traykovski, 2008. Constraining denitrification in permeable wave-influenced marine sediment using linked hydrodynamic and biogeochemical modeling. Earth and Planetary Science Letters 275(1-2):127-137.

Carlson, C. A. & D. A. Hansell, 2015. DOM sources, sinks, reactivity, and budgets Biogeochemistry of marine dissolved organic matter. Elsevier, 65-126.

Caverly, E., J. M. Kaste, G. S. Hancock & R. M. Chambers, 2013. Dissolved and particulate organic carbon fluxes from an agricultural watershed during consecutive tropical storms. Geophysical Research Letters 40(19):5147-5152.

Cerdà-Domènech, M., V. Rodellas, A. Folch & J. Garcia-Orellana, 2017. Constraining the temporal variations of Ra isotopes and Rn in the groundwater end-member: Implications for derived SGD estimates. Science of the total environment 595:849-857.

Charette, M. A., 2007. Hydrologic forcing of submarine groundwater discharge: Insight from a seasonal study of radium isotopes in a groundwater-dominated salt marsh estuary. Limnology and Oceanography 52(1):230-239.

Charette, M. A. & M. C. Allen, 2006. Precision ground water sampling in coastal aquifers using a direct-push, shielded-screen well-point system. Ground Water Monitoring and Remediation 26(2):87-93.

Charette, M. A. & K. O. Buesseler, 2004. Submarine groundwater discharge of nutrients and copper to an urban subestuary of Chesapeake bay (Elizabeth River). Limnology and Oceanography 49(2):376-385.

Charette, M. A., K. O. Buesseler & J. E. Andrews, 2001. Utility of radium isotopes for evaluating the input and transport of groundwater-derived nitrogen to a Cape Cod estuary. Limnology and Oceanography 46(2):465-470.

Charette, M. A., R. Splivallo, C. Herbold, M. S. Bollinger & W. S. Moore, 2003. Salt marsh submarine groundwater discharge as traced by radium isotopes. Marine Chemistry 84(1-2):113-121.

Chowdhury, A. H., S. Wade, R. E. Mace & C. Ridgeway, 2004. Groundwater availability model of the central gulf coast aquifer system: numerical simulations through 1999. Texas Water Development Board, unpublished report 1:14.

Collins, A., 1975. Geochemistry of oilfield waters, vol 1. Elsevier.

D'Andrilli, J., W. T. Cooper, C. M. Foreman & A. G. Marshall, 2015. An ultrahigh-resolution mass spectrometry index to estimate natural organic matter lability. Rapid Communications in Mass Spectrometry 29(24):2385-2401 doi:10.1002/rcm.7400.

D'Unger, C., D. Chapman & R. S. Carr, 1996. Discharge of oilfield-produced water in Nueces Bay, Texas: A case study. Environmental Management 20(1):143-150.

Dalsgaard, T. & B. Thamdrup, 2002. Factors controlling anaerobic ammonium oxidation with nitrite in marine sediments. Appl Environ Microbiol 68(8):3802-3808.

Danielescu, S., K. T. MacQuarrie & R. N. Faux, 2009. The integration of thermal infrared imaging, discharge measurements and numerical simulation to quantify the relative contributions of freshwater inflows to small estuaries in Atlantic Canada. Hydrological processes 23(20):2847-2859.

Diener, R. A., 1975. Cooperative Gulf of Mexico Estuarine Inventory and Study--Texas: Area Description. National Oceanic and Atmospheric Administration, docs.lib.noaa.gov.

Dimova, N., W. C. Burnett, E. P. Horwitz & D. Lane-Smith, 2007. Automated measurement of Ra-224 and Ra-226 in water. Applied Radiation and Isotopes 65(4):428-434.

Dimova, N. T., P. W. Swarzenski, H. Dulaiova & C. R. Glenn, 2012. Utilizing multichannel electrical resistivity methods to examine the dynamics of the fresh water-seawater interface in two Hawaiian groundwater systems. Journal of Geophysical Research-Oceans 117.

Dittmar, T., 2008. The molecular level determination of black carbon in marine dissolved organic matter. Organic Geochemistry 39(4):396-407.

Dittmar, T., B. Koch, N. Hertkorn & G. Kattner, 2008. A simple and efficient method for the solid-phase extraction of dissolved organic matter (SPE-DOM) from seawater. Limnology and Oceanography-Methods 6:230-235.

Dixon, J. L., C. L. Osburn, H. W. Paerl & B. L. Peierls, 2014. Seasonal changes in estuarine dissolved organic matter due to variable flushing time and wind-driven mixing events. Estuarine, Coastal and Shelf Science 151:210-220.

Douglas, A., D. Murgulet, M. S. Wetz, N. Spalt, C. Lopez & H. Wang, 2017. Evaluating groundwater inflow and nutrient transport to Texas coastal embayments. Texas General Land Office, Austin, TX.

Douglas, A. R., D. Murgulet & P. A. Montagna, 2020a. Hydroclimatic variability drives submarine groundwater discharge and nutrient fluxes in an anthropogenically disturbed, semi-arid estuary. Science of The Total Environment 755 doi:https://doi.org/10.1016/j.scitotenv.2020.142574.

Douglas, A. R., D. Murgulet & R. N. Peterson, 2020b. Submarine groundwater discharge in an anthropogenically disturbed, semi-arid estuary. Journal of Hydrology 580:124369.

Dulaiova, H., R. Peterson, W. C. Burnett & D. Lane-Smith, 2005. A multi-detector continuous monitor for assessment of Rn-222 in the coastal ocean. Journal of Radioanalytical and Nuclear Chemistry 263(2):361-365 doi:10.1007/s10967-005-0063-8.

Durridge Company Inc., 2017. RAD7 Radon Detector User Manual. vol Revision 7.4.5, Billerica, MA, USA.

El-Gamal, A. A., R. N. Peterson & W. C. Burnett, 2012. Detecting Freshwater Inputs via Groundwater Discharge to Marina Lagoon, Mediterranean Coast, Egypt. Estuaries and Coasts 35(6):1486-1499 doi:10.1007/s12237-012-9539-2.

EPA, U., 2011. 40 CFR APPENDIX B TO PART 136 - DEFINITION AND PROCEDURE FOR THE DETERMINATION OF THE METHOD DETECTION LIMIT-REVISION 1.11. In: U.S. Government Publishing Office. https://www.gpo.gov/fdsys/granule/CFR-2011-title40-vol23/CFR-2011-title40-vol23-part136-appB/content-detail.html Accessed 7/20/18.

Felix, J. D. & J. Campbell, 2019. Investigating Reactive Nitrogen Sources that Stimulate Algal Blooms in Baffin Bay.

Fernando, N., 2017. RE: Daily modelled runoff for ungauged watershed 20005 from 2014 through 2016. In: Douglas, A. (ed).

Fetter, C. W., 2001. Applied Hydrogeology, Fourth edn. Prentice-Hall, Inc., New Jersey.

Gerla, P. J., 1992. The relationship of water-table changes to the capillary fringe, evapotranspiration, and precipitation in intermittent wetlands. Wetlands 12(2):91-98 doi:10.1007/bf03160590.

Giblin, A. E., C. R. Tobias, B. Song, N. Weston, G. T. Banta & V. H. RIVERA-MONROY, 2013. The importance of dissimilatory nitrate reduction to ammonium (DNRA) in the nitrogen cycle of coastal ecosystems. Oceanography 26(3):124-131.

Gomez-Saez, G. V., J. Niggemann, T. Dittmar, A. M. Pohlabeln, S. Q. Lang, A. Noowong, T. Pichler, L. Wörmer & S. I. Bühring, 2016. Molecular evidence for abiotic sulfurization of dissolved organic matter in marine shallow hydrothermal systems. Geochimica et Cosmochimica Acta 190:35-52.

Gonneea, M. E., P. J. Morris, H. Dulaiova & M. A. Charette, 2008. New perspectives on radium behavior within a subterranean estuary. Marine Chemistry 109(3):250-267 doi:https://doi.org/10.1016/j.marchem.2007.12.002.

Gonsior, M., M. Zwartjes, W. J. Cooper, W. Song, K. P. Ishida, L. Y. Tseng, M. K. Jeung, D. Rosso, N. Hertkorn & P. Schmitt-Kopplin, 2011. Molecular characterization of effluent organic matter identified by ultrahigh resolution mass spectrometry. Water research 45(9):2943-2953.

Granger, J. & S. D. Wankel, 2016. Isotopic overprinting of nitrification on denitrification as a ubiquitous and unifying feature of environmental nitrogen cycling. Proceedings of the National Academy of Sciences 113(42):E6391-E6400.

Gunnars, A. & S. Blomqvist, 1997. Phosphate exchange across the sediment-water interface when shifting from anoxic to oxic conditions an experimental comparison of freshwater and brackish-marine systems. Biogeochemistry 37(3):203-226.

Gunnars, A., S. Blomqvist, P. Johansson & C. Andersson, 2002. Formation of Fe (III) oxyhydroxide colloids in freshwater and brackish seawater, with incorporation of phosphate and calcium. Geochimica et Cosmochimica Acta 66(5):745-758.

Hammes, U., R. Loucks, L. Brown, R. Trevino, R. Remington & P. Montoya, 2004. Structural setting and sequence architecture of a growth-faulted lowstand subbasin, Frio Formation, South Texas.

Hansen, L. S., M. Holmer & T. H. Blackburn, 1993. Mineralization of organic nitrogen and carbon (fish food) added to anoxic sediment microcosms: role of sulphate reduction. Marine Ecology Progress Series:199-204.

Hawkes, J. A., T. Dittmar, C. Patriarca, L. Tranvik & J. Bergquist, 2016. Evaluation of the Orbitrap mass spectrometer for the molecular fingerprinting analysis of natural dissolved organic matter. Analytical chemistry 88(15):7698-7704.

Hedges, J. I., R. G. Keil & R. Benner, 1997. What happens to terrestrial organic matter in the ocean? Organic geochemistry 27(5-6):195-212.

Hernes, P. J. & R. Benner, 2006. Terrigenous organic matter sources and reactivity in the North Atlantic Ocean and a comparison to the Arctic and Pacific oceans. Marine Chemistry 100(1-2):66-79.

Hill, E. M. & B. Nicolau, 2014. Nueces Bay Zinc in Sediment Profiling Assessment.

Hobday, D. & W. Galloway, 1999. Groundwater processes and sedimentary uranium deposits. Hydrogeology Journal 7(1):127-138.

Hood, E., M. N. Gooseff & S. L. Johnson, 2006. Changes in the character of stream water dissolved organic carbon during flushing in three small watersheds, Oregon. Journal of Geophysical Research: Biogeosciences 111(G1) doi:10.1029/2005jg000082.

Hooper, E., 1991. Fluid migration along growth faults in compacting sediments. Journal of Petroleum Geology 14(S1):161-180.

Hupfer, M. & J. Lewandowski, 2008. Oxygen controls the phosphorus release from lake sediments–a long-lasting paradigm in limnology. International Review of Hydrobiology 93(4-5):415-432.

Hur, M., R. L. Ware, J. Park, A. M. McKenna, R. P. Rodgers, B. J. Nikolau, E. S. Wurtele & A. G. Marshall, 2018. Statistically significant differences in composition of petroleum crude oils revealed by volcano plots generated from ultrahigh resolution fourier transform ion cyclotron resonance mass spectra. Energy & fuels 32(2):1206-1212.

Hvorslev, M. J., 1951. Time lag and soil permeability in ground-water observations.

Hwang, D.-W., I.-S. Lee, M. Choi & T.-H. Kim, 2016. Estimating the input of submarine groundwater discharge (SGD) and SGD-derived nutrients in Geoje Bay, Korea using 222Rn-Si mass balance model. Marine Pollution Bulletin 110(1):119-126 doi:https://doi.org/10.1016/j.marpolbul.2016.06.073.

Jäntti, H. & S. Hietanen, 2012. The effects of hypoxia on sediment nitrogen cycling in the Baltic Sea. Ambio 41(2):161-169.

Jickells, T., 1998. Nutrient biogeochemistry of the coastal zone. Science 281(5374):217-222.

Johnson, A. G., C. R. Glenn, W. C. Burnett, R. N. Peterson & P. G. Lucey, 2008. Aerial infrared imaging reveals large nutrient-rich groundwater inputs to the ocean. Geophysical Research Letters 35(15).

Jørgensen, B. B., 1982. Mineralization of organic matter in the sea bed—the role of sulphate reduction. Nature 296(5858):643.

Jung, B.-J., J.-K. Lee, H. Kim & J.-H. Park, 2014. Export, biodegradation, and disinfection byproduct formation of dissolved and particulate organic carbon in a forested headwater stream during extreme rainfall events. Biogeosciences 11(21):6119-6129.

Kadko, D., J. K. Cochran & M. Lyle, 1987. The effect of bioturbation and adsorption gradients on solid and dissolved radium profiles in sediments from the eastern equatorial Pacific. Geochimica et Cosmochimica Acta 51(6):1613-1623.

Kazakis, N., I. Matiatos, M.-M. Ntona, M. Bannenberg, K. Kalaitzidou, E. Kaprara, M. Mitrakas, A. Ioannidou, G. Vargemezis & K. Voudouris, 2020. Origin, implications and management strategies for nitrate pollution in surface and ground waters of Anthemountas basin based on a δ15N-NO3− and δ18O-NO3− isotope approach. Science of The Total Environment 724:138211 doi:https://doi.org/10.1016/j.scitotenv.2020.138211.

Kelly, J. L., C. R. Glenn & P. G. Lucey, 2013. High-resolution aerial infrared mapping of groundwater discharge to the coastal ocean. Limnol Oceanogr: Methods 11:262-277.

Kendall, C., 1998. Tracing nitrogen sources and cycling in catchments. Isotope tracers in catchment hydrology 1:519-576.

Kendall, C., E. M. Elliott & S. D. Wankel, 2007. Tracing anthropogenic inputs of nitrogen to ecosystems. Stable Isotopes in Ecology and Environmental Science, 2nd Edition:375-449 doi:DOI 10.1002/9780470691854.ch12.

Kennish, M. J., 2002. Environmental threats and environmental future of estuaries. Environmental conservation 29(1):78-107.

Kim, G., W. C. Burnett, H. Dulaiova, P. W. Swarzenski & W. S. Moore, 2001. Measurement of Ra-224 and Ra-226 activities in natural waters using a radon-in-air monitor. Environmental Science & Technology 35(23):4680-4683.

Kitidis, V. & G. Uher, 2008. Photochemical mineralisation of dissolved organic nitrogen. Biological oceanography research trends Nova Science Publishers, New York:131-156.

Knee, K. L., E. Garcia-Solsona, J. Garcia-Orellana, A. B. Boehm & A. Paytan, 2011. Using radium isotopes to characterize water ages and coastal mixing rates: A sensitivity analysis. Limnology and Oceanography-Methods 9:380-395 doi:10.4319/lom.2011.9.380.

Komada, T., D. J. Burdige, C. Magen, H.-L. Li & J. Chanton, 2016. Recycling of Organic Matter in the Sediments of Santa Monica Basin, California Borderland. Aquatic Geochemistry 22(5):593-618 doi:10.1007/s10498-016-9308-0.

Kraemer, T. F. & D. F. Reid, 1984. The occurrence and behavior of radium in saline formation water of the U.S. Gulf Coast region. Chemical Geology 46(2):153-174 doi:https://doi.org/10.1016/0009-2541(84)90186-4.

Krauk, J. M., T. A. Villareal, J. A. Sohm, J. P. Montoya & D. G. Capone, 2006. Plasticity of N:P ratios in laboratory and field populations of Trichodesmium spp. Aquatic Microbial Ecology 42(3):243-253.

Kraus, T. E., R. A. Dahlgren & R. J. Zasoski, 2003. Tannins in nutrient dynamics of forest ecosystems-a review. Plant and soil 256(1):41-66.

Kreitler, C. W., 1993. Geochemical techniques for identifying sources of ground-water salinization. CRC press.

Krest, J. M., W. S. Moore & Rama, 1999. 226Ra and 228Ra in the mixing zones of the Mississippi and Atchafalaya Rivers: indicators of groundwater input. Marine Chemistry 64(3):129-152 doi:https://doi.org/10.1016/S0304-4203(98)00070-X.

Kroeger, K. D. & M. A. Charette, 2008. Nitrogen biogeochemistry of submarine groundwater discharge. Limnology and Oceanography 53(3):1025-1039.

Lambert, M. J. & W. C. Burnett, 2003. Submarine groundwater discharge estimates at a Florida coastal site based on continuous radon measurements. Biogeochemistry 66(1-2):55-73.

Lamontagne, S., C. L. G. La Salle, G. J. Hancock, I. T. Webster, C. T. Simmons, A. J. Love, J. James-Smith, A. J. Smith, J. Kämpf & H. J. Fallowfield, 2008. Radium and radon radioisotopes in regional groundwater, intertidal groundwater, and seawater in the Adelaide Coastal Waters Study area: implications for the evaluation of submarine groundwater discharge. Marine Chemistry 109(3):318-336.

Lee, C. M., J. J. Jiao, X. Luo & W. S. Moore, 2012. Estimation of submarine groundwater discharge and associated nutrient fluxes in Tolo Harbour, Hong Kong. Science of the total environment 433:427-433.

Lee, D. R., 1977. A device for measuring seepage flux in lakes and estuaries. Limnology and Oceanography 22(1):140-147.

Letourneau, M. L. & P. M. Medeiros, 2019. Dissolved organic matter composition in a marsh-dominated estuary: Response to seasonal forcing and to the passage of a hurricane. Journal of Geophysical Research: Biogeosciences.

Li, X., B. X. Hu, W. C. Burnett, I. R. Santos & J. P. Chanton, 2009. Submarine ground water discharge driven by tidal pumping in a heterogeneous aquifer. Ground Water 47(4):558-568.

Liu, Z. & K. Lu, 2019. Molecular level analysis reveals changes in chemical composition of dissolved organic matter from south Texas rivers after high flow events. Frontiers in Marine Science 6:673.

Longley, W. L., G. L. Powell, A. W. Green & T. W. D. Board, 1994. Freshwater inflows to Texas bays and estuaries: ecological relationships and methods for determination of needs. Texas Water Development Board, Austin, TX.

Longnecker, K. & E. B. Kujawinski, 2011. Composition of dissolved organic matter in groundwater. Geochimica Et Cosmochimica Acta 75(10):2752-2761 doi:10.1016/j.gca.2011.02.020.

Lopez-Veneroni, D. & L. A. Cifuentes, 1994. Transport of dissolved organic nitrogen in Mississippi River Plume and Texas-Louisiana continental shelf near-shore waters. Estuaries 17:796-808.

Lopez, C., D. Murgulet, A. Douglas & V. Murgulet, 2018. Impacts of Temporal and Spatial Variation of Submarine Groundwater Discharge on Nutrient Fluxes to Texas Coastal Embayments, Phase III (Baffin Bay). Texas General Land Office, Austin, TX.

Luo, X., J. J. Jiao, W. S. Moore & C. M. Lee, 2014. Submarine groundwater discharge estimation in an urbanized embayment in Hong Kong via short-lived radium isotopes and its implication of nutrient loadings and primary production. Marine Pollution Bulletin 82(1-2):144-154.

Ma, H. & C. M. Aelion, 2005. Ammonium production during microbial nitrate removal in soil microcosms from a developing marsh estuary. Soil Biology and Biochemistry 37(10):1869-1878 doi:https://doi.org/10.1016/j.soilbio.2005.02.020.

Mace, R. E., W. F. Mullican, E. S. Angle, S. C. Davidson & Texas Water Development Board., 2006. Aquifers of the Gulf coast of Texas. Texas Water Development Board, Austin, Tex.

Maher, D. T., M. Call, P. Macklin, J. R. Webb & I. R. Santos, 2019. Hydrological Versus Biological Drivers of Nutrient and Carbon Dioxide Dynamics in a Coastal Lagoon. Estuaries and Coasts 42(4):1015-1031 doi:10.1007/s12237-019-00532-2.

Majidzadeh, H., H. Uzun, A. Ruecker, D. Miller, J. Vernon, H. Zhang, S. Bao, M. T. Tsui, T. Karanfil & A. T. Chow, 2017. Extreme flooding mobilized dissolved organic matter from coastal forested wetlands. Biogeochemistry 136(3):293-309 doi:https://doi.org/10.1007/s10533-017-0394-x.

Majumdar, D. & N. Gupta, 2000. Nitrate pollution of groundwater and associated human health disorders. Indian journal of environmental health 42(1):28-39.

Maria, E., P. Crançon, G. Lespes & M. C. Bridoux, 2019. Spatial Variation in the Molecular Composition of Dissolved Organic Matter from the Podzol Soils of a Temperate Pine Forest. ACS Earth and Space Chemistry 3(8):1685-1696.

Martin, J. B., J. E. Cable, P. W. Swarzenski & M. K. Lindenberg, 2004. Enhanced submarine ground water discharge from mixing of pore water and estuarine water. Groundwater 42(7):1000-1010.

Medeiros, P. M., M. Seidel, N. D. Ward, E. J. Carpenter, H. R. Gomes, J. Niggemann, A. V. Krusche, J. E. Richey, P. L. Yager & T. Dittmar, 2015. Fate of the Amazon River dissolved organic matter in the tropical Atlantic Ocean. Global Biogeochemical Cycles 29(5):677-690.

Michael, H. A., A. E. Mulligan & C. F. Harvey, 2005. Seasonal oscillations in water exchange between aquifers and the coastal ocean. Nature 436(7054):1145.

Millero, F. J., 1993. What is PSU? Oceanography 6(3):67.

Montagna, P. A., X. Hu, T. A. Palmer & M. Wetz, 2018. Effect of hydrological variability on the biogeochemistry of estuaries across a regional climatic gradient. Limnology and Oceanography 63(6):2465-2478.

Montagna, P. A. & R. D. Kalke, 1992. The Effect of Fresh-Water Inflow on Meiofaunal and Macrofaunal Populations in the Guadalupe and Nueces Estuaries, Texas. Estuaries 15(3):307-326.

Montluçon, D. & S. A. Sañudo-Wilhelmy, 2001. Influence of Net Groundwater Discharge on the Chemical Composition of a Coastal Environment: Flanders Bay, Long Island, New York. Environmental Science & Technology 35(3):480-486 doi:10.1021/es9914442.

Mooney, R. F. & J. W. McClelland, 2012. Watershed Export Events and Ecosystem Responses in the Mission–Aransas National Estuarine Research Reserve, South Texas. Estuaries and coasts 35(6):1468-1485.

Moore, W. S., 1996. Large groundwater inputs to coastal waters revealed by Ra-226 enrichments. Nature 380(6575):612-614 doi:DOI 10.1038/380612a0.

Moore, W. S., 2000. Ages of continental shelf waters determined from Ra-223 and Ra-224. Journal of Geophysical Research-Oceans 105(C9):22117-22122 doi:Doi 10.1029/1999jc000289.

Moore, W. S., 2010. The Effect of Submarine Groundwater Discharge on the Ocean. Annual Review of Marine Science 2:59-88.

Mori, C., I. R. Santos, H.-J. Brumsack, B. Schnetger, T. Dittmar & M. Seidel, 2019. Non-conservative behavior of dissolved organic matter and trace metals (Mn, Fe, Ba) driven by porewater exchange in a subtropical mangrove-estuary. Frontiers in Marine Science 6:481.

Mortimer, R. J., S. J. Harris, M. D. Krom, T. E. Freitag, J. I. Prosser, J. Barnes, P. Anschutz, P. J. Hayes & I. M. Davies, 2004. Anoxic nitrification in marine sediments. Marine Ecology Progress Series 276:37-52.

Mulligan, A. E. & M. A. Charette, 2006. Intercomparison of submarine groundwater discharge estimates from a sandy unconfined aquifer. Journal of Hydrology 327(3-4):411-425.

Murgulet, D., A. Douglas, C. Lopez, B. Gyawali & V. Murgulet, 2019. Impacts of Temporal and Spatial Variation of Submarine Groundwater Discahrge on Nutrient Fluxes to Texas Coastal Embayments. Texas General Land Office, Austin, TX.

Murgulet, D., V. Murgulet, N. Spalt, A. Douglas & R. G. Hay, 2016. Impact of hydrological alterations on river-groundwater exchange and water quality in a semi-arid area: Nueces River, Texas. Science of The Total Environment 572:595-607.

Murgulet, D. & G. R. Tick, 2013. Understanding the sources and fate of nitrate in a highly developed aquifer system. Journal of Contaminant Hydrology 155:69-81.

Murgulet, D. & G. R. Tick, 2016. Effect of variable-density groundwater flow on nitrate flux to coastal waters. Hydrological Processes 30(2):302-319.

Murgulet, D., M. Trevino, A. Douglas, N. Spalt, X. Hu & V. Murgulet, 2018. Temporal and spatial fluctuations of groundwater-derived alkalinity fluxes to a semiarid coastal embayment. Science of The Total Environment 630:1343-1359 doi:https://doi.org/10.1016/j.scitotenv.2018.02.333.

Murgulet, D., M. Valeriu, R. R. Hay, P. Tissot & A. M. Mestas-Nuñez, 2017. Relationships between sea surface temperature anomalies in the Pacific and Atlantic Oceans and South Texas precipitation and streamflow variability. Journal of Hydrology 550:726-739.

Murgulet, D., M. S. Wetz, A. Douglas, W. McBee, N. Spalt & K. Linares, 2015. Evaluating Groundwater Inflow and Nutrient Transport to Texas Coastal Embayments. Texas General Land Office.

NBBEST (Nueces River and Corpus Christi and Baffin Bays Basin and Bay Expert Science Team), 2011. Environmental Flows Recommendations Report. Final Submission to the Environmental Flows Advisory Group, Nueces River and Corpus Christi and Baffin Bays Basin and Bay Area Stakeholders Committee, and Texas Commission on Environmental Quality.

Nelson, K. & P. A. Montagna, 2009. Causes and Monitoring of Hypoxia in Corpus Christi Bay.

Nicolau, B. A. & E. M. Hill, 2013. Nueces Bay Total Maximum Daily Load Project--Year-seven Implementation Effectiveness Monitoring Data Report. Texas Commission on Environmental Quality, Austin, TX.

Nyquist, J. E., P. A. Freyer & L. Toran, 2008. Stream bottom resistivity tomography to map ground water discharge. Ground water 46(4):561-569.

Oberdorfer, J. A., M. Charette, M. Allen, J. B. Martin & J. E. Cable, 2008. Hydrogeology and geochemistry of near-shore submarine groundwater discharge at Flamengo Bay, Ubatuba, Brazil. Estuarine Coastal and Shelf Science 76(3):457-465.

Oberdorfer, J. A., M. A. Valentino & S. V. Smith, 1990. Groundwater Contribution to the Nutrient Budget of Tomales Bay, California. Biogeochemistry 10(3):199-216.

Ockerman, D. J., 2001. Water Budget for the Nueces Estuary, Texas, May-October 1998. U.S. Geological Survey.

Ohno, T., R. L. Sleighter & P. G. Hatcher, 2016. Comparative study of organic matter chemical characterization using negative and positive mode electrospray ionization ultrahigh-resolution mass spectrometry. Analytical and bioanalytical chemistry 408(10):2497-2504.

Osterholz, H., D. L. Kirchman, J. Niggemann & T. Dittmar, 2016. Environmental drivers of dissolved organic matter molecular composition in the Delaware Estuary. Frontiers in Earth Science 4:95.

Paerl, H. W., 1997. Coastal eutrophication and harmful algal blooms: Importance of atmospheric deposition and groundwater as "new" nitrogen and other nutrient sources. Limnology and oceanography 42(5part2):1154-1165.

Paerl, H. W., 2009. Controlling eutrophication along the freshwater–marine continuum: dual nutrient (N and P) reductions are essential. Estuaries and Coasts 32(4):593-601.

Paudel, B. & P. A. Montagna, 2014. Modeling inorganic nutrient distributions among hydrologic gradients using multivariate approaches. Ecological Informatics 24:35-46.

Paudel, B., P. A. Montagna & L. Adams, 2019. The relationship between suspended solids and nutrients with variable hydrologic flow regimes. Regional Studies in Marine Science 29:100657.

Pena, M., 2017. Assessment of Historical Oil-Field Brine Discharge Influences on Sediment-supported Radionuclide Activities McNair Scholars Research Journal. vol IX. Texas A&M University-Corpus Christi.

Peterson, R. N., W. C. Burnett, M. Taniguchi, J. Y. Chen, I. R. Santos & T. Ishitobi, 2008. Radon and radium isotope assessment of submarine groundwater discharge in the Yellow River delta, China. Journal of Geophysical Research-Oceans 113(C9).

Pohlabeln, A. M., G. V. Gomez-Saez, B. E. Noriega-Ortega & T. Dittmar, 2017. Experimental evidence for abiotic sulfurization of marine dissolved organic matter. Frontiers in Marine Science 4:364.

Powers, L. C., J. L. Luek, P. Schmitt-Kopplin, B. J. Campbell, C. Magen, L. W. Cooper & M. Gonsior, 2018. Seasonal changes in dissolved organic matter composition in Delaware Bay, USA in March and August 2014. Organic Geochemistry 122:87-97 doi:https://doi.org/10.1016/j.orggeochem.2018.05.005.

Pulich Jr., W., 2007. Texas Coastal Bend. In: Handley, L., D. Altsman & R. DeMay (eds) Seagrass Status and Trends in the Northern Gulf of Mexico: 1940–2002. U.S. Geological Survey Scientific Investigations Report 2006-5287, 267.

Rabalais, N. N., 2002. Nitrogen in aquatic ecosystems. Ambio 31(2):102-112 doi:10.1579/0044-7447-31.2.102.

Rabalais, N. N., R. E. Turner, R. J. Díaz & D. Justić, 2009. Global change and eutrophication of coastal waters. ICES Journal of Marine Science 66(7):1528-1537.

Raymond, P. A. & J. E. Saiers, 2010. Event controlled DOC export from forested watersheds. Biogeochemistry 100(1-3):197-209.

Raymond, P. A., J. E. Saiers & W. V. Sobczak, 2016. Hydrological and biogeochemical controls on watershed dissolved organic matter transport: Pulse-shunt concept. Ecology 97(1):5-16.

Repeta, D. J., 2015. Chemical characterization and cycling of dissolved organic matter Biogeochemistry of marine dissolved organic matter. Elsevier, 21-63.

Rettman, P., 1983. Water levels and salinities of water within the Evangeline Aquifer in an area southwest of Corpus Christi, Texas. US Geological Survey.

Robinson, C., L. Li & H. Prommer, 2007. Tide-induced recirculation across the aquifer-ocean interface. Water Resources Research 43(7).

Rodellas, V., J. Garcia-Orellana, A. Tovar-Sánchez, G. Basterretxea, J. M. López-Garcia, D. Sánchez-Quiles, E. Garcia-Solsona & P. Masqué, 2014. Submarine groundwater discharge as a source of nutrients and trace metals in a Mediterranean bay (Palma Beach, Balearic Islands). Marine Chemistry 160:56-66.

Rossel, P. E., C. Bienhold, A. Boetius & T. Dittmar, 2016. Dissolved organic matter in pore water of Arctic Ocean sediments: Environmental influence on molecular composition. Organic Geochemistry 97:41-52 doi:https://doi.org/10.1016/j.orggeochem.2016.04.003.

Rossel, P. E., C. Bienhold, L. Hehemann, T. Dittmar & A. Boetius, 2020. Molecular Composition of Dissolved Organic Matter in Sediment Porewater of the Arctic Deep-Sea Observatory HAUSGARTEN (Fram Strait). Frontiers in Marine Science 7(428) doi:10.3389/fmars.2020.00428.

RRC (Railroad Commision of Texas), 2018. Public GIS Viewer (Map). In. http://www.rrc.state.tx.us/about-us/resource-center/research/gis-viewers/ Accessed July 2018.

Russoniello, C. J., C. Fernandez, J. F. Bratton, J. F. Banaszak, D. E. Krantz, A. S. Andres, L. F. Konikow & H. A. Michael, 2013. Geologic effects on groundwater salinity and discharge into an estuary. Journal of hydrology 498:1-12.

Sadat-Noori, M., I. R. Santos, C. J. Sanders, L. M. Sanders & D. T. Maher, 2015. Groundwater discharge into an estuary using spatially distributed radon time series and radium isotopes. Journal of Hydrology 528(Supplement C):703-719 doi:https://doi.org/10.1016/j.jhydrol.2015.06.056.

Sánchez-Murillo, R., L. G. Romero-Esquivel, J. Jiménez-Antillón, J. Salas-Navarro, L. Corrales-Salazar, J. Álvarez-Carvajal, S. Álvarez-McInerney, D. Bonilla-Barrantes, N. Gutiérrez-Sibaja & M. Martínez-Arroyo, 2019. DOC transport and export in a dynamic tropical catchment. Journal of Geophysical Research: Biogeosciences 124(6):1665-1679.

Santos, I. R., W. C. Burnett, J. Chanton, B. Mwashote, I. Suryaputra & T. Dittmar, 2008a. Nutrient biogeochemistry in a Gulf of Mexico subterranean estuary and groundwater-derived fluxes to the coastal ocean. Limnology and Oceanography 53(2):705.

Santos, I. R., W. C. Burnett, T. Dittmar, I. G. N. A. Suryaputra & J. Chanton, 2009. Tidal pumping drives nutrient and dissolved organic matter dynamics in a Gulf of Mexico subterranean estuary. Geochimica Et Cosmochimica Acta 73(5):1325-1339 doi:10.1016/j.gca.2008.11.029.

Santos, I. R., P. L. Cook, L. Rogers, J. d. Weys & B. D. Eyre, 2012a. The "salt wedge pump": Convection-driven pore-water exchange as a source of dissolved organic and inorganic carbon and nitrogen to an estuary. Limnology and Oceanography 57(5):1415-1426.

Santos, I. R., J. de Weys, D. R. Tait & B. D. Eyre, 2013. The Contribution of Groundwater Discharge to Nutrient Exports from a Coastal Catchment: Post-Flood Seepage Increases Estuarine N/P Ratios. Estuaries and Coasts 36(1):56-73 doi:10.1007/s12237-012-9561-4.

Santos, I. R., B. D. Eyre & M. Huettel, 2012b. The driving forces of porewater and groundwater flow in permeable coastal sediments: A review. Estuarine, Coastal and Shelf Science 98:1-15 doi:http://dx.doi.org/10.1016/j.ecss.2011.10.024.

Santos, I. R., F. Niencheski, W. Burnett, R. Peterson, J. Chanton, C. F. Andrade, I. B. Milani, A. Schmidt & K. Knoeller, 2008b. Tracing anthropogenically driven groundwater discharge into a coastal lagoon from southern Brazil. Journal of Hydrology 353(3):275-293.

Sañudo-Wilhelmy, S. A., F. K. Rossi, H. Bokuniewicz & R. J. Paulsen, 2002. Trace metal levels in uncontaminated groundwater of a coastal watershed: importance of colloidal forms. Environmental science & technology 36(7):1435-1441.

Sawyer, A., 2015. Enhanced removal of groundwater-borne nitrate in heterogeneous aquatic sediments. Geophysical Research Letters 42(2):403-410.

Sawyer, A. H., O. Lazareva, K. D. Kroeger, K. Crespo, C. S. Chan, T. Stieglitz & H. A. Michael, 2014. Stratigraphic controls on fluid and solute fluxes across the sediment—water interface of an estuary. Limnology and Oceanography 59(3):997-1010 doi:10.4319/lo.2014.59.3.0997.

Scavia, D. & S. B. Bricker, 2006. Coastal eutrophication assessment in the United States Nitrogen Cycling in the Americas: Natural and Anthropogenic Influences and Controls. Springer, 187-208.

Schmidt, F., M. Elvert, B. P. Koch, M. Witt & K.-U. Hinrichs, 2009. Molecular characterization of dissolved organic matter in pore water of continental shelf sediments. Geochimica et Cosmochimica Acta 73(11):3337-3358.

Schmidt, F., B. P. Koch, T. Goldhammer, M. Elvert, M. Witt, Y.-S. Lin, J. Wendt, M. Zabel, V. B. Heuer & K.-U. Hinrichs, 2017. Unraveling signatures of biogeochemical processes and the depositional setting in the molecular composition of pore water DOM across different marine environments. Geochimica et Cosmochimica Acta 207:57-80 doi:https://doi.org/10.1016/j.gca.2017.03.005.

Schwartz, F. W. & H. Zhang, 2003. Fundamentals of ground water. Wiley, [New York].

Shafer, G. & E. Baker Jr, 1973. Ground water resources of Kleberg, Kenedy, and southern Jim Wells Counties. Texas Tex Water Devel Board Rep 173.

Shafer, G. H., 1968. Ground-water Resouces of Nueces and San Patricio Counties, Texas. U.S. Geological Survey.

Shellenbarger, G. G., S. G. Monismith, A. Genin & A. Paytan, 2006. The importance of submarine groundwater discharge to the near shore nutrient supply in the Gulf of Aqaba (Israel). Limnology and Oceanography 51(4):1876-1886 doi:10.4319/lo.2006.51.4.1876.

Shideler, G. L., C. E. Stelting & J. H. McGowen, 1981. Maps showing textural characteristics of benthic sediments in the Corpus Christi Bay estuarine system, South Texas. US Geological Survey, Reston, VA.

Sholkovitz, E., C. Herbold & M. Charette, 2003. An automated dye-dilution based seepage meter for the time-series measurement of submarine groundwater discharge. Limnology and Oceanography: Methods 1(1):16-28.

Silliman, S. E., B. Berkowitz, J. Simunek & M. T. van Genuchten, 2002. Fluid Flow and Solute Migration Within the Capillary Fringe. Ground Water 40(1):76-84 doi:10.1111/j.1745-6584.2002.tb02493.x.

Simon, C., H. Osterholz, A. Koschinsky & T. Dittmar, 2019. Riverine mixing at the molecular scale – An ultrahigh-resolution mass spectrometry study on dissolved organic matter and selected metals in the Amazon confluence zone (Manaus, Brazil). Organic Geochemistry 129:45-62 doi:https://doi.org/10.1016/j.orggeochem.2019.01.013.

Simon, C., V.-N. Roth, T. Dittmar & G. Gleixner, 2018. Molecular signals of heterogeneous terrestrial environments identified in dissolved organic matter: A comparative analysis of Orbitrap and ion cyclotron resonance mass spectrometers. Frontiers in Earth Science 6.

Sipler, R. E. & D. A. Bronk, 2015. Dynamics of Dissolved Organic Nitrogen. Biogeochemistry of Marine Dissolved Organic Matter, 2nd Edition:127-232 doi:10.1016/B978-0-12-405940-5.00004-2.

Sleighter, R. L., Y.-P. Chin, W. A. Arnold, P. G. Hatcher, A. J. McCabe, B. C. McAdams & G. C. Wallace, 2014. Evidence of incorporation of abiotic S and N into prairie wetland dissolved organic matter. Environmental Science & Technology Letters 1(9):345-350.

Sleighter, R. L. & P. G. Hatcher, 2008. Molecular characterization of dissolved organic matter (DOM) along a river to ocean transect of the lower Chesapeake Bay by ultrahigh resolution electrospray ionization Fourier transform ion cyclotron resonance mass spectrometry. Marine chemistry 110(3-4):140-152.

Sleighter, R. L., Z. Liu, J. Xue & P. G. Hatcher, 2010. Multivariate Statistical Approaches for the Characterization of Dissolved Organic Matter Analyzed by Ultrahigh Resolution Mass Spectrometry. Environmental Science & Technology 44(19):7576-7582 doi:10.1021/es1002204.

Slomp, C. P. & P. Van Cappellen, 2004. Nutrient inputs to the coastal ocean through submarine groundwater discharge: controls and potential impact. Journal of Hydrology 295(1-4):64-86.

Smith, C. G. & L. L. Robbins, 2012. Surface-Water Radon-222 Distribution along the Western-Central Florida Shelf. U.S. Geological Survey, 26.

Spalt, N., D. Murgulet & H. Abdulla, 2020. Spatial variation and availability of nutrients at an oyster reef in relation to submarine groundwater discharge. Science of The Total Environment 710:136283.

Spalt, N., D. Murgulet & X. Hu, 2018. Relating estuarine geology to groundwater discharge at an oyster reef in Copano Bay, TX. Journal of hydrology 564:785-801.

Spencer, R. G., G. R. Aiken, K. D. Butler, M. M. Dornblaser, R. G. Striegl & P. J. Hernes, 2009. Utilizing chromophoric dissolved organic matter measurements to derive export and reactivity of dissolved organic carbon exported to the Arctic Ocean: A case study of the Yukon River, Alaska. Geophysical Research Letters 36(6).

Stedmon, C. A., S. Markager, L. Tranvik, L. Kronberg, T. Slätis & W. Martinsen, 2007. Photochemical production of ammonium and transformation of dissolved organic matter in the Baltic Sea. Marine Chemistry 104(3):227-240 doi:https://doi.org/10.1016/j.marchem.2006.11.005.

Stewart, B. T., K. R. Bryan, C. A. Pilditch & I. R. Santos, 2018. Submarine groundwater discharge estimates using radium isotopes and related nutrient inputs into Tauranga Harbour (New Zealand). Estuaries and coasts 41(2):384-403.

Stieglitz, T., M. Taniguchi & S. Neylon, 2008. Spatial variability of submarine groundwater discharge, Ubatuba, Brazil. Estuarine, Coastal and Shelf Science 76(3):493-500.

Stocker, T., 2014. Climate change 2013: the physical science basis: Working Group I contribution to the Fifth assessment report of the Intergovernmental Panel on Climate Change. Cambridge University Press.

Stubbins, A., E. Hood, P. A. Raymond, G. R. Aiken, R. L. Sleighter, P. J. Hernes, D. Butman, P. G. Hatcher, R. G. Striegl & P. Schuster, 2012a. Anthropogenic aerosols as a source of ancient dissolved organic matter in glaciers. Nature Geoscience 5(3):198-201.

Stubbins, A., J. Niggemann & T. Dittmar, 2012b. Photo-lability of deep ocean dissolved black carbon. Biogeosciences 9(5):1661-1670.

Stubbins, A., R. G. Spencer, P. J. Mann, R. M. Holmes, J. W. McClelland, J. Niggemann & T. Dittmar, 2015. Utilizing colored dissolved organic matter to derive dissolved black carbon export by arctic rivers. Frontiers in Earth Science 3:63.

Sugimoto, R., H. Honda, S. Kobayashi, Y. Takao, D. Tahara, O. Tominaga & M. Taniguchi, 2016. Seasonal changes in submarine groundwater discharge and associated nutrient transport into a tideless semi-enclosed embayment (Obama Bay, Japan). Estuaries and Coasts 39(1):13-26.

Sun, Y. & T. Torgersen, 1998. The effects of water content and Mn-fiber surface conditions on Ra-224 measurement by Rn-220 emanation. Marine Chemistry 62(3-4):299-306.

Swarzenski, P. W., 2007. U/Th series radionuclides as coastal groundwater tracers. Chemical Reviews 107(2):663-674.

Swarzenski, P. W., W. C. Burnett, W. J. Greenwood, B. Herut, R. Peterson, N. Dimova, Y. Shalem, Y. Yechieli & Y. Weinstein, 2006a. Combined time-series resistivity and geochemical tracer techniques to examine submarine groundwater discharge at Dor Beach, Israel. Geophysical Research Letters 33(24).

Swarzenski, P. W., W. H. Orem, B. F. McPherson, M. Baskaran & Y. Wan, 2006b. Biogeochemical transport in the Loxahatchee River estuary, Florida: The role of submarine groundwater discharge. Marine Chemistry 101(3-4):248-265 doi:10.1016/j.marchem.2006.03.007.

Swarzenski, P. W., C. Reich, K. D. Kroeger & M. Baskaran, 2007a. Ra and Rn isotopes as natural tracers of submarine groundwater discharge in Tampa Bay, Florida. Marine Chemistry 104(1-2):69-84.

Swarzenski, P. W., F. W. Simonds, A. J. Paulson, S. Kruse & C. Reich, 2007b. Geochemical and geophysical examination of submarine groundwater discharge and associated nutrient loading estimates into Lynch Cove, Hood Canal, WA. Environmental Science & Technology 41(20):7022-7029.

Szabo, Z., V. T. dePaul, J. M. Fischer, T. F. Kraemer & E. Jacobsen, 2012a. Occurrence and geochemistry of radium in water from principal drinking-water aquifer systems of the United States. Applied Geochemistry 27(3):729-752 doi:https://doi.org/10.1016/j.apgeochem.2011.11.002.

Szabo, Z., J. M. Fischer & T. C. Hancock, 2012b. Principal Aquifers Can Contribute Radium to Sources of Drinking Water Under Certain Geochemical Conditions: U.S. Geological Survey Fact Sheet 2010-3113. U.S. Department of the Interior, 6.

Szymczycha, B., Ż. Kłostowska, M. Lengier & L. Dzierzbicka-Głowacka, 2020. Significance of nutrient fluxes via submarine groundwater discharge in the Bay of Puck, southern Baltic Sea. Oceanologia 62(2):117-125 doi:https://doi.org/10.1016/j.oceano.2019.12.004.

Taniguchi, M., W. C. Burnett, J. E. Cable & J. V. Turner, 2002. Investigation of submarine groundwater discharge. Hydrological Processes 16(11):2115-2129 doi:10.1002/hyp.1145.

Taniguchi, M. & Y. Fukuo, 1993. Continuous measurements of ground-water seepage using an automatic seepage meter. Ground water 31(4):675-679.

TDWR (Texas Department of Water Resources), 1981. Nueces and Mission-Aransas Estuaries: A Study of the Influence of Freshwater Inflows.

Toth, J., 1971. Groundwater discharge: a common generator of diverse geologic and morphologic phenomena. Hydrological Sciences Journal 16(1):7-24.

Trenberth, K. E., A. Dai, R. M. Rasmussen & D. B. Parsons, 2003. The changing character of precipitation. Bulletin of the American Meteorological Society 84(9):1205-1218.

Triska, F. J., V. C. Kennedy, R. J. Avanzino, G. W. Zellweger & K. E. Bencala, 1989. Retention and transport of nutrients in a third-order stream in northwestern California: Hyporheic processes. Ecology 70(6):1893-1905.

Groundwater Database (GWDB) Reports: Water Levels by Aquifer 2017. TWDB (Texas Water Development Board),. https://www.twdb.texas.gov/groundwater/data/gwdbrpt.asp#N. Accessed 2017.

TWDB (Texas Water Development Board), 2018. Freshwater Inflow Estimates. In: Water Data for Texas: Coastal. https://waterdatafortexas.org/coastal/hydrology 2018.

Twichell, D., L. Edmiston, B. Andrews, W. Stevenson, J. Donoghue, R. Poore & L. Osterman, 2010. Geologic controls on the recent evolution of oyster reefs in Apalachicola Bay and St. George Sound, Florida. Estuarine, Coastal and Shelf Science 88(3):385-394.

Uddameri, V., S. Singaraju & E. A. Hernandez, 2014. Identifying influencing wells for gradient estimation in the confined portion of the Gulf Coast aquifer near Kingsville, TX. Environmental earth sciences 71(6):2629-2640.

Urquidi-Gaume, M., I. R. Santos & C. Lechuga-Deveze, 2016. Submarine groundwater discharge as a source of dissolved nutrients to an arid coastal embayment (La Paz, Mexico). Environmental Earth Sciences 75(2):1.

Vahatalo, A. V. & M. Jarvinen, 2007. Photochemically produced bioavailable nitrogen from biologically recalcitrant dissolved organic matter stimulates production of a nitrogen-limited microbial food web in the Baltic Sea. Limnology and Oceanography 52(1):132-143.

Vähätalo, A. V. & R. G. Zepp, 2005. Photochemical Mineralization of Dissolved Organic Nitrogen to Ammonium in the Baltic Sea. Environmental Science & Technology 39(18):6985-6992 doi:10.1021/es050142z.

Valiela, I., J. Costa, K. Foreman, J. M. Teal, B. Howes & D. Aubrey, 1990. Transport of Groundwater-Borne Nutrients from Watersheds and Their Effects on Coastal Waters. Biogeochemistry 10(3):177-197.

Wagner, S., T. Dittmar & R. Jaffé, 2015a. Molecular characterization of dissolved black nitrogen via electrospray ionization Fourier transform ion cyclotron resonance mass spectrometry. Organic Geochemistry 79:21-30 doi:https://doi.org/10.1016/j.orggeochem.2014.12.002.

Wagner, S., T. Riedel, J. Niggemann, A. V. Vähätalo, T. Dittmar & R. Jaffé, 2015b. Linking the molecular signature of heteroatomic dissolved organic matter to watershed characteristics in world rivers. Environmental science & technology 49(23):13798-13806.

Wang, X., H. Li, J. Yang, C. Zheng, Y. Zhang, A. An, M. Zhang & K. Xiao, 2017. Nutrient inputs through submarine groundwater discharge in an embayment: A radon investigation in Daya Bay, China. Journal of Hydrology 551:784-792 doi:https://doi.org/10.1016/j.jhydrol.2017.02.036.

Wang, X., H. Li, C. Zheng, J. Yang, Y. Zhang, M. Zhang, Z. Qi, K. Xiao & X. Zhang, 2018. Submarine groundwater discharge as an important nutrient source influencing nutrient structure in coastal water of Daya Bay, China. Geochimica et Cosmochimica Acta 225:52-65 doi:https://doi.org/10.1016/j.gca.2018.01.029.

Warner, N. R., C. A. Christie, R. B. Jackson & A. Vengosh, 2013. Impacts of Shale Gas Wastewater Disposal on Water Quality in Western Pennsylvania. Environmental Science & Technology 47(20):11849-11857 doi:10.1021/es402165b.

Waterstone & Parsons, 2003. Groundwater availability of the central Gulf Coast aquifer--Numerical simulations to 2050, Central Gulf Coast, Texas.

Wilson, A. M., 2005. Fresh and saline groundwater discharge to the ocean: A regional perspective. Water Resources Research 41(2).

Yang, L., W. Guo, N. Chen, H. Hong, J. Huang, J. Xu & S. Huang, 2013. Influence of a summer storm event on the flux and composition of dissolved organic matter in a subtropical river, China. Applied Geochemistry 28:164-171 doi:https://doi.org/10.1016/j.apgeochem.2012.10.004.

Yoon, B. & P. A. Raymond, 2012. Dissolved organic matter export from a forested watershed during Hurricane Irene. Geophysical Research Letters 39(18).

Young, S. C., M. Jigmond, N. Deeds, J. Blainey, T. E. Ewing, D. Banerj, D. Piemonti, T. Jones, C. Griffith, G. Martinez, C. Hudson, S. Hamlin & J. Sutherland, 2016. Final Report: Identification of Potential Brackish Groundwater Production Areas-Gulf Coast Aquifer System. Texas Water Development Board, Austin, TX, 636.

Zarnetske, J. P., R. Haggerty, S. M. Wondzell & M. A. Baker, 2011. Dynamics of nitrate production and removal as a function of residence time in the hyporheic zone. Journal of Geophysical Research: Biogeosciences 116(G1).

Zekt͡ser, I. S., R. G. Dzhamalov & L. G. Everett, 2007. Submarine groundwater. CRC/Taylor & Francis, Boca Raton, FL.

Ziolkowski, L. A. & E. R. Druffel, 2010. Aged black carbon identified in marine dissolved organic carbon. Geophysical Research Letters 37(16).

Zubarev, R. A. & A. Makarov, 2013. Orbitrap mass spectrometry. ACS Publications.